AGU ADVANCING EARTH AND SPACE SCIENCES

Reviews of Geophysics

REVIEW ARTICLE
10.1029/2023RG000833

Key Points:

- Measurement techniques for deep mantle anisotropy have been improved substantially in the last decade
- These improvements enable inferences of deep mantle flow with increasing confidence
- Knowledge of mantle dynamics elucidates the drivers of flow, relationships among structures, and Earth's dynamic evolution

Correspondence to:
J. Wolf,
jonathan.wolf@yale.edu

Citation:
Wolf, J., Li, M., Long, M. D., & Garnero, E. (2024). Advances in mapping lowermost mantle convective flow with seismic anisotropy observations. *Reviews of Geophysics*, *62*, e2023RG000833. https://doi.org/10.1029/2023RG000833

Received 2 FEB 2024
Accepted 26 APR 2024

Author Contributions:
Conceptualization: Jonathan Wolf, Mingming Li, Maureen D. Long, Edward Garnero
Data curation: Jonathan Wolf
Formal analysis: Jonathan Wolf, Mingming Li
Funding acquisition: Mingming Li, Maureen D. Long, Edward Garnero
Investigation: Jonathan Wolf, Mingming Li, Maureen D. Long, Edward Garnero
Methodology: Jonathan Wolf, Mingming Li, Maureen D. Long, Edward Garnero
Resources: Mingming Li, Maureen D. Long, Edward Garnero
Software: Jonathan Wolf, Mingming Li
Supervision: Maureen D. Long, Edward Garnero
Validation: Jonathan Wolf, Mingming Li
Visualization: Jonathan Wolf, Mingming Li, Edward Garnero
Writing – original draft: Jonathan Wolf, Mingming Li
Writing – review & editing: Jonathan Wolf, Mingming Li, Maureen D. Long, Edward Garnero

Advances in Mapping Lowermost Mantle Convective Flow With Seismic Anisotropy Observations

Jonathan Wolf[1], Mingming Li[2], Maureen D. Long[1], and Edward Garnero[2]

[1]Department of Earth and Planetary Sciences, Yale University, New Haven, CT, USA, [2]School of Earth and Space Exploration, Arizona State University, Tempe, AZ, USA

Abstract Convective flow in the deep mantle controls Earth's dynamic evolution, influences plate tectonics, and has shaped Earth's current surface features. Present and past convection-induced deformation manifests itself in seismic anisotropy, which is particularly strong in the mantle's uppermost and lowermost portions. While the general patterns of seismic anisotropy have been mapped for the upper mantle, anisotropy in the lowermost mantle (called D″) is at an earlier stage of exploration. Here we review recent progress in methods to measure and interpret D″ anisotropy. Our understanding of the limitations of existing methods and the development of new measurement strategies have been aided enormously by the availability of high-performance computing resources. We give an overview of how measurements of seismic anisotropy can help constrain the mineralogy and fabric of the deep mantle. Specifically, new and creative strategies that combine multiple types of observations provide much tighter constraints on the geometry of anisotropy than have previously been possible. We also discuss how deep mantle seismic anisotropy provides insights into lowermost mantle dynamics. We summarize what we have learned so far from measurements of D″ anisotropy, how inferences of lowermost mantle flow from measurements of seismic anisotropy relate to geodynamic models of mantle flow, and what challenges we face going forward. Finally, we discuss some of the important unsolved problems related to the dynamics of the lowermost mantle that can be elucidated in the future by combining observations of seismic anisotropy with geodynamic predictions of lowermost mantle flow.

Plain Language Summary Earthquakes cause waves that travel through Earth's interior and are recorded by distant seismometers. These seismic waves behave differently depending on the material that they pass through, revealing Earth's material properties. At the very bottom of the mantle, seismic waves sometimes travel at different speeds depending on their direction. This material property is called seismic anisotropy and is caused by material deformation and flow. Global patterns of mantle flow, which is directly connected to surface processes such as the movement of tectonic plates or hotspot volcanism, can therefore be inferred from seismic anisotropy. Recent years have seen advances in anisotropy imaging in the lowermost mantle as well as in numerical calculations of flow in Earth's lowermost mantle. We review the methods that are used to infer lowermost mantle anisotropy. We further give an overview of previous results and interpretations, which include seismic anisotropy caused by upwelling plumes and ancient slab remnants. Future improvements in the fields of seismology, geodynamics, and mineral physics are needed to improve our understanding of global deep mantle flow.

1. Introduction

More than half a century ago, the lowermost ~300 km of the mantle were suggested to have an anomalous velocity gradient and were therefore given a characteristic name, D″ (Bullen, 1950). D″ corresponds to the lower boundary layer of Earth's mantle, and convective flow in this layer can lead to the preferential alignment of minerals (e.g., Karato et al., 2008; Kocks et al., 2000; Wenk & Houtte, 2004) through the development of crystallographic-preferred orientation (CPO). If the aligned minerals have elastic properties that are directionally dependent, then seismic wavespeeds through the region of deformation can depend on the propagation and/or polarization direction of the wave, a property called seismic anisotropy (Figure 1) (e.g., Karato et al., 2008; Kocks et al., 2000; Wenk & Houtte, 2004). Alternatively, seismic anisotropy can be induced through convective stresses that shape elastically distinct heterogeneities, causing seismic anisotropy through shape-preferred orientation (SPO; e.g., Kendall & Silver, 1998; Lay et al., 1998). Although seismic anisotropy appears to be weak or absent in the bulk of the lower mantle (Figure 2a) (e.g., Chang et al., 2015; French & Romanowicz, 2014; Meade et al., 2005; Niu & Perez, 2004), strong seismic anisotropy has been detected in many regions of D″ (Figure 2b)

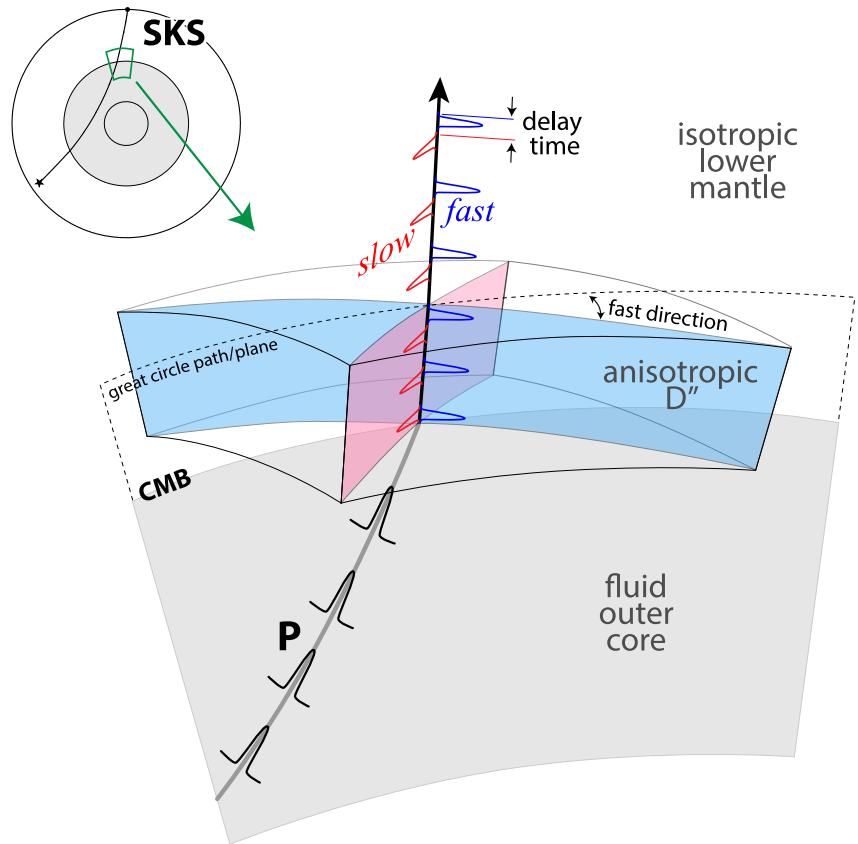

Figure 1. Schematic illustration of shear wave splitting due to lowermost mantle anisotropy. Shear wave splitting is illustrated for the SKS phase (top left), which travels as *P* (black wiggles) through the liquid outer core (gray shading) and then transforms to an SV wave at the core-mantle boundary. SKS splits into fast (blue) and a slow (red) traveling quasi-shear waves, which are polarized in orthogonal planes (slow: red; fast: blue). These components accumulate a time lag (delay time), which can be measured along with the polarization of the fast traveling wave (fast polarization direction). The fast polarization direction ϕ is usually measured at the station with respect to the north direction, but this convention is not explicitly displayed in this D′′-centered illustration.

(e.g., Asplet et al., 2020; Garnero & Lay, 1997; Kendall & Silver, 1996; Lay & Young, 1991; Nowacki et al., 2010). Therefore, measurements of D′′ anisotropy can provide insights into the nature of flow and the mineral phases and physical properties of materials in the deep mantle.

In presence of seismic anisotropy, shear waves split into two orthogonally polarized components (Figure 1; e. g, Silver & Chan, 1991; Vinnik et al., 1989a, 1989b), which travel at the speed of the fast and the slow direction of the anisotropy, respectively. Therefore, shear wave speeds depend on both the propagation and polarization direction of the wave. This implies that D′′ anisotropy can be inferred from (relative) travel times of seismic phases, as done in seismic tomography approaches (e.g., Chang et al., 2015; Moulik & Ekström, 2014), as well as from other data, such as Earth's free oscillations (e.g., Schneider & Deuss, 2020). Alternatively, relative travel times of the slow and fast components can be analyzed via measurements of shear-wave splitting (e.g., Silver & Chan, 1991; Vinnik et al., 1989a, 1989b). Such shear-wave splitting has been measured for many seismic phases (Figure 3). Depending on the seismic phase, and sometimes in comparison with splitting of other phases, the measured shear-wave splitting can be indicative of upper and/or lowermost mantle anisotropy. Another approach involves the use of waveforms in inversions to infer seismic anisotropy instead of measuring splitting parameters. Such inversions can either be conducted for specific seismic phases (e.g., Asplet et al., 2023) or for longer seismogram snippets (e.g., Kawai & Geller, 2010; Suzuki et al., 2021). Such models often assume a radial anisotropic geometry (Chang et al., 2015; Kawai & Geller, 2010; Panning & Romanowicz, 2006; Suzuki et al., 2021), in which there are differences between horizontal and vertical wavespeeds.

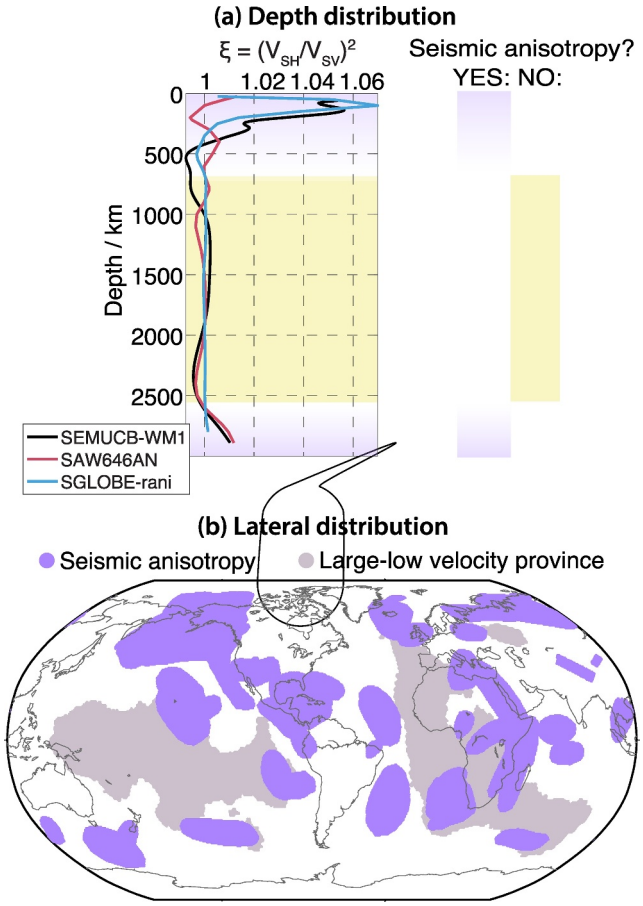

Figure 2. Inferred seismic anisotropy distribution in Earth. (a) Left: Radial anisotropy ζ as a function of depth, as inferred by three radially anisotropic tomography models (Megnin & Romanowicz, 2000), SEMUCB-WM1 (French & Romanowicz, 2014) and SGLOBE-rani (Chang et al., 2015) (see legend). Right: Seismic anisotropy is present in Earth's crust and upper mantle as well as in the deep mantle (violet), while the bulk of the lower mantle is almost isotropic (yellow). (b) Locations for which the presence of deep mantle seismic anisotropy has been suggested in previous regional studies (violet areas), compiled by Wolf, Long, Li, and Garnero (2023). Low velocity features are shown in purple gray, as determined by regions where at least 3 out of 5 tomography models assigned a particular point to a slow cluster at a depth of 2,700 km in the cluster analysis performed by Lekic et al. (2012).

Irrespective of the specific technique used, good ray sampling is crucial for an accurate analysis of D″ anisotropy, preferably from multiple seismic phases, both in terms of the number of raypaths through the mantle region of interest and sampling from different directions (e.g., Wolf, Long, Li, & Garnero, 2023).

Many new strategies to measure deep mantle anisotropy have been suggested in the past two decades (e.g., H. A. Ford et al., 2015; Kawai & Geller, 2010; Niu & Perez, 2004; Pisconti et al., 2019; Thomas et al., 2011; Wang & Wen, 2004; Wolf et al., 2022a; Wolf, Frost, et al., 2023; Wolf, Long, Creasy, & Garnero, 2023; Wolf, Long, Frost, & Nissen-Meyer, 2024; Wookey et al., 2005). Some of these strategies rely on ray theory, which is a high-frequency approximation of the wave equation. The validity of such ray-theoretical assumptions has become possible to test through the increasing availability of computational resources, which allow for the consideration of full-wave effects. Global wavefield simulations have been conducted at the periods at which shear-wave splitting measurements are typically made, in both isotropic (e.g., Borgeaud et al., 2016; Komatitsch et al., 2010; Parisi et al., 2018) and arbitrarily anisotropic (e.g., Cottaar & Romanowicz, 2013; Nowacki & Wookey, 2016; Tesoniero et al., 2020; Wolf et al., 2022a, 2022b) media. Such global wavefield simulations have been used to test measurement strategies that rely on a multitude of body wave phases (e.g., S, ScS, S_{diff}, SKS, SKKS, S3KS; Figure 3). Using simulations of seismic wave propagation, some challenges with existing methods have been identified. Some of these challenges have successfully been resolved (e.g., Cottaar & Romanowicz, 2013; Nowacki & Wookey, 2016; Wolf, Long, Creasy, & Garnero, 2023), but others have proven harder to tackle. We give a detailed overview of these challenges in this paper.

Mitchell and Helmberger (1973) showed evidence for differential SV-SH travel times of S and ScS waves, which they interpreted as an indicator of structural layering. In hindsight, these observations could have been explained by D″ anisotropy, but the authors did not make such an interpretation. The first paper to infer D″ anisotropy was Vinnik et al. (1989a, 1989b), based on differential times between SV_{diff} and SH_{diff}. Inferences of D″ anisotropy became common in the 1990s, but the identification of the causative mechanism has proven challenging. The main reason is that most early D″ anisotropy studies analyzed whether vertically or horizontally polarized shear-waves travel faster in a particular geographic region (i.e., radial anisotropy; e.g., Fouch et al., 2001; Kendall & Silver, 1996; Lay & Young, 1991; Pulliam & Sen, 1998; Russell et al., 1998; Ritsema, Lay, et al., 1998; Vinnik et al., 1995), which has many different possible causes. In the 2000s, techniques to more accurately measure splitting caused by D″ anisotropy were developed (e.g., Wang & Wen, 2004; Wookey et al., 2005), which enabled the inference of plausible anisotropy scenarios that reproduce the measured shear wave splitting parameters, using both forward and inverse modeling methods (e.g., Asplet et al., 2023; Creasy et al., 2017; H. A. Ford et al., 2015; Nowacki et al., 2010; Wolf & Long, 2022). Bridgmanite's (Br) high-pressure polymorph post-perovskite (Ppv) was discovered in 2004 (Murakami et al., 2004) and was invoked as a potential explanation for lowermost mantle anisotropy, along with ferropericlase (Fp). Modeling of seismic anisotropy has allowed the inference of likely D″ compositions of some regions using previously suggested elastic tensors; such studies have often favored post-perovskite as a mechanism for anisotropy and as a dominant mineral (e.g., Asplet et al., 2023; Chandler et al., 2021; Cottaar et al., 2014; Creasy et al., 2017; H. A. Ford et al., 2015; Pisconti et al., 2023; Wenk et al., 2011). These inferences are important because they potentially allow the determination of lowermost mantle mineralogy and

10.1029/2023RG000833

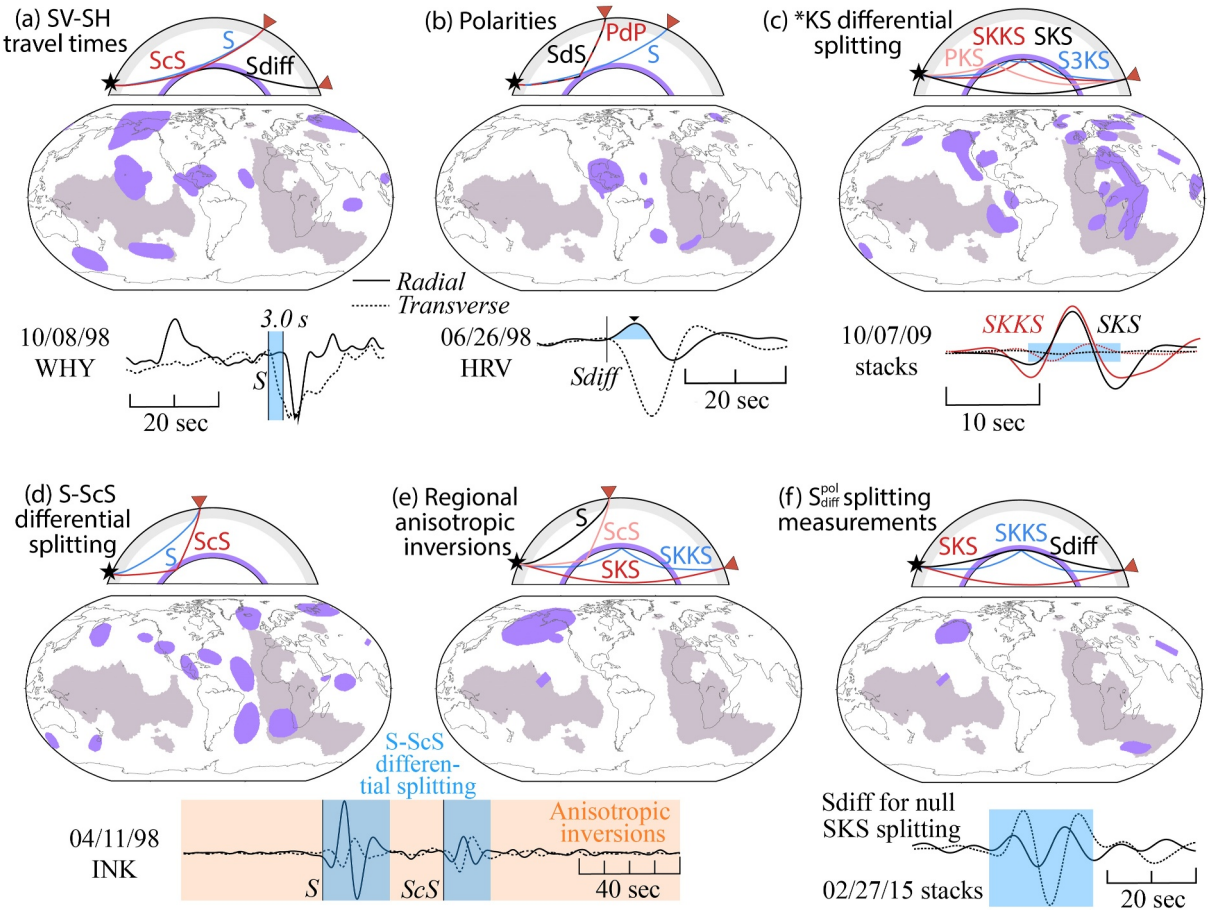

Figure 3. Summary of D′′ anisotropy distribution, based on different measurement methods. Figure and caption are slightly modified from Wolf, Long, Li, and Garnero (2023). (a) Top: Cross-section of seismic phases used to determine differential SV-SH travel times. The source is represented as a black star and stations as red triangles. Middle: Seismic anisotropy locations identified using differential SV-SH travel times. The plotting conventions are as in Figure 2b. Bottom: Real data example after Garnero, Moore, et al. (2004), showing a differential arrival time for the S seismic phase in radial and transverse component seismograms (blue shading). The waveforms were recorded at station WHY for an event that occurred on 8 October 1998. Panel (b) same as panel (a), but showing phases and results from polarity studies; the real data example is after Garnero and Lay (2003) and shows an anomalous radial component S_{diff} polarity (blue shading). Otherwise, as in all other panels, plotting conventions are the same as in panel (a). (c) Phases and results for *KS differential splitting measurements; the real data example is modified from Wolf and Long (2022) and shows differential splitting of SKS and SKKS (blue shading). (d) Phases and results for S-ScS differential splitting; the real data example of S and ScS waveforms is modified from Wolf et al. (2019) (blue shading). (e) Phases and results from regional anisotropic inversions; real data example of a seismogram around S and ScS arrivals (orange shading) is as in panel (d). (f) S_{diff} splitting measurements that explicitly consider the wave's initial polarization; the real data example is modified from Wolf, Long, and Frost (2024), showing example radial and transverse S_{diff} waveforms that exhibit splitting for a case in which SKS splitting is null (blue shading).

thus temperature conditions and the quantification of heat flow across the core-mantle boundary (CMB; Murakami et al., 2004; Hernlund et al., 2005; Lay et al., 2008; Kawai & Tsuchiya, 2009).

While from a seismological perspective, distinguishing different scenarios for the origin of anisotropy (as described by different elastic tensors) is now possible, progress is somewhat hindered by the fact that properties of deep mantle materials are hard to determine at realistic conditions from a mineral physics perspective. Therefore, elastic tensors (which mathematically describe the anisotropy), as well as dominant deformation mechanisms and slip systems, are often estimated via extrapolation. However, disagreements among different studies (e.g., F. Lin et al., 2017; Miyagi et al., 2008; Romanowicz & Wenk, 2017; Yamazaki, Yoshino, et al., 2006, and references therein) lead to substantial uncertainty. Recent advances have included calculations of a large range of elastic tensors for (polycrystalline) aggregates with a variety of candidate dominant slip systems for different minerals (Creasy et al., 2020). This elastic tensor library enables the modeling of observations using more realistic models for anisotropy than single-crystal elastic tensors; however, it still relies on imperfect knowledge of the single-crystal elasticity and the relative strength of different slip systems.

Measurements of seismic anisotropy can be used to infer flow patterns at the base of the mantle, which may help us understand big-picture aspects of lowermost mantle dynamics, such as the behavior of the large-low velocity provinces (LLVPs) and their interaction with the surrounding mantle, the formation of mantle plumes, and the influence of subducted slabs on flow in the deepest mantle (e.g., Garnero et al., 2016; Lithgow-Bertelloni & Silver, 1998; McNamara, 2019; Nowacki et al., 2010; Steinberger & Steinberger, 2023; Tackley, 2000). Similarly, the patterns and drivers of lowermost mantle flow can be elucidated through measurements of seismic anisotropy (e.g., Chandler et al., 2021; McNamara et al., 2002; Nowacki et al., 2010). Over the past two decades, many regional studies have detected particularly strong lowermost mantle seismic anisotropy at LLVP edges (e.g., Cottaar & Romanowicz, 2013; Creasy et al., 2017; Deng et al., 2017; Lynner & Long, 2014; Pisconti et al., 2023; Reiss et al., 2019; Wang & Wen, 2004; Wolf & Long, 2023), although statistical analysis of previous observations of anisotropy in the D′′ layer does not indicate a preferential occurrence of anisotropy at LLVP edges versus elsewhere on a global scale (Wolf, Long, Li, & Garnero, 2023). Strong deep mantle anisotropy near LLVP edges may reflect particularly strong deformation, perhaps due to mantle flow impinging on their sides (e.g., Li & Zhong, 2017; McNamara et al., 2010) or the generation of upwelling flow (e.g., Burke et al., 2008; Heyn et al., 2020; Steinberger & Torsvik, 2012), which would induce deformation and seismic anisotropy. In fact, observations of seismic anisotropy at the roots of the Afar and Iceland plumes are generally consistent with upwelling flow in the lowermost mantle (H. A. Ford et al., 2015; Wolf et al., 2019). Moreover, recent observations of seismic anisotropy at the base of the mantle have been connected to slab remnants (e.g., Asplet et al., 2020; Asplet et al., 2023; Long, 2009; Nowacki et al., 2010; Wolf & Long, 2022; Wolf, Long, & Frost, 2024), implying that subducted slabs are an important driver of deep mantle flow (e.g., Chandler et al., 2021; McNamara et al., 2002; Tackley, 2000). In some cases, D′′ anisotropy is approximately co-located with enigmatic features having extremely low seismic velocities at the base of the mantle, called ultra-low velocity zones (ULVZs) (Garnero et al., 1993; Yu & Garnero, 2018). The interpretation of these findings can yield insights about the role of ULVZs in lowermost mantle dynamics (Wolf & Long, 2023; Wolf, Long, & Frost, 2024). Ongoing progress with respect to inferring mantle dynamics from D′′ anisotropy will further elucidate the drivers of deep mantle flow and the relationships among different lowermost mantle structures.

Mantle flow has been widely explored in geodynamic modeling calculations by solving the conservation equations of mass, momentum, and energy. The present-day instantaneous flow field in the mantle can be calculated from given density and viscosity structures of the mantle (e.g., Hager, 1984; Hager & O'Connell, 1981; X. Liu & Zhong, 2016; Steinberger & Holme, 2008; Walker et al., 2011; Yoshida, 2008b). The past mantle flow field has been predicted by solving the conservation equations backward-in-time (e.g., Steinberger, 2000; Steinberger & O'Connell, 1998), and by performing global convection models in which plate motion history is imposed at the surface to guide the convection pattern (e.g., Bower et al., 2013; Li & Zhong, 2017, 2019; McNamara & Zhong, 2005; Zhang et al., 2010). It is now generally thought that the global-scale convection pattern in the D′′ layer at the present-day is dominated by downwelling flow beneath subduction regions, upwelling flow above the two LLVPs and mostly lateral flows between them. However, the calculated mantle flow in geodynamic models at a regional scale remains controversial and is model dependent (e.g., Bull et al., 2010; Li & Zhong, 2017; Walker et al., 2011; Yoshida, 2008b). Since seismic anisotropy is a result of mantle convection, the former has been predicted using mantle flow field obtained in geodynamic models (e.g., Chandler et al., 2021; Cottaar et al., 2014; McNamara et al., 2002, 2003; Merkel et al., 2007; Nowacki et al., 2011; Walker et al., 2011; Wenk et al., 2011). A comparison of seismic anisotropy between geodynamic predictions and seismic observations thus provides critical information about the connection between mantle flow and seismic anisotropy and helps understand the deformation mechanism, mantle rock properties, and ultimately the mantle flow field for the real Earth (e.g., Nowacki & Cottaar, 2021; Nowacki et al., 2011).

This review will focus on three areas of significant scientific progress in the study of D′′ anisotropy in the last two decades and, in particular, in the last ∼5 years. First, we now clearly understand the strengths and weaknesses of many body-wave strategies to measure deep mantle anisotropy (e.g., Komatitsch et al., 2010; Nowacki & Wookey, 2016; Parisi et al., 2018; Wolf et al., 2022a, 2022b), which have lead to the development of novel measurement and interpretation approaches (e.g., Asplet et al., 2023; Pisconti et al., 2019; Wolf et al., 2022a; Wolf, Frost, et al., 2023; Wolf, Long, Creasy, & Garnero, 2023). Second, we now have the ability to use seismic observations to distinguish among different anisotropy-producing minerals in the deep mantle (e.g., Asplet et al., 2023; Creasy et al., 2017; H. A. Ford et al., 2015; Pisconti et al., 2023; Wenk et al., 2011; Wolf et al., 2019), although this remains limited by the imperfect understanding of the elastic properties and

dominant slip systems of deep mantle materials (e.g., post-perovskite; Romanowicz & Wenk, 2017, and references therein). Third, we are now able to infer possible flow scenarios for the lowermost mantle from observations of seismic anisotropy (e.g., Asplet et al., 2023; Cottaar & Romanowicz, 2013; H. A. Ford et al., 2015; Pisconti et al., 2023; Reiss et al., 2019). This enables us to compare flow inferred from measurements of seismic anisotropy with that from geodynamic predictions (e.g., Chandler et al., 2021; Cottaar et al., 2014; Flament, 2018; Walker et al., 2011). Using this information, we can assess which big-picture questions concerning mantle dynamics can potentially be elucidated, and what progress is needed to achieve this. In this review, we do not aim to provide a complete picture of the current research state on deep mantle mineralogy and composition beyond what is directly applicable to the interpretation of D′′ anisotropy measurements. Detailed discussions on the mineralogical aspects of seismic anisotropy have been provided in previous papers; see, for example, Irifune and Tsuchiya (2007), Shim (2008), Trønnes (2010), Nowacki et al. (2011), Cobden et al. (2015), and Romanowicz and Wenk (2017). We also do not discuss observations and interpretations of seismic anisotropy for other depth regions in the Earth, such as the upper mantle or the inner core. Extensive reviews on these topics have been provided previously, for example, by Long and Becker (2010), Long (2013), Deuss (2014), Tkalčić (2015), Romanowicz and Wenk (2017), and L. N. Hansen et al. (2021).

2. Body Wave Methods to Infer Deep Mantle Anisotropy

Seismic anisotropy in the deep mantle is usually inferred from the polarization-dependent behavior of shear waves. Compressional waves are more difficult to use; thus, to date, no certain picture of P wave anisotropy for the deep mantle has been developed (e.g., Beghein et al., 2006; Boschi & Dziewonski, 2000; Montagner & Kennett, 1996). We therefore focus on how D′′ anisotropy can be measured using shear waves.

2.1. Shear Wave Splitting

A shear wave that travels through an anisotropic medium splits into two components (e.g., Crampin & Lovell, 1991; Silver & Chan, 1991; Vinnik et al., 1989a, 1989b), a process analogous to optical birefringence (Figure 1). One component of the split wave travels at the speed that corresponds to the direction of low-velocity propagation and the other one to the high-velocity direction. Therefore, the slow wave will accumulate a time delay, δt, with respect to the fast wave after traveling through the anisotropic medium (Figure 1). Another parameter that can be measured is the fast polarization direction, usually called ϕ when measured clockwise from the north, and ϕ' (Nowacki et al., 2010) when measured with respect to the backazimuthal direction.

It can be useful to define an additional parameter, the splitting intensity (SI) (Chevrot, 2000), that indicates the strength of splitting on an individual seismogram. Let us designate C_0 as the horizontal component of wave motion in the direction of initial polarization of the incoming wave; $C_{90}(t)$ is oriented 90° away from this direction, ω is the angular frequency and t is time. Assuming that $\omega t \ll 1$, C_0 can be expressed as

$$C_0(t) \simeq \cos \omega t\,. \tag{1}$$

After traveling through the anisotropic medium, $C_{90}(t)$ becomes

$$C_{90}(t) \simeq -0.5\omega\delta t \sin 2(\alpha - \phi) \sin \omega t = 0.5\omega\delta t \sin(-2\phi')\, C_0'(t), \tag{2}$$

where α is the initial polarization direction of the incoming wave and $C_0'(t)$ is the component's time derivative (Silver & Chan, 1991; Vinnik et al., 1989a, 1989b). The splitting intensity (SI) can be expressed as

$$SI = -2\frac{C_{90}(t)C_0'(t)}{|C_0'(t)|^2} \approx \delta t \sin(-2\phi'). \tag{3}$$

The SI is large when the $C_{90}(t)$ amplitude is large and the waveform shape is similar to the time derivative of the $C_0(t)$ component, which is expected in case of shear-wave splitting due to seismic anisotropy (e.g., Silver & Chan, 1991; Vinnik et al., 1989a, 1989b). Because *KS (e.g., PKS, SKS, SKKS or S3KS; see Figure 3) waves are radially polarized upon exiting the core due to the P-to-SV conversion at the CMB, C_0 in this case corresponds to the radial component. On the other hand, for those S_{diff} waves that are almost perfectly SH-polarized, C_0 can be

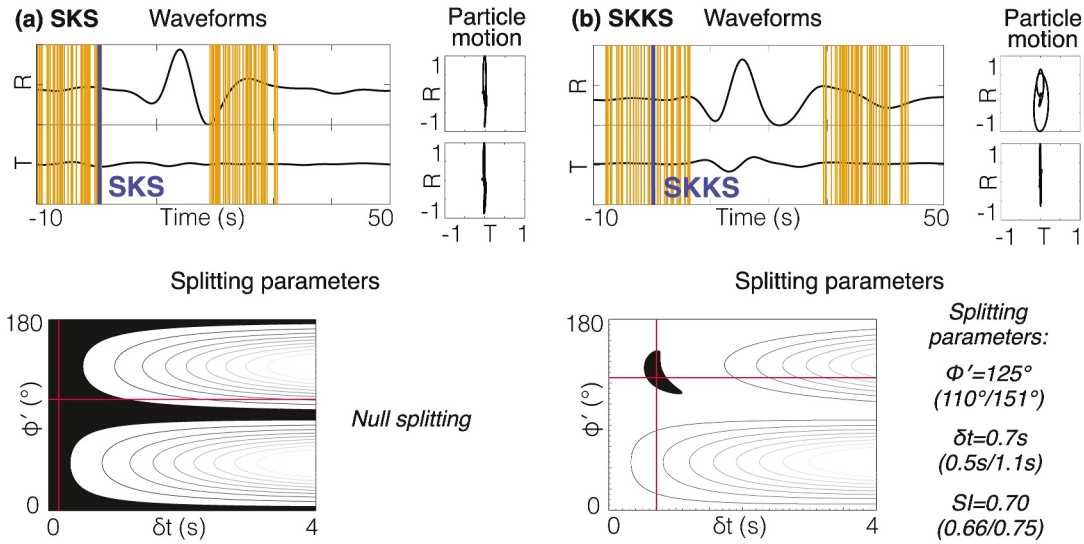

Figure 4. Example of differential SKS-SKKS splitting. Measurements were originally published in Wolf and Long (2022), for stacked seismograms across stations in the northwestern United States. (a) Top left: SKS radial (R) and transverse (T) component waveforms. Blue line indicates expected arrival time of SKS phase. Orange lines indicate the start and end of 50 randomly selected measurement windows for the splitting measurements (Reiss & Rümpker, 2017). Top right: Particle motion before (top) and after (bottom) correcting for the best-fitting splitting parameters. Bottom: Best-fitting splitting parameters in the ϕ'-δt-plane. Black region indicates 95% confidence interval for the splitting measurement (with contour lines showing different transverse energy component levels). The red cross indicates the best-fitting combination of (ϕ', δt). SKS splitting is null. Panel (b) same as panel (a) for SKKS. The values of the best-fitting splitting parameters (ϕ', δt; *splitting intensity*) and their 95% confidence intervals are shown at the bottom.

assumed to correspond to the transverse component. For other shear phases, such as direct S, the direction of $C_0(t)$ is controlled by the focal mechanism of the earthquake. For many anisotropy applications, it is helpful that SI is commutative as long as the assumption $\omega t \ll 1$ is valid. This means that SI values accumulated by a wave traveling through multiple anisotropic layers can simply be summed to obtain the SI after the whole raypath.

Shear-wave splitting is commonly measured from SKS and SKKS seismic waves, typically at epicentral distances from ~90° to ~120° (SKS) or ~108° to ~140° (SKKS) (Long, 2009). Studies often use a bandpass filter retaining periods between 6 and 25 s or similar. Example shear wave splitting measurements for SKS and SKKS seismograms are shown in Figure 4. For SKKS (Figure 4b), most energy arrives on the radial component, while some energy has been partitioned to the transverse component due to splitting. Therefore the particle motion (radial vs. transverse component amplitude; Figure 4b, top right) is elliptical. The best fitting splitting parameters are displayed in a two-dimensional plot showing the fast polarization direction (ϕ') against the time delay (δt; Figure 4b, bottom panel). The 95% confidence interval is shown in black. After correcting the waveforms for the best-fitting splitting parameters, the corrected particle motion is linear, as would be expected in the absence of shear wave splitting (Figure 4b, top right). For SKS recorded for the same source-receiver configuration, shear-wave splitting is null (Figure 4a). Such discrepant SKS-SKKS splitting is indicative of the presence of lowermost mantle anisotropy as further described in Section 2.3.

Splitting parameters (ϕ, δt) can be determined using different methods; examples include the transverse energy minimization (Silver & Chan, 1991; Walsh et al., 2013), the rotation correlation (Ando, 1984; Bowman & Ando, 1987) method, or transfer function inversion (Vinnik et al., 1989a, 1989b) (for a review of these methods, see Long and Silver (2009)). Freely available software packages to measure splitting parameters from seismograms include SplitLab (Fröhlich et al., 2022; Wüstefeld et al., 2008), SplitRacer (Link et al., 2022; Reiss & Rümpker, 2017) and SWSPy (Hudson et al., 2023).

2.2. Differential SV-SH Travel Times

Early studies that characterized seismic anisotropy in the deep mantle relied on the measurement of differential travel times of SV- and SH-polarized waves. These focused on direct S waves that turn in D″ (e.g., S. R. Ford

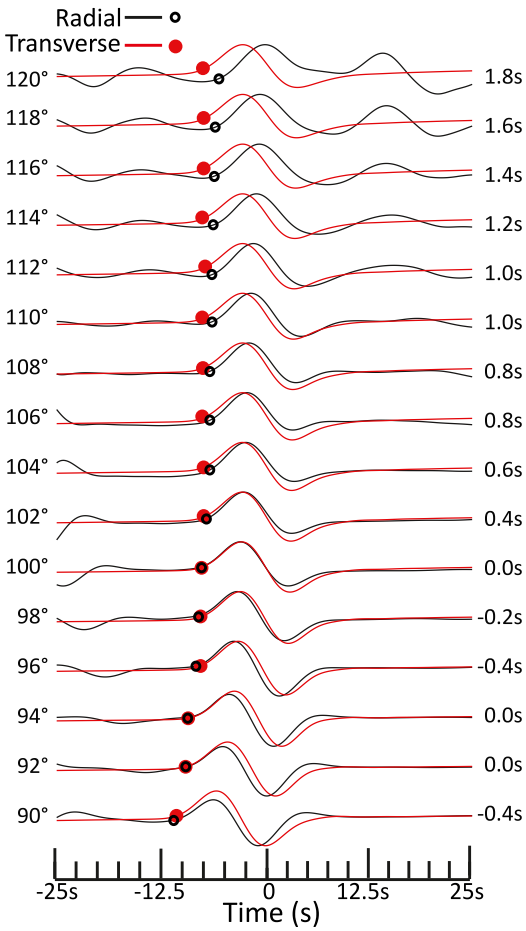

Figure 5. Self-normalized displacement radial (black) and transverse (red) component S and S_{diff} waveforms as a function of distance (left). The waveforms were computed for the IASP91 (Kennett & Engdahl, 1991) model using full-wave simulations. Apparent differences in relative SV-SH arrival times can be measured at some distances (values listed at right). Modified from Parisi et al. (2018).

et al., 2006; Fouch et al., 2001; Kendall & Silver, 1996; Pulliam & Sen, 1998), ScS waves (e.g., Garnero, Maupin, et al., 2004; Matzel et al., 1996; Rokosky et al., 2006; Russell et al., 1998, 1999), and S_{diff} waves (e.g., Lay & Young, 1991; Ritsema, Lay, et al., 1998; Vinnik et al., 1989a, 1989b) (Figure 2a). Differential travel times of 5 s or more have been measured between SV- and SH-polarized shear waves (e.g., Garnero & Lay, 1997; Kendall & Silver, 1996; Wysession et al., 1999), too large to be solely explained by anisotropic structure in the upper mantle. Furthermore, some studies showed that for deeper waves turning in the lowermost mantle, the longer the D′′ path, the larger their accumulated SV-SH time delay times (e.g., Garnero & Lay, 1997; Matzel et al., 1996). Other studies argued that S_{diff} could be expected to be fully SH-polarized for distances >110° irrespective of focal mechanism, and that therefore SV energy arriving with a time shift relative to SH (Equation 2) at larger distances must be due to seismic anisotropy (e.g., Vinnik et al., 1995). However, a strongly negative vertical shear velocity gradient can result in SV_{diff} propagating to large distances; therefore, this argument requires knowledge of the velocity-depth profile, which is usually not precisely known (e.g., Lay & Helmberger, 1983; Ritsema et al., 1997; Ritsema, Ni, et al., 1998). Most studies using these strategies have reported faster velocities for seismic waves polarized in D′′ in the horizontal plane (V_{SH}) than in the vertical plane (V_{SV}) (e.g., Ding & Helmberger, 1997; Fouch et al., 2001; Lay & Young, 1991; Ritsema, 2000; Rokosky et al., 2004; Usui et al., 2008), while the opposite was measured more rarely (e.g., Fouch et al., 2001; Pulliam & Sen, 1998). Using such a strategy, the presence of deep mantle anisotropy was suggested, among other places, in multiple regions beneath the Pacific Ocean, Alaska, the Caribbean and Siberia (Figure 3a; see also compilation by Wolf, Long, Li, and Garnero (2023)).

Komatitsch et al. (2010) suggested that differential travel times of SV- and SH-polarized waves could alternatively be explained by isotropic structure; they successfully reproduced relatively large SV-SH delay times in isotropic input velocity models using global wavefield simulations. Figure 5 shows the results from such a numerical experiment conducted by Komatitsch et al. (2010) and reproduced by Parisi et al. (2018), showing the accumulation of differential SV-SH travel times as a function of distance for an equatorial raypath using the IASP91 (Kennett & Engdahl, 1991) velocity model. This figure illustrates that SV_{diff} interacts differently with lowermost mantle structure and the CMB than SH_{diff}. Some SV_{diff} energy is transmitted into the core and becomes SKS. Some refracts above the CMB, which can lead to complicated waveforms and additional arrivals, such as those visible in Figure 5 at larger distances. Later studies added to these findings; for example, by investigating the influence of attenuation (Borgeaud et al., 2016) on SV-SH delay times and by testing the effects of more realistic 3D tomography models (Parisi et al., 2018). Taken together, these studies (Borgeaud et al., 2016; Komatitsch et al., 2010; Parisi et al., 2018) show that SV-SH delay times of 5 s can be explained by isotropic effects, while larger delay times may also be possible for specific configurations. Therefore, it is unclear how uniquely diagnostic differential SV-SH times are as an indicator of deep mantle anisotropy in Earth. Thus, when interpreting differential SV-SH travel times as being indicative of seismic anisotropy, the possibility of isotropic effects should be fully explored, and/or other seismic phases should be used to obtain independent constraints on D′′ anisotropy.

2.3. *KS Differential Splitting

When splitting parameters differ substantially for two or more *KS phases (Figure 3c) for the same source-receiver configuration, it is often interpreted as evidence of deep mantle anisotropy (e.g., Niu & Perez, 2004). The reason is that the mantle raypaths of different *KS phases are very similar in the upper

mantle, while their sampling volumes and propagation directions are substantially different in the lowermost mantle (Figure 3c). Therefore, large differences in shear wave splitting between two *KS phases most likely reflect a contribution from deep mantle anisotropy. Differential SKS-SKKS splitting is most commonly measured (e.g., Asplet et al., 2020; Creasy et al., 2017; Long, 2009; Lynner & Long, 2014; Niu & Perez, 2004; Reiss et al., 2019; Wang & Wen, 2004; Wolf et al., 2019), but differential splitting of PKS-SKS (e.g., Creasy et al., 2021) and SKS-SKKS-S3KS (Wolf, Frost, et al., 2023) has also been observed. The *KS differential splitting technique is one of the most commonly used techniques and has been applied in many regions worldwide. Regions in which deep mantle anisotropy has been suggested using differential *KS splitting include D′′ beneath western Africa, the northeastern Pacific Ocean, the Caribbean, Iceland, Siberia and central Asia (Figure 3c).

The validity of the *KS differential splitting technique for identifying lowermost mantle anisotropy has recently been investigated using global wavefield simulations (Tesoniero et al., 2020; Wolf et al., 2022a). The method has been shown to generally be able to constrain D′′ anisotropy if certain best practices are followed. First, only relatively large *SI* (>0.4) differences between phases should be regarded as evidence for deep mantle anisotropy, since minor differences in splitting can also be due to upper mantle anisotropy (Y. Lin et al., 2014; Tesoniero et al., 2020). Second, we recommend only using those measurements for which all phases show *SI*-values <1. For larger values, the commutativity of the SI, which is implicitly assumed, is not guaranteed (Wolf et al., 2022a). Third, it has been shown that high levels of noise for one or more phases can influence the accuracy of *KS differential splitting measurements. Therefore, it is a good practice to ensure that the signal-to-noise ratios (SNRs) of the phases under study are high enough to ensure reliable results (e.g., Wolf, Frost, et al., 2023). Most studies therefore use SNRs larger than 2 (e.g., Reiss et al., 2019; Wolf & Long, 2022).

If the aforementioned best practices are followed, the *KS differential splitting technique reliably identifies D′′ anisotropy. However, the interpretation of these results is not always straightforward. A lack of differential *KS splitting (also called nondiscrepant) can either mean that the lowermost mantle is isotropic, that the phases under study are split similarly in D′′, or that one or both phases is sampling D′′ anisotropy but is polarized along the null splitting direction. In the absence of additional constraints, no specific determinations can be made. On the other hand, if splitting between *KS phases is discrepant, this usually indicates that at least one of the phases under study, but potentially all of them, sample D′′ anisotropy (e.g., Tesoniero et al., 2020). To investigate whether a particular phase samples deep mantle anisotropy, more information is needed; for example, using a second D′′ splitting method in addition to *KS differential splitting, or carrying out a careful study of the upper mantle splitting contribution beneath the station(s).

2.4. Differential Splitting of S and ScS Waves

Wookey, Kendall, and Rümpker (2005) suggested that the lowermost mantle anisotropy contribution to ScS can be isolated if the upper mantle anisotropy beneath the station and the source are known (or inferred). They proposed that the upper mantle anisotropy beneath the receiver can be determined via SKS splitting measurements over a range of backazimuths, which mostly reflects the upper mantle contribution (e.g., Long & Silver, 2009). They further argued that the source-side anisotropy contribution to S and ScS—that is, the contribution to splitting from anisotropy close to the earthquake—will be similar for a given source-receiver pair at epicentral distances larger than 60°, while S and ScS will be sufficiently separated in time to measure shear-wave splitting of both phases up to 85°. Therefore, the direct S phase can be used to estimate splitting due to source-side anisotropy, and its effect on the corresponding ScS phase can be explicitly corrected for. Then, if the ScS wave is split after explicitly correcting for receiver- and source-side anisotropy, it is likely due to the presence of D′′ anisotropy. Here, we refer to this procedure as S-ScS differential splitting. Since its invention, the S-ScS differential splitting technique has become increasingly frequently used (e.g., Asplet et al., 2023; Creasy et al., 2017; Nowacki et al., 2010; Pisconti et al., 2023; Rao et al., 2017; Wookey & Kendall, 2008) and has been applied to many regions across the globe, for example, the western edge of the African LLVP, the Caribbean, the western United States and Siberia (Figure 3d). Seismic anisotropy measured using this technique has been associated with slab-driven flow beneath the Caribbean (e.g., Nowacki et al., 2010) and upwelling flow at the base of plumes in the deep mantle beneath Afar and Iceland (e.g., H. A. Ford et al., 2015; Wolf et al., 2019).

Interpretations and measurements of S-ScS differential splitting have been increasingly advanced over time. The initial S-ScS differential splitting technique assumed a near-horizontal raypath of ScS through D″ (Wookey et al., 2005). This assumption was later found to be oversimplified (Nowacki & Wookey, 2016). Moreover, it has been demonstrated that applying the traditional source-side correction may often lead to apparent D″ splitting even in the absence of D″ anisotropy, unless S and ScS are initially perfectly SH-polarized (Wolf et al., 2022a). Although the phase shift that the radial (SV) component undergoes upon the CMB reflection can be explicitly taken into account, and a correction applied (Wolf et al., 2022a), such explicit corrections may lead to inaccurate results in practice (Wolf & Long, 2024).

Therefore, to obtain trustworthy anisotropy results, the best approach to differential S-ScS splitting measurements appears to entirely avoid explicit anisotropy corrections. This is possible if seismic anisotropy is only measured for seismograms recorded at null stations (i.e., stations that overlie apparently isotropic upper mantle, e.g., Lynner & Long, 2013), for which the S phase is unsplit (Wolf & Long, 2024). Furthermore, the S-ScS differential splitting technique should not be applied for epicentral distances <60°. The primary reason is that at smaller distances, radial/transverse component amplitude ratios of ScS will be strongly affected by the CMB reflection, thereby potentially introducing apparent splitting (Wolf et al., 2022a). Furthermore, the assumption that S and ScS raypaths on the source side are sufficiently similar may break down for distances <60°. Wolf and Long (2024) showed that complex phase interferences lead to ScS polarizations that are difficult to predict for epicentral distances larger than 70°, and therefore suggested to limit the use of the S-ScS differential splitting technique to distances between 60° and 70°.

Since the ScS raypath in D″ is not horizontal (e.g., Nowacki & Wookey, 2016), with an angle to the horizontal of approximately 15° for an epicentral distance between 60° and 70°, the measured splitting is a combination of splitting from both the downgoing and upgoing legs of ScS in D″. Therefore, even in the case of a homogeneously anisotropic deep mantle region sampled from a single azimuth by multiple ScS waves with different source polarizations (in absence of upper mantle anisotropy), different apparent fast polarization directions are produced (Silver & Savage, 1994). Thus, it is crucial to both avoid the assumption of horizontal ScS raypaths and explicitly consider the initial polarization of the ScS waves to obtain reliable results. A recently developed approach that overcomes these challenges involves direct waveform inversions of S-ScS splitting (Asplet et al., 2023), using only waveforms that are (mostly) radially initially polarized; more details about this approach are discussed in Section 2.7.2.

2.5. S_{diff}^{pol} Splitting Measurement

As described in Section 2.2, deep mantle seismic anisotropy has been inferred from S_{diff} waves by analyzing differential SV-SH travel times. In light of the challenges with this method, strategies to measure deep mantle anisotropy from S_{diff} have been adjusted over time. Cottaar and Romanowicz (2013) were the first to argue, using global wave simulations, that the S_{diff} waves used in their study would be expected to be almost perfectly SH-polarized in the absence of seismic anisotropy. Such an approach avoids general arguments about how SV_{diff} amplitudes relative to SH_{diff} decrease as a function of distance, which have been shown to be problematic (e.g., Komatitsch et al., 2010; Ritsema et al., 1997). This idea was then expanded and tested in detail by Wolf, Long, Creasy, and Garnero (2023). In the following, we refer to this strategy, which explicitly considers the initial polarization of S_{diff}, as S_{diff}^{pol} splitting. S_{diff}^{pol} splitting measurements have been applied in multiple regions (Figure 3f), including the southern edge of the African LLVP, providing evidence for upwelling mantle flow (Cottaar & Romanowicz, 2013), and beneath the central and northeastern Pacific Ocean, indicating likely slab-driven mantle dynamics (Wolf & Long, 2022) (Figure 3e).

There are multiple best practices that should be considered when applying S_{diff}^{pol} splitting measurements. First, one must ensure (preferably via global wavefield simulations) that S_{diff} would be expected to be almost perfectly SH-polarized in absence of deep mantle anisotropy for the source-receiver configuration under study. Second, a substantial influence of source-side anisotropy should be excluded. Third, receiver-side upper mantle anisotropy should be thoroughly understood and accounted for (e.g., by comparison to S recorded at different distances). Receiver-side upper mantle anisotropy can, for example, be analyzed through SKS splitting over a large range of backazimuths, as is often done in S-ScS differential studies. Fourth, splitting can be measured using traditional techniques that determine δt, ϕ, and SI. We refer the reader to Wolf, Long, Creasy, and Garnero (2023) for additional details on this method.

Detailed testing of the S_{diff}^{pol} splitting technique has revealed some challenges. One challenge is the requirement for S_{diff} to be almost perfectly SH-polarized in absence of seismic anisotropy. In an analysis by Wolf and Long (2023), this requirement was only met by one out of ~20 events for the azimuth range under study. Another challenge is the interpretation of the split SH_{diff} waves: S_{diff} has a long raypath through D″, along which it can accumulate splitting. Without any additional constraints, it is difficult to determine where splitting occurs for a single measurement. A challenge for determining where seismic anisotropy is located is the large finite frequency sensitivity kernel for S_{diff} in the deep mantle (e.g., Zhao & Jordan, 2006). There are general strategies for managing these limitations: if upper mantle anisotropy is known, S_{diff} can be investigated as a function of distance in record sections of data from large and dense arrays of seismic stations (e.g., Vinnik et al., 1998a, 1998b; Wolf & Long, 2022), so that the approximate location of deep mantle anisotropy can be determined. Alternatively, splitting can be measured from a crossing azimuth or using an additional method with a better lateral resolution (e.g., *KS differential splitting).

The S_{diff}^{pol} splitting technique framework is consistent with previous work showing that differential SH_{diff}-SV_{diff} travel times can be accumulated in an isotropic Earth (Borgeaud et al., 2016; Komatitsch et al., 2010; Parisi et al., 2018). The reason for this is that a substantial energy redistribution of SH to SV energy, as measured in the S_{diff}^{pol} technique, cannot be easily explained by isotropic structure. Additionally, if SV_{diff} amplitudes are analyzed across seismic arrays, splitting can be measured at the distance at which it occurs first, such that no substantial δt between SH_{diff} and SV_{diff} can be potentially acquired due to isotropic structure after sampling the anisotropy (Wolf, Long, Creasy, & Garnero, 2023). Additionally, the splitting strategy requires the measurement of splitting parameters (ϕ, δt, SI), which entails waveform shape requirements (Section 2.1), and not simply the measurement of SV-SH differential travel times. There is good global coverage of the CMB using S_{diff} phases from existing data (e.g., H. Lai & Garnero, 2020). Therefore, going forward, we can envision a global inversion of S_{diff} data to obtain a global model of D″ anisotropy. We will discuss the global ray-coverage of different seismic phases, including S_{diff}, in detail in Section 5.1.4.

2.6. Polarity and Amplitude Measurements

The presence of seismic anisotropy has been inferred from anomalous polarities of S waves grazing D″ (Garnero, Maupin, et al., 2004; Maupin et al., 2005). In these studies polarity reversals were modeled as indicating seismic anisotropy with a tilted axis of symmetry (relative to the vertical direction). More recent work on seismic wave polarities has used P and S waves that reflect off the top of D″, often called SdS and PdP (Figure 3b), using array processing techniques such as beamforming to detect these subtle signals (e.g., Pisconti et al., 2019; Pisconti et al., 2023). While, in theory, directional amplitude variations of D″ reflections are indicative of the anisotropy of the reflecting interface, in practice it is challenging to measure subtle directional amplitude changes (e.g., Thomas et al., 2011). Therefore, rather than focusing on directional variations of reflection amplitudes, D″ reflection polarities are sometimes used to analyze seismic anisotropy. The reflection polarities are compared to polarities from other seismic phases such as P/S and PcP/ScS. Such reflection polarity measurements can be ideally used as a complementary constraint along with splitting data (e.g., Creasy et al., 2019; Pisconti et al., 2019, 2023) rather than being interpreted as uniquely indicative of deep mantle anisotropy.

Several best practices have been formulated for the application of polarity measurements to infer deep mantle anisotropy (Pisconti et al., 2019, 2023; Thomas et al., 2011). First, it is important to ensure that the observed reflections in fact occur along the great-circle path and not out-of-plane, since they may otherwise be associated with a different anisotropic region than that under study (e.g., Pisconti et al., 2019, 2023). Second, SdS and PdP polarity measurements are often compared to the polarity of S/ScS and P/PcP. For such comparisons, the source mechanism must be considered because polarity reversals may also be caused by the focal mechanism (e.g., Thomas et al., 2011). Third, variations in SdS/PdP amplitudes can be caused by different factors (e.g., attenuation or scattering), such that amplitude variations as a function of azimuth should not be interpreted as necessarily being indicative of D″ anisotropy. SdS and PdP polarity measurements are often used as an additional constraint alongside with another method (i.e., shear-wave splitting analysis) to detect deep mantle anisotropy (e.g., Creasy et al., 2019, 2021; Pisconti et al., 2019, 2023). In this process, it is assumed that the wave in fact reflects off the same anisotropic layer to which the complementary method is sensitive. Moreover, the reflection interface is often assumed to be horizontal with no topography (e.g., Pisconti et al., 2019, 2023). Future studies that use full-

wave simulations to test various effects on SdS and PdP reflections, such as heterogeneity and reflector topography, are desirable.

2.7. Anisotropy From Waveform Inversions

2.7.1. Regional Inversions for Lowermost Mantle Anisotropy

When seismic waves sample anisotropy, their waveforms and horizontal component amplitude ratios change. Therefore, seismic waveforms can be inverted for anisotropic structure. For the deep mantle, ScS waves (Asplet et al., 2023) or the time-window around them (Kawai & Geller, 2010; Suzuki et al., 2021) are often used, due to their long raypath through D′′. Such inversions sometimes include prior knowledge of candidate elastic tensors of seismic anisotropy. In this case, the elastic tensor orientation and a strength parameter can be inverted for, focusing on one or multiple seismic phases (e.g., Asplet et al., 2023). Alternatively, a simplified radial geometry of deep mantle anisotropy can be assumed, investigating a chosen seismogram time window. In this case, a large number of waveforms can be used to invert for radially anisotropic structure (e.g., Kawai & Geller, 2010).

Inversions of ScS waveforms have revealed seismic anisotropy and likely directions of mantle flow beneath the northeastern Pacific Ocean (Asplet et al., 2023). Through studies that used the whole seismic waveform around the S and ScS arrivals (including triplicated phases, for example D′′ reflections), a detailed map of radial anisotropy in D′′ has been obtained for the central (Kawai & Geller, 2010) and the northern (Suzuki et al., 2021) Pacific Ocean. For the deep mantle beneath the central Pacific Ocean, the observation of $V_{SV} > V_{SH}$ was interpreted as evidence for upwelling flow at the edge of the Pacific LLVP (Kawai & Geller, 2010), while the seismic anisotropy found beneath the northern Pacific Ocean was used to infer the mineralogical composition in that region (Suzuki et al., 2021).

Inversions for localized radially anisotropic structure in the deep mantle (Kawai & Geller, 2010; Suzuki et al., 2021) are a powerful tool to map lateral and depth variations in anisotropic structure. Typical shear-wave splitting methods are often not able to resolve such variations, because the splitting of a single waveform reflects the integrated anisotropic contribution along the whole raypath. While this is also true for single waveforms used in anisotropic inversions, these inversions can generally resolve lateral and depth variations in seismic anisotropy better because they use the full waveform and a large number of seismograms (Kawai & Geller, 2010; Suzuki et al., 2021). So far, however, local anisotropic inversions for the deep mantle have only been applied to map radial anisotropy and have not considered complicated geometries of anisotropy. Therefore, direct comparison to splitting measurements is challenging, although splitting measurements and results from anisotropic inversions have been shown to be compatible with each other in some cases (e.g., Kawai & Geller, 2010; Wolf & Long, 2023).

2.7.2. Global Anisotropic Inversions

For global studies, horizontal component travel times are often used, often in combination with other types of data, to invert for radially symmetric anisotropy in the deep mantle, sometimes also using relative travel times between different seismic phases (e.g., Chang et al., 2015; Moulik & Ekström, 2014). Seismic phases for such inversions include, for example, S, SS, ScS, S_{diff}, SKS, SKKS and their corresponding depth phases (e.g., Chang et al., 2015; Moulik & Ekström, 2014). As an alternative to travel-time tomography, full-waveform inversion techniques have been used (e.g., French & Romanowicz, 2014; Panning & Romanowicz, 2006). Global tomography models of radial anisotropy are well-suited to resolve features with wavelengths of 1,000's of kilometers, while variations of D′′ anisotropy on scales smaller than this are often characterized using regionally focused techniques.

Multiple global models of radial anisotropy have been published (e.g., Auer et al., 2014; Chang et al., 2015; French & Romanowicz, 2014; Kustowski et al., 2008; Moulik & Ekström, 2014; Panning et al., 2010; Panning & Romanowicz, 2020), two of which are displayed in Figure 6. While the smaller scale details of these models differ, they all show the same general pattern of $V_{SV} > V_{SH}$ (faster velocities of vertically than horizontally polarized shear waves) within LLVPs and $V_{SH} > V_{SV}$ outside of them (Figure 6). These patterns are generally consistent with early findings of D′′ anisotropy studies (Fouch et al., 2001; Kendall & Silver, 1996; Lay & Helmberger, 1983; Lay & Young, 1991; Pulliam & Sen, 1998; Ritsema, Lay, et al., 1998; Rokosky et al., 2006;

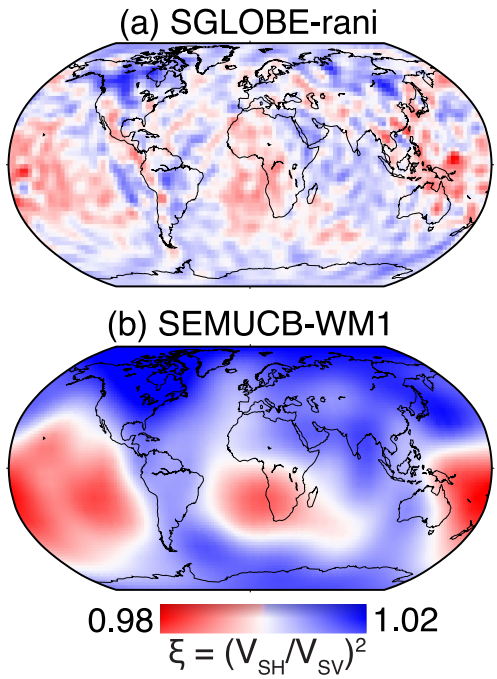

Figure 6. Radial anisotropy ζ (see legend) at a depth of 2,700 km for the two models SGLOBE-rani (a; Chang et al., 2015) and SEMUCB-WM1 (b; French & Romanowicz, 2014).

Russell et al., 1998; Vinnik et al., 1995). However, it has been demonstrated that tradeoffs between isotropic and anisotropic structures exist when inverting for radial anisotropy in the deep mantle (Chang et al., 2014; Kustowski et al., 2008), which is why the smaller-scale patterns in radially anisotropic tomography models may not be reliable to interpret. While the overall pattern is consistent, its interpretation in terms of flow at the base of the mantle is unclear (e.g., Karato, 1998; Yamazaki & Karato, 2007), as further discussed in Section 4.3.

Overall, global radially anisotropic tomography models give a valuable indication of the large-scale patterns of seismic anisotropy. However, due to the fact that only large scale features can be reliably resolved, they are generally difficult to compare to local shear wave splitting studies. Also, their simplified radially anisotropic parameterization makes comparisons with local shear wave splitting observations difficult. The relationship between global radially anisotropic tomography models and local shear-wave splitting studies for the lowermost mantle is somewhat analogous to surface wave inversions and shear-wave splitting for the upper mantle. While one method is able to resolve large-scale patterns globally (tomography/surface waves), the other can provide a more detailed characterization of laterally constrained anisotropy (shear wave splitting). Studies that have explicitly sought to reconcile surface wave and shear-wave splitting observations of upper mantle anisotropy have been fruitful (e.g., Becker & Lebedev, 2021; Becker et al., 2012; Wüstefeld et al., 2009). Similar work applied to lowermost mantle anisotropy would also be helpful.

2.8. Techniques to Map D″ Anisotropy: Possible Future Directions

Shear wave splitting techniques applied to the study of D″ anisotropy have been tested extensively over the last one and a half decades. If the caveats mentioned above are considered, *KS differential splitting, S-ScS differential splitting, local anisotropic tomography, and S_{diff}^{pol} splitting are all promising techniques for future use. Also, the implementation of global S_{diff} waveform inversions to obtain a picture of D″ anisotropy appears to have a great potential. The use of polarity measurements along with splitting measurements to obtain tighter constraints on deep mantle anisotropy is auspicious; however, the potential pitfalls should be explored in detail using global wavefield simulations. Uncertainties from differential SV-SH travel times as indicators of D″ anisotropy will be greatly reduced by implementing global wavefield simulations for realistic mantle models at the relevant periods to show that observed waveform effects cannot be explained by isotropic D″ structure. Global maps of radial anisotropy, with increasing computing power, will be able to move toward imaging smaller structures with time. The application of array techniques such as beamforming in the study of lowermost mantle anisotropy also holds promise. It has been shown that the splitting of stacked or beamformed data reflects an average of the splitting contributing to the single-station seismograms, and beamforming often leads to higher SNRs and more robust splitting measurements (Frost et al., 2024; Wolf, Frost, et al., 2023). Therefore, when dense seismic arrays are available, it may be helpful to apply the commonly used shear wave splitting techniques to stacked or beamformed data instead of single-station seismograms. This way, the number of seismic phases and distances ranges suitable for shear wave splitting measurements for different seismic phases will be increased (Figure 7; for more details see Section 5.1.4).

3. Causes of Deep Mantle Anisotropy

Observations of deep mantle anisotropy are usually interpreted as being caused by one of two different anisotropy-producing mechanisms: SPO and CPO. In the deep Earth, materials may have elastic properties significantly different from the surrounding matrix. If their shapes are directionally oriented, causing SPO, then seismic waves can travel faster in certain directions than in others (Figure 8). CPO, on the other hand, is caused by the preferential alignment of individual crystals in an aggregate (Figure 8) due to deformation from convective

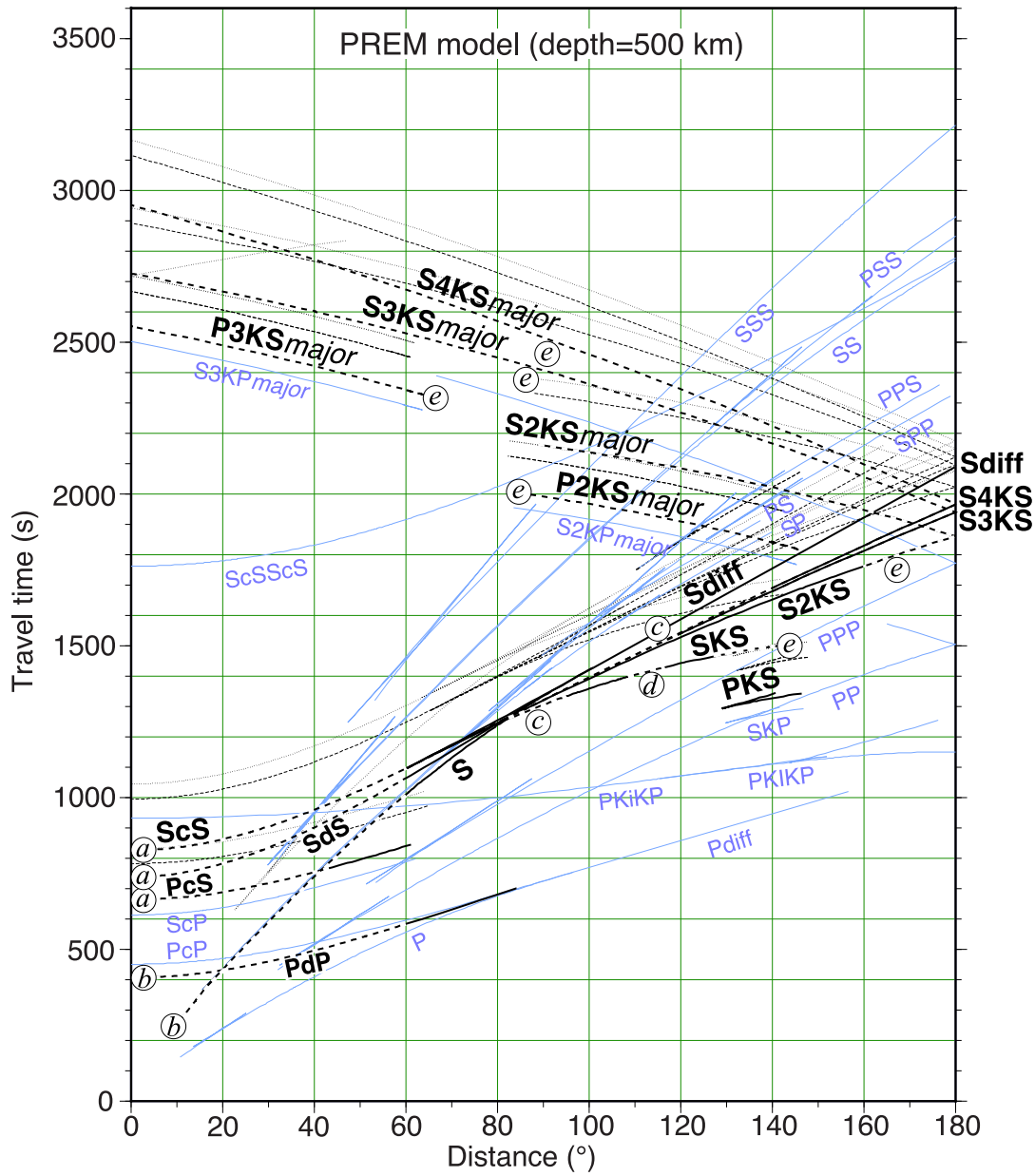

Figure 7. Body wave travel time curve, highlighting seismic phases that do (black) or do not (blue) hold promise for inferring lowermost mantle anisotropy. Curves were calculated for an earthquake depth of 500 km using the PREM velocity model (Dziewonski & Anderson, 1981). *Major* labels indicate major arc phases. Thin dashed and dotted lines show depth phases, but are only displayed for waves that have been used to infer seismic anisotropy. ⓐ Seismic waves are usually not used to map D″ anisotropy at low distances because of wave interference, for example, from surface waves. ⓑ D″-reflected waves are usually not visible at low distances due to low reflection coefficients. ⓒ Potential interference of S or SmKS waves. ⓓ Potential waveform complications due to SPdKS (e.g., Thorne et al., 2021). ⓔ Low wave amplitudes due to large epicentral distance.

flow in the deep mantle. Here we discuss how these two mechanisms can potentially explain observations of seismic anisotropy in D″.

3.1. Shape-Preferred Orientation

D″ is located just above the CMB, which marks the largest density and temperature contrast within Earth (e.g., Davies et al., 2015; Mundl-Petermeier, 2021). Over the course of Earth's history, the deep mantle has likely

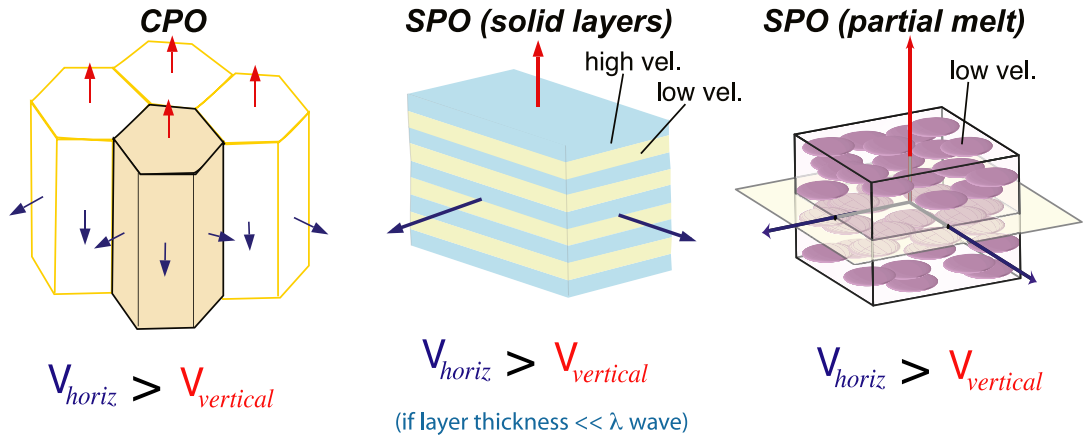

Figure 8. Schematic illustrations of crystallographic-preferred orientation (CPO) and shape-preferred orientation (SPO) leading to $V_{SH} > V_{SV}$ (after Moore et al. (2004)). Left: CPO of preferentially oriented minerals. Middle: SPO caused by layering of solid materials (yellow and green) with contrasting seismic velocities. Right: SPO caused by pockets of melt (violet).

become a storehouse for significant chemical heterogeneity, potentially including previously subducted materials (e.g., Andrault et al., 2014; Christensen & Hofmann, 1994; Hirose et al., 1999; Li, 2021, 2023b; Nakagawa et al., 2010; Tackley, 2011), remnants of the crystallizing of magma ocean (Labrosse et al., 2008), remnants of the Moon-forming impactor (Yuan et al., 2023), and products of CMB reaction (e.g., Kellogg, 1997; Ko et al., 2022; Manga & Jeanloz, 1996; Otsuka & Karato, 2012). For example, the LLVPs and the ULVZs may be formed by these chemical heterogeneities (e.g., see review by McNamara, 2019). In fact, D′′ is the only layer in Earth that seems to exhibit a similar degree of wavespeed heterogeneity as the lithosphere (e.g., Tkalčić et al., 2015). If deformed due to convective stresses, elastically distinct heterogeneities can become elongated, potentially causing seismic anisotropy if the contrast in elastic properties with the surrounding matrix is large enough. In places where flow and shearing of the deep mantle are horizontal, horizontally laminated structures can lead to faster velocities of horizontally than vertically polarized waves, while vertical velocities would be faster in the case of vertical shearing (e.g., Backus, 1962; Kendall & Silver, 1998).

Backus (1962) demonstrated that alternating layers with contrasting properties (Figure 8), much thinner than the seismic wavelength, can produce transverse isotropy (anisotropy that is symmetric about an axis, isotropy in the perpendicular plane). The stronger the contrast, the larger the effective seismic anisotropy becomes (Moore et al., 2004). There are several candidates to produce such thin layering, including stretched and elongated filaments of deeply subducted former oceanic crust, thin lenses of Ppv (e.g., in regions in which Br transforms to Ppv with depth and then transforms back to Br closer to the CMB), partial melt of some deep mantle component, or even compositionally distinct LLVP material that has been upwardly entrained and then recirculated back into the deep mantle in whole mantle convection. Of these (and other plausible) mechanisms, partially molten material possesses the strongest elastic contrast with the surrounding mantle, and is thus one viable scenario for strong shear-wave splitting due to SPO. Partial melts are weak and easy to shear (e.g., Kendall & Silver, 1998), thereby causing SPO. However, it is still debated whether enough partial melt is present in the lowermost mantle to cause SPO-induced anisotropy, partially because the wetting behavior of such melts at the CMB is unknown (e.g., Karato, 2014).

3.2. Crystallographic-Preferred Orientation

Deformation via propagation of dislocations through the crystal lattice (dislocation creep) can cause the preferential alignment of minerals (CPO; Figure 8), likely a main cause of D′′ anisotropy (e.g., Murakami et al., 2004; Nowacki et al., 2011; Romanowicz & Wenk, 2017; Wookey, Stackhouse, et al., 2005). However, the mechanism (s) causing CPO in D′′ are only partially understood. The most abundant mineral in the lowermost mantle is likely Br and/or its high-pressure polymorph Ppv, while Fp is less abundant (e.g., Irifune & Tsuchiya, 2007; Trønnes, 2010). Although Fp is not the dominant mineral in D′′, its strong single-crystal anisotropy at lowermost mantle pressures means that it may contribute significantly to anisotropy (e.g., Long et al., 2006; Yamazaki &

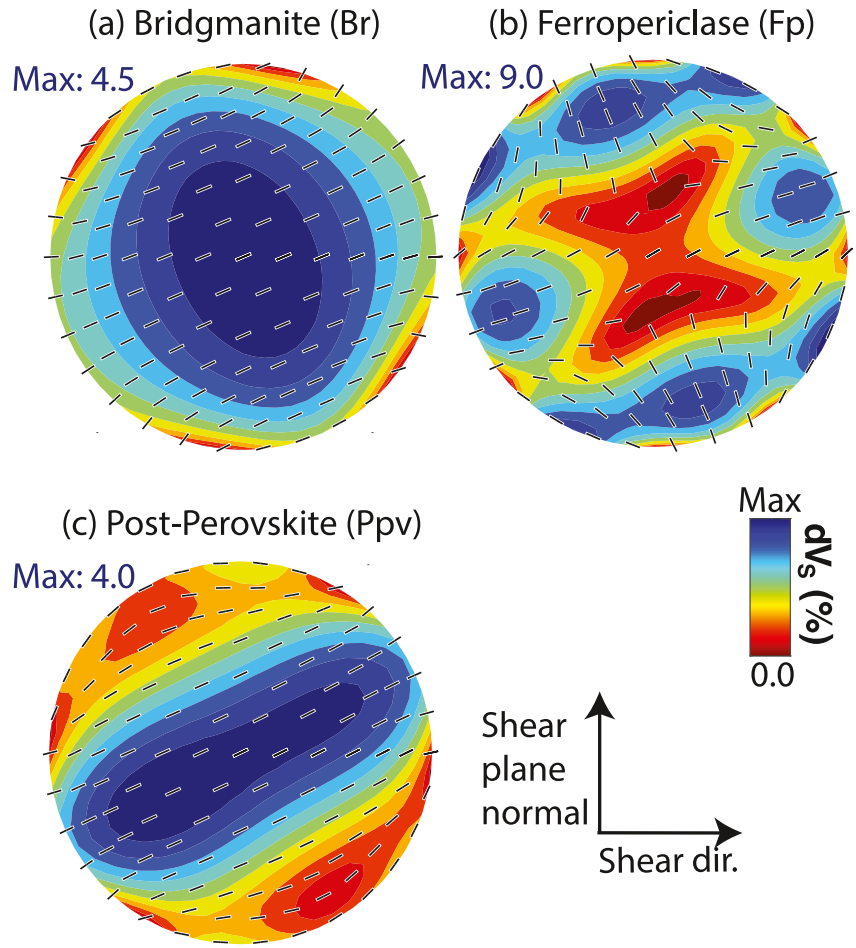

Figure 9. Upper hemisphere representations of seismic wave behavior predicted for example, elastic tensors for (a) Br, based on single-crystal results from Wookey, Stackhouse, et al. (2005) (pressure = 126 GPa, temperature = 2,800 K); (b) Fp, based on Karki et al. (1999) (pressure = 135 GPa, temperature = 3,000 K) and (c) Ppv, based on Stackhouse et al. (2005) (pressure = 136 GPa, temperature = 3,000 K). All elastic tensors are from Creasy et al. (2020). Colors represent the difference in wave speed of the fast and the slow traveling wave in percent (see legend) as a function of propagation direction. Fast polarization directions are indicated by small black sticks. The shear plane orientation and shear direction are indicated in the legend.

Karato, 2002; Yamazaki & Karato, 2007). Whether Br or Ppv dominates in any particular region depends strongly on temperature and composition, and the stability of Ppv in the lower mantle is still a subject of active research (e.g., Koelemeijer et al., 2018; Murakami et al., 2004; Romanowicz & Wenk, 2017; Yamazaki & Karato, 2007). The response of materials to deformation, via the formation of CPO, controls how seismic velocities will vary with the propagation direction through the material. The (anisotropic) elasticity can be described via a fourth-rank tensor with 21 independent components, called the elastic tensor. For a thorough mathematical description of the elastic tensor we refer the reader to Backus (1970), Browaeys and Chevrot (2004), and Nowacki et al. (2011). Different potential single-crystal elastic tensors and dominant slip systems have been proposed for relevant minerals (Br, Fp, Ppv) at lowermost mantle conditions, as summarized by Nowacki et al. (2011) and Romanowicz and Wenk (2017). These elastic tensors can be visualized as stereographic plots (Figure 9) that show the strength of seismic anisotropy, defined as the difference in slow and fast seismic shear wavespeeds, and the polarization direction of the fast traveling wave as a function of propagation direction through the material.

3.3. Discriminating Among Elastic Tensors Describing Deep Mantle Anisotropy

SPO in the lowermost mantle can be described by an effective elastic tensor derived through effective medium theory, which assumes that inclusions with contrasting properties are much smaller than the dominant wavelength

(e.g., Kendall & Silver, 1996, 1998; Tandon & Weng, 1984). This makes it possible to compare different SPO and CPO scenarios (e.g., Asplet et al., 2023). In order to distinguish among different anisotropy scenarios (described by different elastic tensors) in the lowermost mantle, the anisotropy must be sampled from different azimuths, ideally using multiple types of seismic waves that sample the anisotropy at different incidence angles (Creasy et al., 2019).

The number of strategies that we can use to measure splitting due to lowermost mantle anisotropy has increased through recent methodological progress (Section 2). Moreover, the amount of available seismic data is growing exponentially. This makes it possible now to distinguish among different CPO anisotropy scenarios in certain well-sampled regions (e.g., Asplet et al., 2023; H. A. Ford et al., 2015; Pisconti et al., 2023). While the modeling often does not lead to unique results (e.g., Asplet et al., 2023; Creasy et al., 2017), most previous studies are consistent with Ppv anisotropy outside of the two LLVP regions (Asplet et al., 2023; Creasy et al., 2017, 2021; H. A. Ford et al., 2015; Pisconti et al., 2019, 2023; Walker et al., 2011; Wenk et al., 2011; Wolf et al., 2019; see also Romanowicz & Wenk, 2017). Aligned Ppv as a mechanism for anisotropy is also suggested by the lower than average temperatures in these regions, implying a relatively shallow Br-Ppv transition (Murakami et al., 2004).

Traditionally, mineralogical modeling of anisotropy observations has often relied on single-crystal elastic tensors from mineral physics experiments (e.g., H. A. Ford et al., 2015), which significantly overpredict anisotropy strength. Recent progress has been made on testing more realistic elastic tensors for deep Earth materials from previously suggested single-crystal elastic tensors and from knowledge of the relative strength of various slip systems obtained from experiments. A library of elastic tensors for deep Earth materials (including polyphase aggregates), predicted via numerical deformation experiments using viscoplastic self-consistent modeling (Lebensohn & Tomé, 1993) to simulate texture development, has recently been published (Creasy et al., 2020). This database can now be used routinely to conduct modeling of measured splitting parameters (e.g., Wolf & Long, 2022; Wolf, Long, & Frost, 2024).

It is important to note two significant challenges when trying to distinguish between the causes of deep mantle anisotropy using anisotropy observations. First, while we are able to distinguish between different elastic tensors describing deep mantle anisotropy from a seismological perspective, our knowledge about elastic tensors describing deep Earth minerals remains limited. Laboratory experiments at lowermost mantle temperature and pressure conditions are challenging to conduct, such that many published single-crystal elastic tensors and dominant slip systems have been obtained via extrapolation or from first-principle calculations. This makes it unclear how well they describe lowermost mantle materials in the real Earth (e.g., Romanowicz & Wenk, 2017). Second, much of the previously performed modeling to discriminate among different causes of lowermost mantle anisotropy has relied on ray-theoretical assumptions, which have significant limitations (e.g., Nowacki & Wookey, 2016; Wolf et al., 2022b). While ray-theoretical modeling is still popular due to its computational efficiency, we can now model wave propagation through arbitrary seismic anisotropy using global 3D wave propagation solvers (e.g., Cottaar & Romanowicz, 2013; Nowacki & Wookey, 2016; Tesoniero et al., 2020). AxiSEM3D (Fernando et al., 2024; Leng et al., 2016, 2019) is very efficient in this context and, therefore, frequently used (e.g., Tesoniero et al., 2020; Wolf & Long, 2022; Wolf et al., 2022a, 2022b; Wolf, Long, & Frost, 2024; Wolf, Long, Frost, & Nissen-Meyer, 2024).

4. Lowermost Mantle Convective Flow and Seismic Anisotropy

4.1. Numerical Models of Deep Mantle Flow

While seismic anisotropy is an observational measurement that reflects mantle flow, mantle flow has also been widely explored in geodynamic modeling calculations. In geodynamic models, the velocity field at a single time step can be computed by solving the conservation equations for mass and momentum:

$$(\partial u_i)_{,i} = 0, \tag{4}$$

$$-P_{,i} + \tau_{ij,i} - \delta\rho g \delta_{ir} = 0, \tag{5}$$

where ρ the density, u is the velocity, P is the dynamic pressure, $\delta\rho$ is the density anomaly, g is the gravitational acceleration, δ_{ir} is the Kroneker delta tensor with r indicating the radial direction, and τ_{ij} is the deviatoric stress tensor which is determined by a rheology equation of:

$$\tau_{ij} = \eta\left(u_{i,j} + u_{j,i} - \frac{2}{3}u_{k,k}\delta_{ij}\right) \quad (6)$$

where η is the viscosity. Comma-separated subscripts denote with respect to which variable a partial derivative is taken. The solution of Equations 4 and 5, which are governed by the density anomaly $\delta\rho$ and the viscosity field η, has been widely explored in models of mantle flow.

To calculate the mantle flow at the present-day, the density and viscosity structures need to be specified. The density structure is often derived from seismic velocity anomalies in global tomography models, often assuming a scaling relationship between the two as constrained in mineral physics experiments and calculations (e.g., Bull et al., 2010; Hager, 1984; Hager & Richards, 1989; Li et al., 2024; X. Liu & Zhong, 2016; Steinberger & Holme, 2008; Walker et al., 2011; Yoshida, 2008a). For the viscosity structure, some studies assume a 1D viscosity profile in which mantle is separated into multiple layers with each layer assigned a viscosity (e.g., Hager, 1984; Hager & Richards, 1989; Rudolph et al., 2015; Walker et al., 2011). Typically, a 10–100 times viscosity increase from upper mantle to lower mantle is used, as suggested by results from geoid inversion studies (e.g., Hager, 1984; Hager & Richards, 1989). The temperature anomaly can also be derived from the density anomaly by considering the effects of thermal expansion on density. In this case, the viscosity can be temperature dependent (e.g., Čadek & Fleitout, 2006; Ghosh et al., 2010; Yang & Gurnis, 2016; Yoshida, 2008b). An additional viscosity reduction can be applied to the Ppv phase (e.g., Shahraki et al., 2015; Yoshida, 2008a), as mineral physics experiments have suggested that the Br to Ppv phase transition could lead to 10–1,000 times viscosity reduction (e.g., Ammann et al., 2010; Hunt et al., 2009), although this remains a matter of debate (Karato, 2011).

The solution of Equations 4 and 5 also provides the stress field (including both the dynamic pressure and the deviatoric stress in Equation 5). The radial stress at the surface and the CMB can be used to determine the dynamic topography at the surface and the CMB (e.g., Flament, 2018; Flament et al., 2013; Hager et al., 1985; Kiefer & Kellogg, 1998; Panasyuk & Hager, 2000; Rubey et al., 2017; Steinberger et al., 2019; Yang & Gurnis, 2016). The density anomalies in the mantle's interior and at these boundaries have been used to calculate the geoid anomaly which can be compared to observation of the geoid anomaly (e.g., Čadek & Fleitout, 2006; Ghosh et al., 2010; Hager, 1984; Hager et al., 1985; X. Liu & Zhong, 2016; Yang & Gurnis, 2016). Fitting calculated surface dynamic topography and geoid anomaly with observations provides tighter constraints on the density and viscosity structures in the mantle which, in turn, provides better constraints on the instantaneous mantle flow field (e.g., Walker et al., 2011).

Previous studies have shown that the instantaneous mantle flow field in the D′′ layer is characterized by convergent flow toward the two LLVP regions at a global scale, although the magnitude of the flow velocity, and the direction of the velocity at a regional scale, depend on model parameters such as the tomography model used to specify density, depth-dependent viscosity profiles and lateral variation of viscosity, and the relationship between density and seismic velocity anomalies (e.g., Walker et al., 2011; Yoshida, 2008a). To illustrate this with an example (Figure 10), we show two geodynamic models here. Model 1 is from the geodynamic simulations presented in Wolf, Li, et al. (2024). In this model, the thermal density anomaly is derived from tomography model S40RTS (Ritsema et al., 2011) with $\delta\rho_T/\rho = -C\delta V_s/V_s$, where $C = 0.4$ is a constant scaling factor. The density anomaly is then converted to temperature variation via $\delta T = \delta\rho_T/\alpha\rho$, with $\alpha = 3 \times 10^{-5}$/K the thermal expansivity. An additional 2.25 % positive compositional density anomalies are included in the LLVP regions, where the V_s anomaly is $<-0.5\%$ in the lowermost 600 km of the mantle. The viscosity is temperature dependent with an activation energy of 191 kJ/mol. A viscosity jump of 70 times is applied from upper mantle to lower mantle. Furthermore, a 100 times viscosity reduction is applied to Ppv regions in the D′′ layer. More details about the model setup and parameters are in Wolf, Li, et al. (2024). Model 2 is the same as model 1, except that the density anomaly is derived from tomography model SEMUCB-WM1 (French & Romanowicz, 2014). As shown in Figure 10, the V_s in the two tomography models (S40RTS and SEMUCB-WM1) agree on a large scale, with both including by LLVPs beneath the central Pacific Ocean and the Africa, but they differ at local scales. Flow is often directed from regions outside the LLVPs toward the LLVPs, although this is not true for all regions (Figure 10).

The mantle flow velocity in the past has also been explored, using two main approaches. The first approach is to impose plate motion history from plate reconstruction models as the surface velocity boundary condition to guide the large-scale convection pattern, solving the energy conservation equation in addition to Equations 4 and 5 (e.g.,

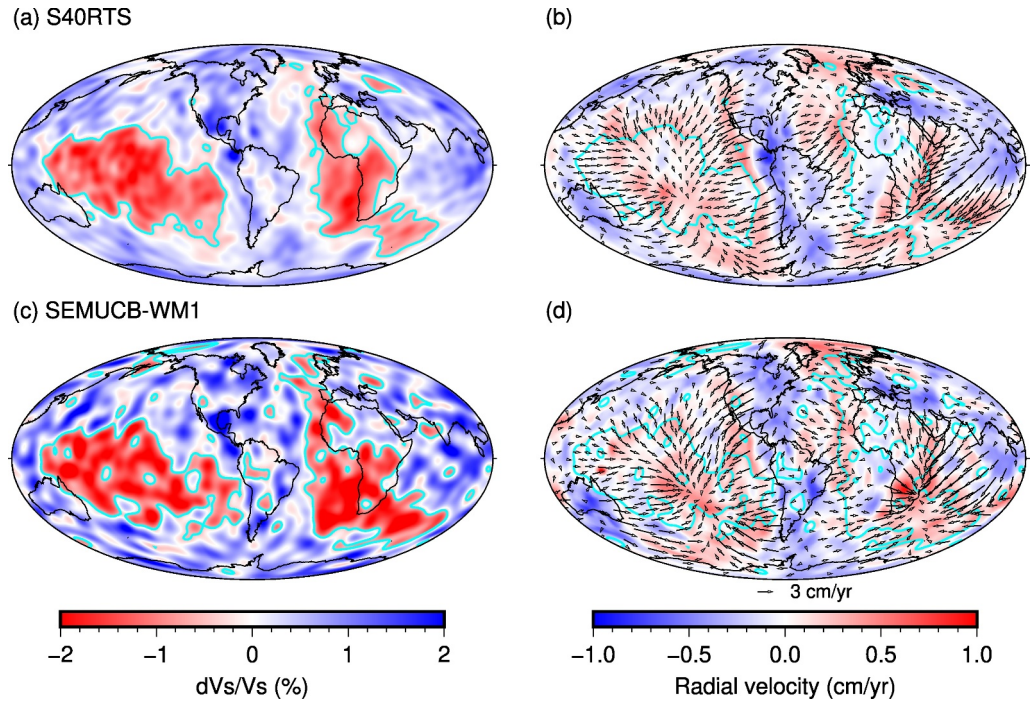

Figure 10. Seismic tomography models (a, c) (French & Romanowicz, 2014; Ritsema et al., 2011) and predicted mantle flow velocity from inferred density variations (b, d) at 2,800 km depth. Cyan lines indicate contours of the V_S anomaly at −0.5 %. (a, c) Background colors (see legend) represent shear velocity perturbation with respect to 1D reference models. (b, d) Arrows show horizontal flow directions and velocities, which are proportional to the arrow length (see legend). Radial velocities (see legend) are indicated by the background color.

Bower et al., 2013; Li & Zhong, 2017, 2019; McNamara & Zhong, 2005; Zhang et al., 2010). These types of models suffer from unknown initial conditions; furthermore, the resulting mantle structures are model dependent and may be different from those of the real Earth—even the calculated present-day mantle structures are not the same as the real Earth, as expressed in seismic tomography. Another approach is to use the present-day mantle structure and flow field as initial conditions and run models backward-in-time by solving Equations 4 and 5 (e.g., Steinberger, 2000; Steinberger & O'Connell, 1998). Because thermal diffusion is forward in nature, it is ignored in these models. Therefore, the further backward in time the models are run, the larger the errors will be in the models. As investigated by Li (2023a), the propagation of an uncertain present-day mantle flow field into the past could lead to large errors. Even assuming a precise understanding of the present-day mantle flow field and mantle density and viscosity structures, these backward-in-time models could lead to ∼10%–30% errors in mantle flow velocities after ∼40 Ma. These issues may be alleviated somewhat by using an adjoint method (e.g., Bunge et al., 2003; Horbach et al., 2014; L. Liu & Gurnis, 2008; Spasojevic et al., 2009), in which a trial of past mantle structure is first obtained by running models backward-in-time and is set as the initial condition for forward-in-time models. Then, the mismatch between the calculated present-day structure in forward-in-time models with that from observations is used to correct the initial mantle structures. This iterative process continues until a convergence is met.

4.2. Previous Interpretations of Deep Mantle Anisotropy and Mantle Flow

4.2.1. Slab-Driven Flow

Increasingly detailed seismic tomography images (e.g., Fukao & Obayashi, 2013; Grand et al., 1997; Lei et al., 2020; Ritsema et al., 2011; van der Hilst et al., 1997) have shown that some subducting slabs penetrate down to the CMB. In some instances, studies have suggested approximate locations where previously subducted slabs can be found in the lowermost mantle (e.g., Qayyum et al., 2022; van der Meer et al., 2018), although there is substantial uncertainty in such determinations (e.g., Sigloch et al., 2008; van der Hilst et al., 1997). Slabs that reach the CMB will induce deformation and CPO, thereby causing seismic anisotropy (Garnero & McNamara, 2008; McNamara et al., 2002, 2003; Wenk et al., 2006, 2011). The interpretation of deep mantle anisotropy as indicating

10.1029/2023RG000833

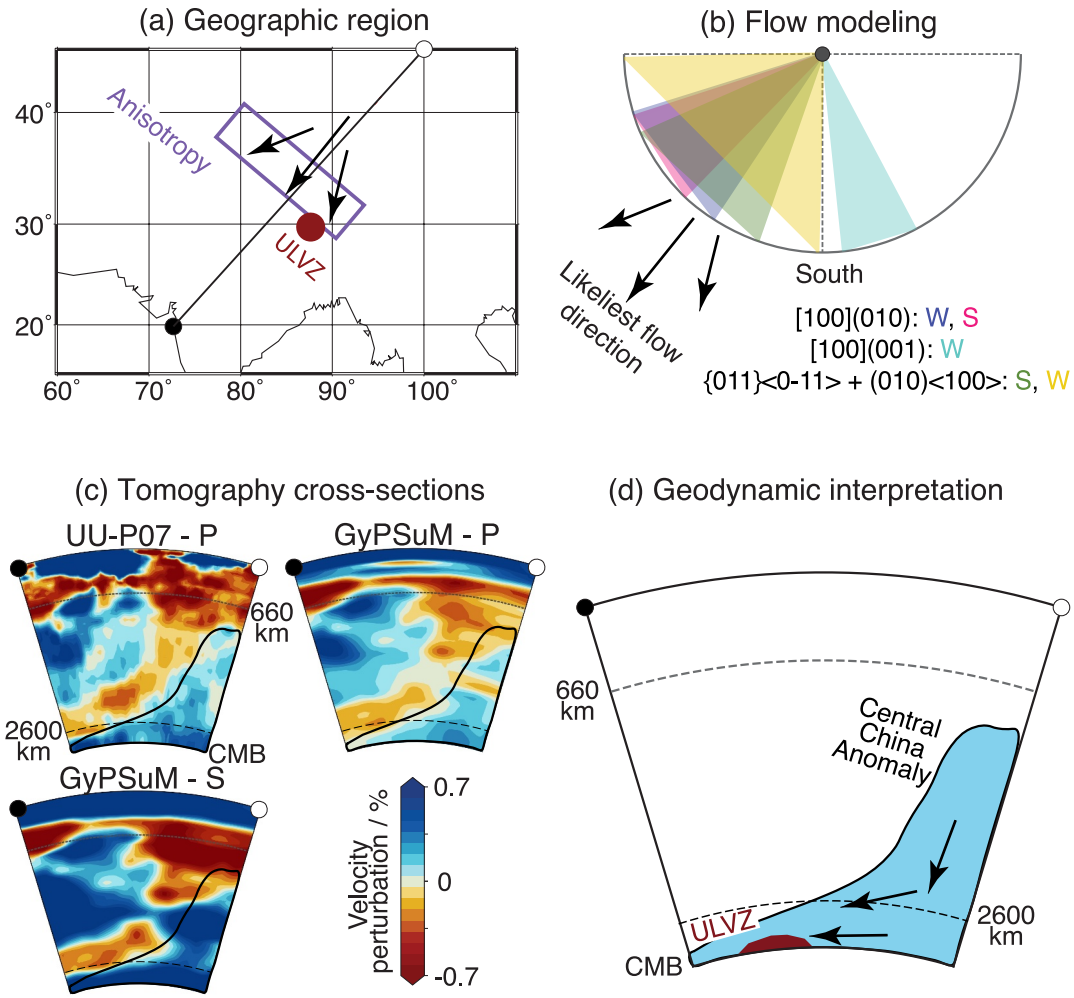

Figure 11. Geodynamic interpretation of shear wave splitting measurements for the deep mantle beneath the Himalayas. Figure and caption are slightly modified from Wolf, Long, and Frost (2024). Black arrows are indicating flow directions (a) Anisotropic region (violet) and ultra-low velocity zone (ULVZ; red) identified by Wolf, Long, and Frost (2024). Here and in panels (b) and (d), black arrows schematically indicate inferred flow directions. (b) Modeling suggests southwestwards (or, alternatively, northeastwards) flow, with differently colored triangles representing the range of potential flow directions that match the observations for different elastic tensors. Only southeast and southwest quadrants are shown; however, there is a 180° ambiguity in the potential shear direction. (c) Vertical slice of velocity structure from tomography models UU-P07 (Amaru, 2007) and GyPSuM (Simmons et al., 2010), with the start and end points of the cross-sections shown as black and white circles in panel (a). (d) Interpretation of fast velocity anomalies from panel (c), after (Qayyum et al., 2022). The ULVZ (dark red; vertically and laterally exaggerated for clarity) is interpreted to have been transported southwestwards through slab-driven flow.

slab-driven flow in the seismically faster lowermost mantle regions has been put forth in a number of studies (e.g., Asplet et al., 2020; Chandler et al., 2021; Grund & Ritter, 2019; Long, 2009; Nowacki et al., 2010; Wolf & Long, 2022). For example, anisotropic deep mantle structure has been linked to the subducted Farallon slab beneath North America (Asplet et al., 2020; Long, 2009; Lutz et al., 2020; Nowacki et al., 2010; Wolf & Long, 2022), remnant slab material of imprecisely known origin beneath Siberia (Creasy et al., 2021; Grund & Ritter, 2019), and the central China slab located beneath the Himalayas (Wolf, Long, & Frost, 2024). To determine likely flow directions beneath the Himalayas, Wolf, Long, and Frost (2024) conducted mineral-physics-informed forward modeling, which indicated likely southwestwards (or, alternatively, northeastwards) flow in this region (Figures 11a and 11b). Using these and other constraints, they argued that slab remnants had moved southwestwards along the CMB, potentially leading to the displacement of ULVZ material that has been detected in this region (Figures 11c and 11d).

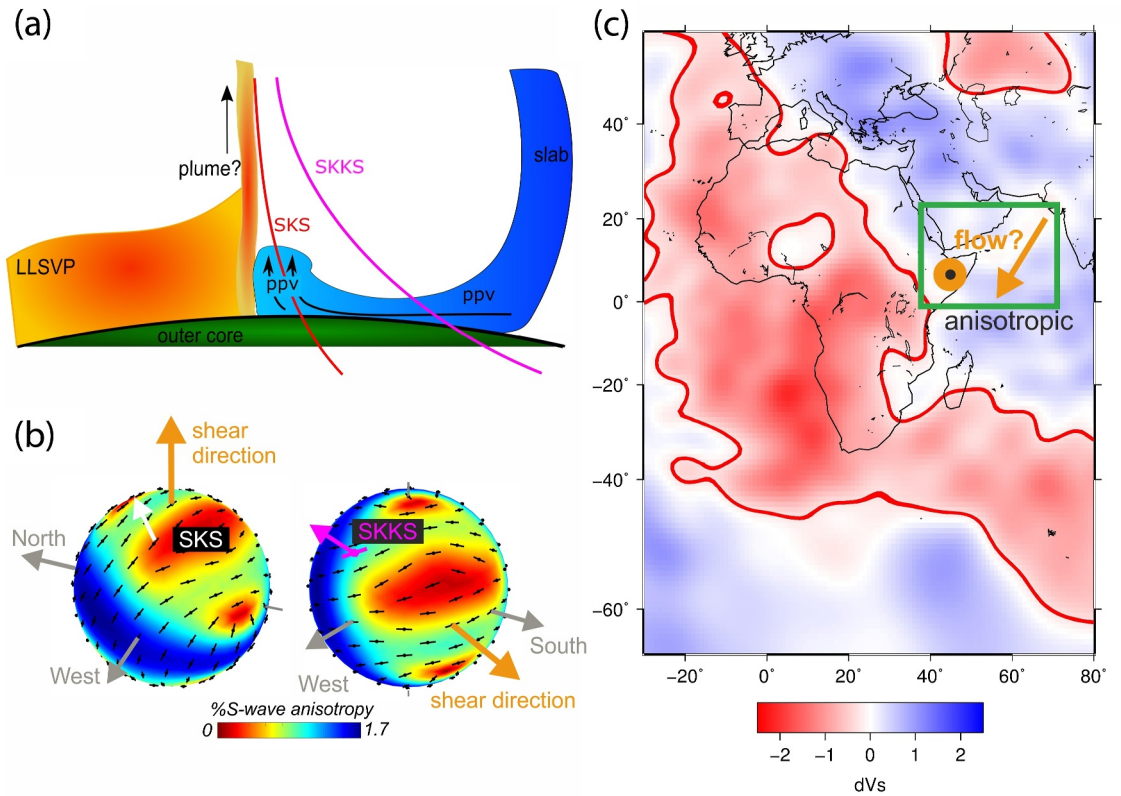

Figure 12. Geodynamic interpretation of shear wave splitting measurements for the deep mantle close to the edge of the African large-low velocity province (LLVP). Figure and caption are slightly modified from Reiss et al. (2019). (a) Schematic illustration of inferred D″ structure at the northeastern edge of the African LLVP (shown as green box in panel c). The cross-section is perpendicular to the LLVP edge. SKS and SKKS raypaths are shown as red and pink solid lines. Suggested flow directions are shown as black arrows. (b) Upper hemisphere representation (looking down on Earth from above) of splitting predicted for textured Ppv, similar to the elastic tensors shown in Figure 9. Colors indicate the shear wave anisotropy percentage (see legend). Yellow solid lines represent the shear direction and white/pink solid lines SKS/SKKS raypaths. The left and right plots represent the seismic anisotropy inferred to be sampled by SKS and SKKS, respectively. (c) Horizontal slice through the S40RTS tomography model (Ritsema et al., 2011) at 2,800 km depth (see legend). The LLVP boundary, as defined by the 0.5 % slow-velocity contour (Garnero et al., 2016), is shown as a thick red line. Orange arrow and circle represent flow directions shown in panel (a). The green box indicates the study region.

4.2.2. Upwelling Flow at LLVP Edges

Multiple regional studies have shown evidence for particularly strong seismic anisotropy in the lowermost mantle at the edges of the two LLVPs (e.g., Cottaar & Romanowicz, 2013; Deng et al., 2017; H. A. Ford et al., 2015; Lynner & Long, 2014; Reiss et al., 2019; To et al., 2005; Wang & Wen, 2004; Wolf & Long, 2023). However, although seismic anisotropy along LLVP edges has been found to be particularly strong at regional scales, a global compilation of D″ observations shows that anisotropy is just as likely to be found away from LLVP edges as near it (Wolf, Long, Li, & Garnero, 2023). Seismic anisotropy along LLVP edges may be especially strong due to the origination of plumes, which has been suggested to be particularly likely in these regions (e.g., Burke et al., 2008; Steinberger & Torsvik, 2012). In agreement with this idea, observations of deep mantle anisotropy near LLVP edges have often been connected to upwelling flow (e.g., Cottaar & Romanowicz, 2013; H. A. Ford et al., 2015; Reiss et al., 2019; Vanacore & Niu, 2011). In any case, if LLVPs are thermochemical structures with a rheological contrast with the mantle outside of them (e.g., McNamara, 2019), complex flow patterns with particularly strong deformation can be expected at LLVP edges, therefore causing strong seismic anisotropy. A previously proposed model of upwelling flow at the edge of the African LLVP near the Afar plume from Reiss et al. (2019) is shown in Figure 12. Reiss et al. (2019) interpreted differential SKS-SKKS splitting observations as being indicative of deep mantle flow deflected upwards along the LLVP edge in several regions close to the edge of the African LLVP.

4.2.3. Upwelling Flow at the Root of Plumes

An interesting target for measurements of D″ anisotropy are regions that coincide with suspected roots of plumes in the deep mantle. Previous studies have focused on the Afar (H. A. Ford et al., 2015), the Iceland (Wolf et al., 2019) and the Yellowstone (Wolf, Li, et al., 2024) plumes. These studies suggest that splitting measurements indicate anisotropy due to upwelling flow close to the plume root and mostly horizontal flow in the surrounding regions, pointing toward a deep mantle source for both plumes. Even if measurements of deep mantle anisotropy cannot always be uniquely linked to flow directions, such as SKS-SKKS differential splitting measurements (e.g., Wolf et al., 2019; Wolf, Li, et al., 2024), the D″ anisotropy signature near suspected deep mantle plume roots can be compared to the signature in the surrounding regions, potentially indicating unique anisotropy at the suspected plume root location.

4.3. Linking Seismic Models to Geodynamics Interpretations

Analogously to the upper mantle (e.g., Long & Becker, 2010), observations of larger velocities for horizontally than vertically polarized shear waves ($V_{SH} > V_{SV}$) have traditionally been interpreted as evidence for approximately horizontal flow at the CMB (and vice versa) (e.g., Kendall & Silver, 1998). This assumption is true if seismic anisotropy is caused by SPO; however, if CPO of anisotropic minerals induces seismic anisotropy, the validity of this relationship depends on the details of CPO development in the relevant minerals (e.g., Yamazaki & Karato, 2007). Therefore, interpretations of seismic anisotropy in terms of flow are challenging if only radial anisotropy is known. However, improved measurement techniques have allowed the measurement of deep mantle splitting parameters, enabling the inference of plausible flow directions under the assumption that anisotropy is caused by CPO.

One possible strategy to infer deep mantle flow from splitting observations, which has been frequently applied (e.g., Creasy et al., 2021; H. A. Ford et al., 2015; Nowacki et al., 2010; Wolf & Long, 2022), is to assume a plausible deformation geometry in the deep mantle and test predictions for this geometry against splitting observations for a variety of elasticity scenarios and flow directions. This could be horizontal simple shear, where slab remnants move horizontally along the CMB (e.g., Pisconti et al., 2019; Wolf & Long, 2022), or vertical extension at the root of plumes at the CMB (e.g., H. A. Ford et al., 2015). Additionally, a probable composition can be assumed; for example, it has been argued that regions likely dominated by slab remnants imply lower than average temperatures and a relatively shallow bridgmanite-postperovskite transition (Murakami et al., 2004), thereby making Ppv the likely dominant phase (e.g., Asplet et al., 2020; Wolf & Long, 2022). Under such assumptions, forward modeling can be performed for multiple plausible elastic tensors and slip systems with the aim of matching the measured splitting parameters. Sometimes, such forward modeling will lead to similar flow directions for a large group of candidate elasticity and deformation scenarios (e.g., Wolf & Long, 2022), enabling relatively robust inferences on flow. An alternative modeling strategy involves ray-theoretical forward modeling or inversions using multiple independent observations (e.g., D″ reflections combined with S-ScS differential splitting) to infer the most likely deep mantle mineralogy from a suite of elastic tensors (e.g., Creasy et al., 2021; Pisconti et al., 2019; Pisconti et al., 2023). Such ray-theoretical calculations do not consider all the potential full-wave effects that influence splitting parameters (e.g., Nowacki & Wookey, 2016; Wolf et al., 2022a). However, they are substantially more computationally efficient, allowing the testing of more potential orientations of the anisotropy.

CPO induced seismic anisotropy is an expression of mineral deformation and alignment, which are related to the mantle flow field that can be computed in geodynamic models. Therefore, seismic observations of anisotropy, physical properties of minerals, and mantle flow in geodynamic models are linked. Interdisciplinary collaborations have made progress in understanding their connections, enabling the usage of seismic anisotropy observations to unveil the nature of mantle dynamics and mineral structures in the D″ layer (e.g., Chandler et al., 2021; Cottaar et al., 2014; McNamara et al., 2002, 2003; Merkel et al., 2007; Walker et al., 2011; Wenk et al., 2011). These studies typically start with calculations of mantle flow field in geodynamic models. Lagrange tracers are introduced to the model domains and are advected with the mantle flow field. The tracers track the deformation history along their trajectories, which can be compared with regions with observations of seismic anisotropy. Furthermore, the time-integrated deformation of tracers can be fed into mineral physics calculations to compute the anisotropy of mineral assemblages. When compared with seismic observations, such models could provide critical information about elasticity and dominant slip systems of minerals in the D″ layer (Chandler et al., 2021; Cottaar et al., 2014; Merkel et al., 2007; Walker et al., 2011; Wenk et al., 2011).

10.1029/2023RG000833

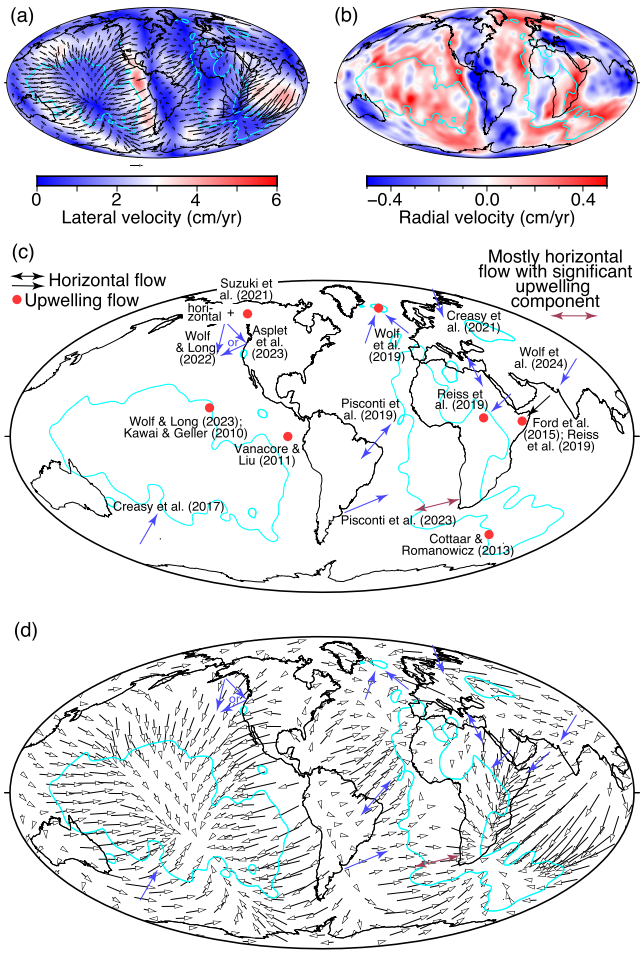

Figure 13. Comparison of deep mantle flow directions inferred from seismic anisotropy with predictions from geodynamics. (a) Global map of lateral flow directions (arrows) and velocities (colorbar, see legend) inferred from geodynamical modeling (Section 4.1) based on tomography model S40RTS (Ritsema et al., 2011). (b) Corresponding radial velocities (colorbar, see legend). Studies are labeled on the map and include Kawai and Geller (2010), Vanacore and Niu (2011), Cottaar and Romanowicz (2013), H. A. Ford et al. (2015), Creasy et al. (2017), Pisconti et al. (2019), Reiss et al. (2019), Wolf et al. (2019), Creasy et al. (2021), Suzuki et al. (2021), Wolf and Long (2022), Asplet et al. (2023), Pisconti et al. (2023), Wolf and Long (2023), Wolf, Long, and Frost. (2024). (c) Flow directions (see legend) inferred from measurements of seismic anisotropy. Studies are mentioned on the map. (d) Combination of panels (a) and (c), showing geodynamically inferred lateral flow directions (black arrows) and lateral flow directions inferred from seismic anisotropy (blue).

Following these procedures, McNamara et al. (2002) and McNamara et al. (2003) created 2D time-dependent mantle convection models in spherical geometry and showed that large strain preferentially occurs beneath subduction regions in the lowermost mantle, suggesting that seismic anisotropy in these regions may be caused by CPO. Through mineral physics experiments, Merkel et al. (2007) found that plastic deformation of Ppv dominantly occurs with slip on the (100) and (110) planes. They also combined mantle flow fields obtained via in 2D geodynamic models with mineral physics calculations of anisotropy; their calculations predicted significant depth-dependent anisotropy near and beyond the turning point of a downwelling slab. It should be noted, however, that the calculated anisotropy is strongly dependent on the choice of elastic moduli and may or may not uniformly agree with features of seismic observations of anisotropy in the D″ layer. Walker et al. (2011) incorporated instantaneous global mantle flow fields with mineral physics calculations and showed that, if the deformation of Ppv is accommodated by slip on the (010) or (100) plane, the computed anisotropy displays similar global patterns as observations of radial anisotropy. In contrast, for models where dislocations move on (001) planes, the predicted anisotropy shows anti-correlation with seismic observations. Wenk et al. (2011) combined flow in 2D convection models and polycrystal plasticity modeling of Br, Ppv, and Fp to calculate anisotropy in the D″ layer. They found that Ppv with predominant (001) slip and Fp with {110} and {111} slip produce similar anisotropy patterns as seismic observations, but Br with dominant (001) slip and Ppv with dominant slip on (010) and (100) produce anisotropy that is inconsistent with observations. Later, Cottaar et al. (2014) extended the convection models of Wenk et al. (2011) to 3D and showed that seismic observations of radial anisotropy and splitting in subhorizontal seismic phases are mostly consistent with dominant deformation of Ppv along (010) and (001) planes. They further showed that the fast axis directions of azimuthal anisotropy for (001)-slip at the edges of the slab are (sub-)parallel to flow directions. Chandler et al. (2021) further extended the 3D convection models of Cottaar et al. (2014) by including thermochemical piles in the lowermost mantle that represent the compositionally-distinct LLVPs and studied their interaction with subducted slabs. They also found that Ppv with dominant (001) and (010) slip can explain the seismically observed anisotropy in colder regions, where downwellings turn to horizontal flow; however, only a model of Ppv with dominant (001) slip matches seismic observations at the root of hotter large-scale upwellings.

We emphasize that, although these previous studies have shown that deformation of Ppv phase could explain seismic observations of anisotropy in the D″ layer, these studies do not exclude the contribution of other mechanisms for the origin of seismic anisotropy in this layer, including SPO. As discussed in Section 3.1, the Earth's lowermost mantle could include a mixture of chemical heterogeneities (e.g., Christensen & Hofmann, 1994; Ferrick & Korenaga, 2023; Keller et al., 2023; Kellogg, 1997; Ko et al., 2022; Labrosse et al., 2008; Li, 2021; Li, 2023a; Manga & Jeanloz, 1996; Nakagawa et al., 2010; Tackley, 2011; Yuan et al., 2023), and perturbations of the basal thermal boundary layer by the arrival of subducted slabs could induce small-scale convection involving linear-, sheet-, and ridge-like shapes of thermal and/or thermochemical structures (e.g., Davies & Davies, 2009; Li, 2020; Lowman et al., 2004). Such structures may or may not include partial melting, but in any case may contribute to seismic anisotropy in the D″ layer as well.

Figure 13 shows both lowermost mantle flow directions inferred from geodynamic simulations (Figures 13a and b) and a summary of all previously inferred flow directions from measurements of lowermost mantle anisotropy (Figures 13c and 13d). The general patterns inferred from geodynamics and measurements of seismic anisotropy agree: both find upwelling flow more likely beneath the LLVPs and horizontal flow in the higher velocity regions

near the CMB. Also, inferred flow directions agree in many places, such as the lowermost mantle beneath New Zealand, the northeastern Pacific Ocean, the Atlantic Ocean and western Africa. However, due to the limited number of previous studies that have modeled flow directions from measurements of seismic anisotropy, it is not useful to perform systematic quantitative comparisons at this point. However, reconciling geodynamic flow models and interpretations on a global scale is a promising line of future research.

5. Challenges and New Directions

5.1. Seismology

5.1.1. Understanding Methodological Limitations Through Global Wavefield Simulations

As discussed in detail in Section 2, recent modeling of global seismic wave propagation has revealed some limitations of methods that have been commonly used for the detection of deep mantle anisotropy (e.g., Komatitsch et al., 2010; Nowacki & Wookey, 2016; Wolf et al., 2022a). The methods that have been most thoroughly investigated so far are the S-ScS differential splitting technique (Nowacki & Wookey, 2016; Wolf & Long, 2024; Wolf et al., 2022a), differential SV-SH travel times (Borgeaud et al., 2016; Komatitsch et al., 2010; Parisi et al., 2018), S_{diff}^{pol} splitting (Cottaar & Romanowicz, 2013; Wolf, Long, Creasy, & Garnero, 2023) and SKS-SKKS differential splitting (Tesoniero et al., 2020; Wolf et al., 2022a). By construction, full-wave anisotropic tomography inversions consider finite-frequency effects (Kawai & Geller, 2010; Suzuki et al., 2021). One strategy that still needs to be more thoroughly tested to understand the consequences of ray theoretical assumptions is polarity measurements of D″-reflected phases (e.g., Thomas et al., 2011).

There are many unknowns that can be explored using global wavefield simulations in future work, whose understanding will greatly help improve measurements and interpretations of D″ anisotropy. Such open research questions pertain to specific aspects of individual methods or the development of new strategies. Some questions worth exploring include:

- Under what conditions and for which distance ranges can differential S, ScS, and S_{diff} SV-SH travel times be reliably interpreted as evidence for D″ anisotropy? Are there, for example, requirements with respect to waveform shape that allow the reliable distinction between differential travel times accumulated in isotropic versus anisotropic media?
- What are the effects of a gradual (as opposed to a sharp) D″ discontinuity on D″-reflected waves?
- What are the effects of D″ discontinuity topography on D″-reflected waves, in particular their polarity? What are the effects of CMB topography on ScS and other seismic phases?
- Can we identify new splitting strategies using seismic phases that are not commonly used to investigate deep mantle anisotropy? For example, are there new splitting strategies to measure seismic anisotropy at epicentral distances that are not commonly used (see Figure 5)?
- Are there seismic phases that can be used to investigate different aspects of D″ structure simultaneously with the analysis of seismic anisotropy? For example, S_{diff}, which can be used to measure D″ anisotropy, is also commonly used to investigate (mega-)ULVZ structure. Can we leverage such phases to learn more about the causative mechanism for D″ anisotropy?

5.1.2. Null Detections: Identification of Isotropic Regions of D″

Wolf, Long, Li, and Garnero (2023) provided a detailed compilation of locations at which deep mantle anisotropy has been detected in the past (Figures 2 and 3). From this compilation, it is clear that only a few studies confidently report the absence of splitting due to deep mantle anisotropy in some regions (e.g., Garnero, Maupin, et al., 2004; Wang & Wen, 2007; Wolf, Li, et al., 2024). The limited number of null detections (i.e., confident identification of D″ isotropy, as opposed to null splitting observations, which may have other causes) does not allow reliable deduction of deep mantle settings in which D″ anisotropy may be weak or absent. However, elucidating such regimes is crucial for our understanding of deep mantle dynamics. A major challenge is that the measurement of null splitting in the lowermost mantle anisotropy does not necessarily imply that seismic anisotropy is absent; alternatively, the measurement can be caused by the propagation of seismic waves along the fast or slow direction of the anisotropy. These two scenarios can only be distinguished if (null) splitting is measured from multiple azimuths. Despite these challenges, however, the identification of truly isotropic regions of D″, if they exist, should be a priority for future studies.

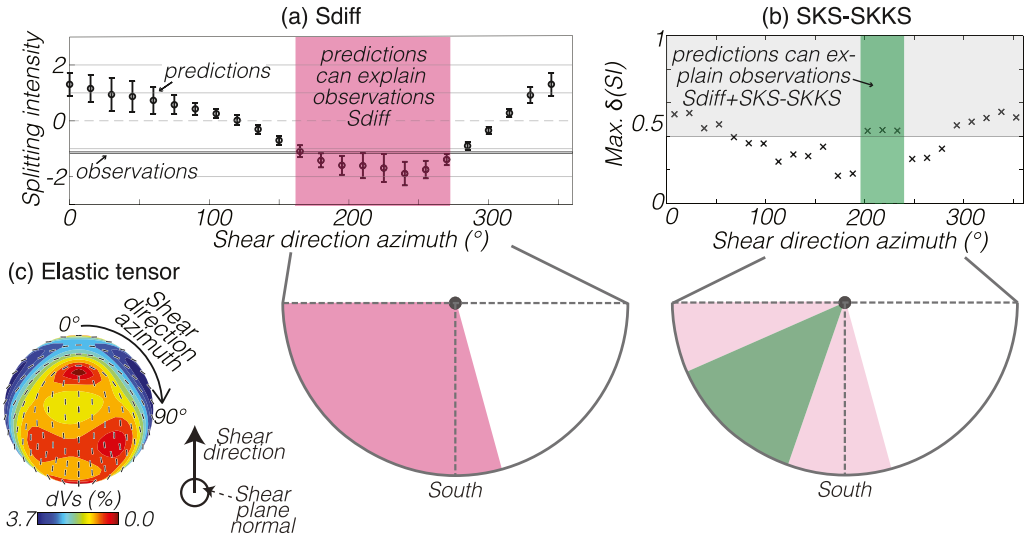

Figure 14. An illustration of how of S_{diff}^{pol} and SKS-SKKS can be combined to infer deep mantle flow directions. These measurements were obtained by Wolf, Long, and Frost (2024) for the lowermost mantle beneath the Himalayas. Our models assume an anisotropic layer at the base of the mantle of thickness 150 km to carry out the synthetic splitting predictions. (a) Top: Predicted synthetic splitting intensity (SI) measurements (circles) as a function of shear direction azimuth (or, equivalently, the propagation direction through the anisotropy) for a Br elastic tensor in a horizontal simple shear configuration (panel c). Error bars represent 95% confidence intervals for splitting intensities estimated from synthetic seismograms. 95% confidence intervals of observed S_{diff} splitting intensities due to lowermost mantle anisotropy are shown as the thin gray shaded area. Predictions of the strength of splitting for the range of shear direction azimuths shown with the pink shaded area. Bottom: Circular representation of possible shear direction azimuths. (b) Top: Maximum (assuming anisotropy affects either one or both phases) differential SKS-SKKS splitting intensities as a function of shear direction azimuth. Observed SKS-SKKS SI differences for this example are larger than 0.4 and are shown with the gray area. Synthetic predictions are shown as black crosses. The green area shows the range of potential shear direction azimuths that can simultaneously fit both the S_{diff} splitting observations and the SKS-SKKS differential splitting observations. This range is significantly reduced from the range obtained from modeling the S_{diff} splitting observations alone. Bottom: Circular representation of possible shear direction azimuths inferred from S_{diff} (pink) and S_{diff} + SKS-SKKS differential splitting measurements (green); compare range of pink and green swaths. (c) Visual representation of the elastic tensor used in the forward modeling. We show an upper hemisphere plot for a Br elastic tensor with a dominant slip system of {011} <0−11> + (010)<100> from Creasy et al. (2020), based on single-crystal elasticity from Stackhouse et al. (2005). Plotting convention is as in Figure 9.

5.1.3. Extracting More Information From the Seismic Wavefield: Combining Measurement Strategies

In cases of particularly favorable ray coverage (e.g., Creasy et al., 2017; H. A. Ford et al., 2015; Nowacki et al., 2010; Reiss et al., 2019), seismic anisotropy can sometimes be sampled from multiple directions using the same splitting measurement strategy. However, in most cases, limitations in ray coverage only allow the reliable measurement of deep mantle anisotropy from waves measured at similar backazimuths (e.g., Asplet et al., 2023; Pisconti et al., 2023; Wolf & Long, 2022). If measurements cannot be made from waves with crossing raypaths, inferring flow directions from measurements of deep mantle anisotropy is often not possible due to a large number of plausible scenarios (e.g., Wolf & Long, 2023). However, making measurements of D″ anisotropy in the same region using multiple methods can substantially facilitate interpretations of deep mantle anisotropy (e.g., Creasy et al., 2019). Methods that are particularly straightforward to combine include SdS and PdP polarity measurements with S-ScS differential splitting, because they can be applied over the same epicentral distance range (Pisconti et al., 2019, 2023). Other methods that have been combined to measure deep mantle anisotropy include S-ScS and SKS-SKKS differential splitting (Asplet et al., 2023; Creasy et al., 2017; H. A. Ford et al., 2015) as well as S_{diff} and SKS-SKKS differential splitting (Wolf & Long, 2023; Wolf, Long, & Frost, 2024). The combination of different methods to measure deep mantle anisotropy is particularly powerful because they provide independent constraints on the geometry of the anisotropy. Figure 14 shows an example in which SKS-SKKS differential splitting and S_{diff} splitting were successfully applied simultaneously. In this case, only the combination of S_{diff} and SKS-SKKS results enables the successful determination of a relatively small range of rotation angles of an elastic tensor that the splitting measurements are consistent with. In case of a simple shear geometry,

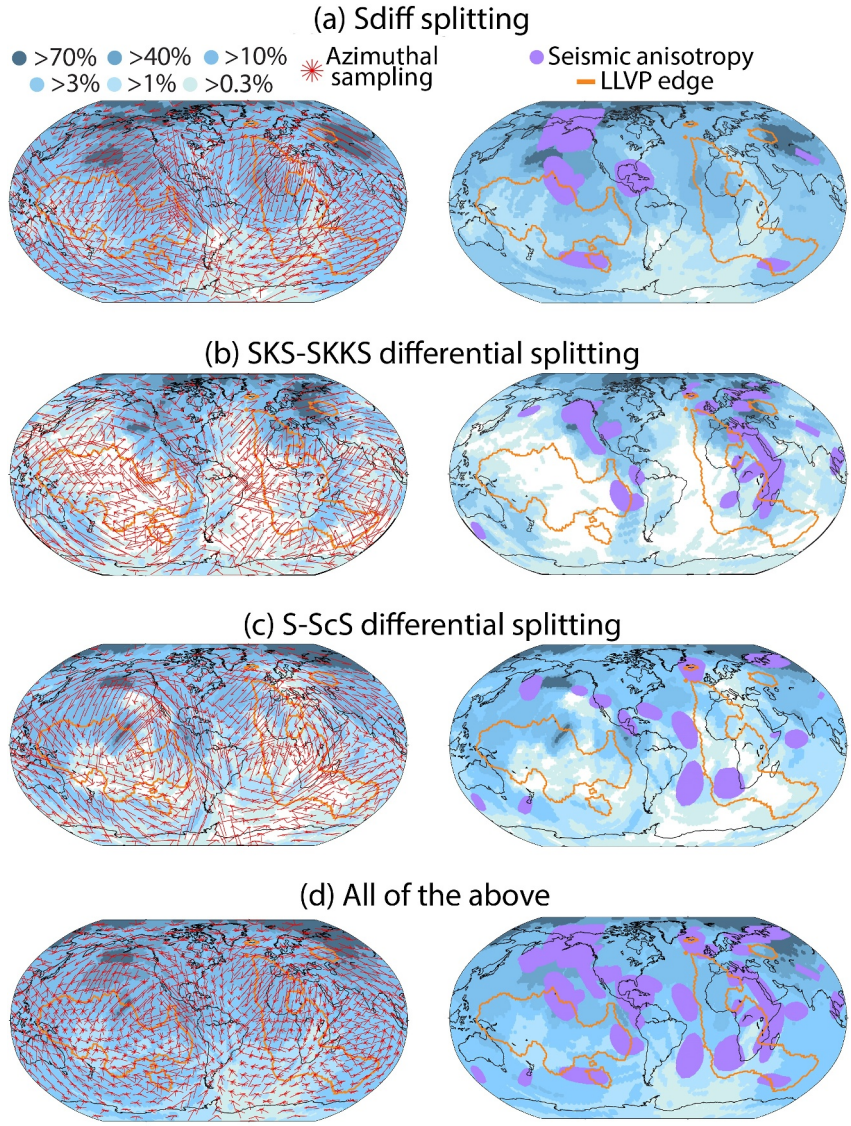

Figure 15. Global raypath coverage for (a) S_{diff} splitting, (b) SKS-SKKS differential splitting, (c) S-ScS differential splitting measurements and (d) all these methods together. Ray coverage is reported relative to the maximum bin (100 %, see legend). Red lines show azimuthal coverage in 30° azimuth bins (legend). The overall length of the sticks is locally normalized to the same value. Large-low velocity province edges, defined as in Figure 2b, are indicated by orange lines. Right and left columns are similar, but the right column shows locations for which the presence of seismic anisotropy has been previously suggested (violet color) instead of azimuthal coverage. Figure and caption are modified from Wolf, Long, Li, and Garnero (2023).

the shear direction approximately agrees with the direction of material flow. It is conceivable that observations of deep mantle anisotropy can be made by combining more than two splitting strategies in several regions, such as North America and eastern Europe/western Asia, given the favorable data coverage in these regions.

5.1.4. Limitations in Ray Coverage

One of the major limitations preventing the determination of a more complete picture of deep mantle anisotropy through regionally focused studies is the ray coverage. Figure 15 shows the ray coverage in the deep mantle for the three particularly popular methods to measure deep mantle anisotropy (S_{diff} splitting, SKS-SKKS differential splitting, S-ScS differential splitting). A detailed characterization of seismic anisotropy in the region under study requires both a large number of waves and abundant directional sampling; therefore, Figure 15 shows both. In general, the regions that hold most promise for an accurate analysis of D″ anisotropy are those that show good

sampling, both in terms of the absolute number of waves as well as the directional coverage (as well as coverage from different seismic phases, Section 5.1.3). This map considers all seismic events that occurred between 01/1990 and 03/2023 and a large majority of available broadband seismic stations world-wide (Wolf, Long, Li, & Garnero, 2023). Ray coverage is highly uneven and generally much denser in the northern than in the southern hemisphere. Therefore, it is unsurprising that most previously detected D″ anisotropy is located in the northern hemisphere (Figure 2b).

Many observations of D″ anisotropy have relied on seismic stations in and around the United States. Many of these studies primarily used data from USArray (IRIS Transportable Array, 2003) (e.g., Asplet et al., 2020, 2023; Lutz et al., 2020; Nowacki et al., 2010; Wolf & Long, 2022), which underlines the importance of the availability of dense array data for many approaches. It can be expected that recent, ongoing and future deployments of large, dense broadband networks (e.g., the AlpArray Seismic Network, 2015) will have a similar effect of expanding our understanding of deep mantle anisotropy through regional studies. Because continental landmasses are primarily located in the northern hemisphere, better raypath coverage of the southern hemisphere will likely require the installation of significant numbers of ocean bottom seismometers. While such an endeavor is technically possible, it would be costly; however, the potential science payoff is large (e.g., Eilon et al., 2021).

Additionally, to increase ray coverage, it is important to continue to improve existing methods and to develop new ones that can be applied at different epicentral distance ranges and to new rarely used seismic phases. Figure 7 shows which phases are commonly used to map seismic anisotropy and at what distances they can be used. Often, limitations on measurements of seismic anisotropy exist because of the low amplitudes at certain distances of key phases (dashed black lines in Figure 7). This challenge can be mitigated by using stacking techniques to array data, which have been shown to enable splitting measurements from low-amplitude seismic phases (Wolf, Frost, et al., 2023). For example, the application of array techniques may enable differential *KS splitting measurements up to distances of 180° (Wolf, Frost, et al., 2023). Array techniques may be applied to other phases as well, helping to expand our repertoire. For example, S_{diff} can potentially be measured up to a larger distance range using array techniques as opposed to single-station seismograms (Wolf, Long, Creasy, & Garnero, 2023). Similarly, using array techniques, PcS splitting can be reliably measured for epicentral distances between 45 and ∼63° (Wolf, Long, Frost, & Nissen-Meyer, 2024), allowing the inference of seismic anisotropy at shorter distances than other commonly applied methods.

5.2. Mineral Physics

To properly interpret shear wave splitting measurements that reflect D″ anisotropy, it is crucial to have accurate measurements of the properties of lowermost mantle minerals at the relevant pressures and temperatures. These properties include (a) the single-crystal elasticity of the phases that may potentially affect deep mantle anisotropy (including Br, Ppv, Fp), (b) the dominant deformation mechanisms in the deepest mantle (e.g., diffusion creep vs. dislocation creep, dislocation glide and dislocation climb), and (c) the relative strength of different slip systems of candidate minerals in the dislocation creep regime. Because experiments at the relevant pressure and temperature conditions are generally difficult to perform, much of our knowledge comes from computational studies, from the extrapolation of results obtained at less extreme conditions, or from experiments performed on analog materials. For example, experiments that have explored the development of CPO in Ppv (or analogs) have often been performed at substantially lower pressures than the lowermost mantle, and realistic mantle strain rates are impossible to achieve in the laboratory (e.g., F. Lin et al., 2017; Miyagi et al., 2008; Yamazaki, Shinmei, et al., 2006; Yamazaki, Yoshino, et al., 2006). Furthermore, experiments are often carried out on single-phase aggregates, although some progress has been made on relatively high-pressure and -temperature experiments on polyphase samples (e.g., Girard et al., 2016), helping us to understand how deformation may be partitioned among different phases with different properties (e.g., viscosity). While substantial progress has been made over the past several years to increase our knowledge of material properties, our understanding of the elasticity and deformation of deep Earth materials at high temperatures and pressures remains incomplete.

Despite the challenges inherent in studying the elasticity and deformation of Earth materials at lowermost mantle pressures, there has been significant recent progress (e.g., Chandler et al., 2021). These challenges include new computational approaches to identifying the most likely dominant slip system in materials such as Ppv (e.g., Goryaeva et al., 2016, 2017), novel experimental approaches that allow for experiments at relevant pressures and temperatures (e.g., Wu et al., 2017), and investigations of novel deformation mechanisms at the base of the mantle

(e.g., Cordier et al., 2023; Dobson et al., 2019). While limitations in our knowledge of elasticity and deformation of lowermost mantle minerals remain a challenge for seismic anisotropy studies, ongoing and future progress will continue to narrow the range of plausible scenarios. Furthermore, we now have a significant arsenal of modeling tools and approaches (e.g., Chandler et al., 2021; Cottaar et al., 2014; Creasy et al., 2020, 2021; H. A. Ford et al., 2015; Pisconti et al., 2019; Tesoniero et al., 2020; Walker et al., 2011; Wolf & Long, 2022; Wolf, Long, & Frost, 2024) that allow us (a) to test different scenarios for anisotropy based on new mineral physics results, and to (b) use seismic observations discriminate among different candidate mechanisms.

5.3. Geodynamics

The present-day Earth's mantle flow field can be determined by solving Equations 4 and 5 with appropriate initial and boundary conditions. The solutions of these two equations are controlled by the density and viscosity anomalies in the mantle. Therefore, the main challenge in calculating the instantaneous mantle flow field at the present day is to better understand the density and viscosity structure of the mantle. One way to improve constraints on the density structure is to improve seismic tomography of the Earth's mantle (e.g., French & Romanowicz, 2014; Houser et al., 2008; Koelemeijer et al., 2015; Lekic et al., 2012; Moulik & Ekström, 2014; Ritsema et al., 2011) and to better understand the scaling relationships between seismic velocities and density (Simmons et al., 2009; Steinberger & Calderwood, 2006; Stixrude & Lithgow-Bertelloni, 2011). The latter needs more comprehensive understanding on mantle composition and temperature, and more mineral physics experiments and calculations to determine the physical properties of mantle minerals and rocks under high-temperature-pressure conditions. Studies have shown that the Earth's free oscillations and solid tides are sensitive to deep mantle density structures and thus can be used to place additional constraints on the density at depth (Ishii & Tromp, 1999; Koelemeijer et al., 2017; Lau et al., 2017; Richards et al., 2023), although the resolution could be improved.

Constraining mantle viscosity is challenging, as it is strongly sensitive to a variety of physical parameters including temperature, pressure, and stress, and it also varies with grain size, composition (including the concentration of volatiles), and different mineral structures and phases, such as the presence and amount of partial melting (e.g., Karato & Wu, 1993; Kohlstedt & Hansen, 2015). It has also been found that viscosity is sensitive to lattice strain as well (e.g., Marquardt & Miyagi, 2015). Additionally, whether a rock deforms dominantly by diffusion creep or dislocation creep also determines whether and how these physical parameters affect the rock viscosity. Nevertheless, our understanding of mantle viscosity is improving through mineral physics experiments and calculations elucidating how these parameters affect viscosity, as well as through enhanced constraints on these parameters within the Earth's mantle. For example, Br is more viscous than other minerals in Earth's lower mantle (Yamazaki & Karato, 2001). An intriguing idea is that the strong Br-enriched ancient mantle structures, which may be even more viscous than both cold downwellings and hot upwellings, could remain unmixed in Earth's lower mantle after 4.5 billions of years of convection (Ballmer et al., 2017). Additionally, mantle viscosity and density structures control the surface and CMB dynamic topography, geoid anomaly, and the rate of post-glacial rebound. Our understanding of mantle density and viscosity structures has also been improving through the comparison of these observables calculated in geodynamic models with that from observations (e.g., Čížková et al., 2012; Kido et al., 1998; Kohlstedt & Hansen, 2015; X. Liu & Zhong, 2016; Mao & Zhong, 2021; Mitrovica & Forte, 2004; Rudolph et al., 2015; Steinberger & Calderwood, 2006; Wang & Li, 2020; Yang & Gurnis, 2016). For example, while a viscosity jump of about 10–100 times at 660 km depth from the upper to the lower mantle was constrained in the 1980s and 1990s based on geoid modeling (e.g., Hager, 1984; Hager & Richards, 1989), Rudolph et al. (2015) showed that the depth for this viscosity jump may occur at ∼1,000 km which could explain flattening of subducted slabs around this depth, although later studies found that to explain the presence of flattened slabs at ∼1,000 km depth for the Earth does not require a viscosity jump at this depth (Mao & Zhong, 2019; Wang & Li, 2020). One of the major challenges of constraining mantle viscosity from geoid modeling originates from non-uniqueness; that is, geoid anomalies can be explained reasonably well by a large variety of viscosity and density structures of the mantle.

Comparisons between geodynamic models and anisotropy observations will become much more accurate as our knowledge of the mantle viscosity structure improves. Geodynamic modeling experiments could be conducted to explore how the remaining large uncertainties in mantle density and viscosity structures affect the computations of mantle flow field. This requires systematic exploration of the parameter space. Geodynamic models that use parameters whose values are consistent with those constrained in mineral physics experiments/calculations, and

that predict outputs that are consistent with observations such as gravity, topography, seismic images, and geochemical observations, are of particular interest. Particularly relevant to mantle flow in the D′′ layer is the combination of mantle flow calculations with mineral physics constraints on anisotropy. Also, its comparison with seismic observations is an appealing direction to continue to pursue, as it provides critical information about mantle dynamics, deformation mechanism of minerals, and the patterns and drivers of flow. For this type of interdisciplinary collaboration, previous geodynamic studies have computed time-dependent mantle flow fields in both 2D and 3D geometry but only for regional models, whereas global models have mostly focused on instantaneous mantle flow at the present-day. In addition, only a few mantle convection models have been tested in previous anisotropy studies. Therefore, possible future studies could include (a) continuing to explore the parameter space in convection models to better understand how model parameters (e.g., density and viscosity structures) control seismic anisotropy in different regions (e.g., beneath downwelling and upwelling centers and in regions dominated by horizontal flow, at/near the edges of the LLVPs, within LLVPs), (b) testing more possible mixture of mineral phases and dominant slip planes for these minerals, (c) computing anisotropy in global 3D convection models with time-dependent mantle flow fields to investigate how mantle flow in the past differs from the present-day and how this difference affects the evolution of anisotropic structure, and (d) investigating the morphology of small-scale D″ layer structures that may induce SPO.

6. Open Science Questions That Deep Mantle Anisotropy Studies Can Address

Mantle convection controls the expression of plate tectonics on Earth's surface, which plays a key role in creating Earth's surface conditions. To understand the mantle's convective system, we must decipher how convection operates at depth. In the following, we discuss a range of open science questions about Earth's interior that can be addressed, and perhaps resolved, by future studies of deep mantle anisotropy.

What causes anisotropy in the lowermost mantle, and what does this tell us about lowermost mantle dynamics? Different mechanisms for D′′ anisotropy have been suggested, including SPO (Section 3.1; Figure 16) and CPO (Section 3.2; Figure 16). It is likely that deep mantle anisotropy is often caused by CPO of anisotropic minerals; however, it is often challenging to distinguish between SPO and CPO for a given set of anisotropy observations. Furthermore, if seismic anisotropy in D′′ is induced by CPO, uncertainties remain as to whether Br, Ppv, Fp, Ca-perovskite or any combination of these minerals is causing it. Some previous studies have preferred CPO of Ppv (e.g., Asplet et al., 2023; H. A. Ford et al., 2015; Pisconti et al., 2019, 2023; Walker et al., 2011) to explain their observations. However, as discussed in Section 3.2, deep mantle elastic tensors are uncertain because many proposed elastic tensors have been obtained via extrapolation to the relevant pressure and temperature conditions. However, the combination of improved mineral physics constraints with increasingly detailed observations of D′′ anisotropy holds promise to eventually lead to a detailed picture of deep mantle mineralogy and the prevailing deformation conditions in D′′.

Are predictions of global models for flow and elasticity at the base of the mantle consistent with body wave observations? Multiple regional studies have suggested likely flow directions using observations of deep mantle anisotropy (e.g., Asplet et al., 2023; Creasy et al., 2017; Pisconti et al., 2019; Wolf & Long, 2022; Wolf, Long, & Frost, 2024). These observations are often compared to flow predictions for the base of the mantle (e.g., Creasy et al., 2021; H. A. Ford et al., 2016), as in Figure 13. As the number of studies that infer directions of deep mantle flow from anisotropy observations grows, we can move away from local comparisons to evaluating the whole global set of flow directions against the predictions from global models for flow and elasticity at the base of the mantle. It is worth noting that the choices of model parameters in previously published calculations of flow at the base of the mantle differ (e.g., Flament, 2018; Forte et al., 2015; Walker et al., 2011). Comparing geodynamically predicted flow directions with those inferred from measurements of seismic anisotropy may thus help constrain model parameters and illuminate the patterns and drivers of deep mantle flow on a global scale.

What are the dynamic relationships among low shear velocity provinces, mantle plumes, and subducted paleoslabs? Elucidating the interaction among LLVPs, mantle plumes, and subducted slab remnants in the deep mantle is important for understanding the origin and evolution of deep mantle structures and how they interact with mantle convection (Figure 16). Many studies have suggested that LLVPs are chemically distinct (e.g., Flament et al., 2017; Labrosse et al., 2008; Li & McNamara, 2022; McNamara & Zhong, 2005; Wang & Wen, 2004; Yuan et al., 2023), although others argued that they may be purely thermal structures (e.g., Davies et al., 2015; Schuberth et al., 2009). It has been suggested that LLVPs are stable over hundreds of millions of years

10.1029/2023RG000833

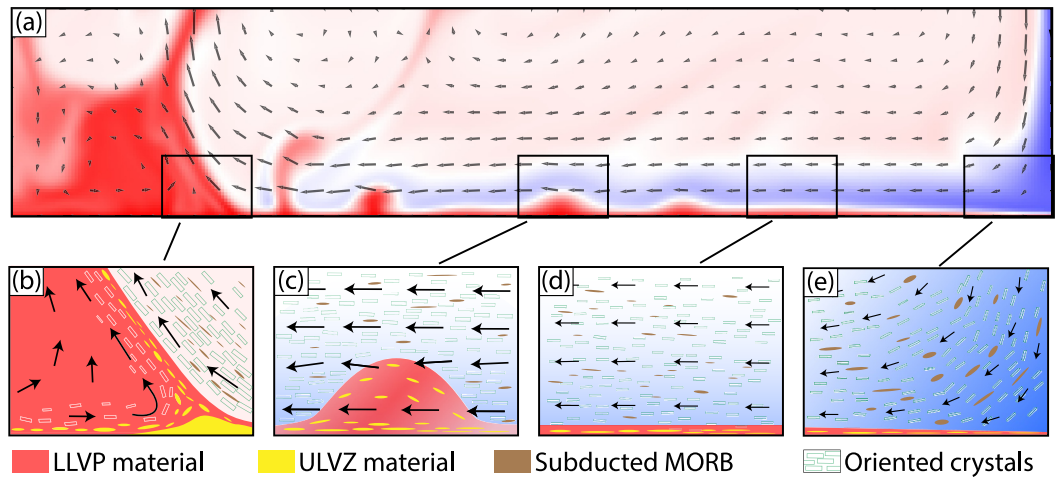

Figure 16. Schematic diagram of the types of regions and flow scenarios that can potentially be elucidated via a combination of seismic anisotropy observations and geodynamic simulations. (a) Mantle flow field (arrows: flow directions, length proportional to flow velocity; background colors indicate temperature) for a geodynamic simulation that includes sinking cold material (blue), reminiscent of a slab, a hot (red) structure similar to a large-low velocity province (LLVP) (left), and rising plumes (close to LLVP edge). (b–e) Zoom-ins representing different flow scenarios. Ultra-low velocity zone (ULVZ) material is shown in yellow, subducted mid-ocean ridge basalts in brown, aligned crystals in green and LLVP material in red. (b) Representation of flow near LLVP edge. ULVZ materials and partial melts potentially cause shape-preferred orientation, while crystals are aligned via CPO; either scenario causes seismic anisotropy. (c) Flow near a developing thermal upwelling. (d) A region of horizontal flow, with a potential thin and hot layer of chemically distinct material at the base of the mantle. (e) A region of slab-downwelling. Note that in contrast to panel (a), in which reddish colors show regions with relative higher temperature, the reddish colors in panels (b)–(e) represent chemically distinct LLVP materials.

and that large igneous provinces, kimberlites, and plumes are preferentially found at the surface close to their edges (e.g., Burke et al., 2008; Torsvik, 2019). However, it has been argued that LLVPs could only have remained stable beyond ~300 million years in the past if they were able to withstand impingement by downgoing slabs (e.g., Wolf & Evans, 2022). Other studies have argued that the shape of low velocity anomalies is controlled by downgoing slabs and that they evolve over time (e.g., McNamara, 2019; Yuan & Li, 2022; Zhong et al., 2007; Zhong & Rudolph, 2015). This notion agrees with inferences, based on seismic tomography, that plumes occur where slabs do not suppress them, which is not necessarily (always) spatially coincident with LLVP edges (Davaille & Romanowicz, 2020). An improved understanding of flow patterns at the base of the mantle, through observations and models of deep mantle anisotropy, will help answer these open questions. Figure 16 shows how geodynamic simulations can illuminate the dynamic relationships among different deep mantle structures such as LLVPs, subducted paleoslabs, and deep mantle upwellings. From such simulations, flow direction can be inferred, crystal orientation that can cause CPO (Figure 16e) and material elongation that can cause SPO (Figure 16b) are possible to predict.

What are ULVZs, and how do they reflect the dynamical evolution of the planet? It has been speculated that ULVZs may be remnants of an ancient magma ocean (e.g., Labrosse et al., 2008), originate from interactions with the liquid iron of the outer core (e.g., Otsuka & Karato, 2012), be enriched in ferric iron of unknown origin (e.g., V. H. Lai et al., 2022) and/or consist of subducted materials (e.g., S. E. Hansen et al., 2023). It is still a matter of debate whether they are solid or made of partial melt (e.g., Dobrosavljevic et al., 2019, 2023; Simmons & Grand, 2002; Thorne et al., 2019; Williams & Garnero, 1996). Previous work (Wolf & Long, 2023; Wolf, Long, & Frost, 2024) has found seismic anisotropy in the deep mantle that is co-located with or adjacent to ULVZ material. These measurements of seismic anisotropy were then used to infer likely directions of flow around the ULVZs. If such analyses are performed systematically in many regions with known ULVZ structure, this will potentially lead to insights into the role of ULVZs in Earth's dynamic evolution as well as their origin(s) and properties. Moreover, investigations of deep mantle anisotropy near ULVZs have potential to elucidate the interactions of ULVZs with other deep mantle structures. Geodynamic simulations will help suggest and distinguish between plausible scenarios (Figure 16b).

What drives flow at the base of the mantle? The discussion of the relationships among different deep mantle structures touches upon the fundamental question of what is driving flow in the deep mantle. Sinking slabs may play a major role by perturbing LLVPs (Figure 16a); however, we still do not precisely understand the nature of LLVPs and their role in mantle dynamics (e.g., Garnero et al., 2016; McNamara, 2019). Upwelling plumes at LLVP edges (Figure 16b) may have a significant influence on mantle convection, but this is still uncertain (e.g., Burke et al., 2008; Garnero et al., 2016; McNamara, 2019). A better understanding of seismic anisotropy in the deep mantle is a promising avenue to answer some of these open questions. The availability of improved measurement methods and the increasing number of local D″ anisotropy studies will enable us to systematically compare the patterns of deep mantle flow inside LLVPs (e.g., Reiss et al., 2019), in areas believed to be dominated by paleoslabs (e.g., Nowacki et al., 2010; Wolf & Long, 2022), and areas coinciding with likely deep mantle upwellings (e.g., H. A. Ford et al., 2015; Wolf et al., 2019). Future work on seismic anisotropy, from an observational as well as a mineral physics perspective, will help to illuminate the dynamic interactions among deep mantle structures, revealing the main driver(s) of flow.

What is the rheology of the deep mantle? More detailed knowledge about the relationships among different deep mantle structures and the patterns (Figure 16) of deep mantle flow will reveal information about their respective rheology. The effective viscosity in the deep mantle has been suggested to decrease as a function of depth as a consequence of the steep temperature gradient in D″ (e.g., Nakada & Karato, 2012). Lateral variations of the effective viscosity have also been suggested, due to changes in temperature and composition (e.g., Čadek & Fleitout, 2006). If the rheology of the deep mantle is laterally and radially variable as suggested, this will modify flow patterns, which can be inferred via observations of seismic anisotropy. For example, lateral contrasts in viscosity would manifest in how subducted slabs interact dynamically with LLVPs.

7. Summary and Outlook

In this work, we have reviewed methods to map and characterize lowermost mantle anisotropy, summarizing weaknesses, strengths, and directions for future improvements. We have explored how measurements of seismic anisotropy can be used to distinguish among different anisotropy-producing minerals, potentially helping to constrain deep mantle mineralogy. Combining seismological and mineral physics constraints, we are also now able to infer possible flow scenarios from observations of lowermost mantle anisotropy and compare them to predictions of geodynamical models. A main limitation in such work is the understanding of the deep Earth elastic properties, which continues to improve with advances in mineral physics. Promising previous and future work includes approaches that combine seismological, geodynamical and mineral physics results in interpretations of flow in the deepest mantle. With increasing seismic sampling of the lowermost mantle, new geodynamic modeling approaches, and progress in mineral physics, such an interdisciplinary strategy has potential to shed new light on important outstanding questions about deep Earth dynamics.

Data Availability Statement

No new data analysis was conducted in this work.

Acknowledgments
This work was funded by Yale University and by the U.S. National Science Foundation via Grant EAR-2026917 to MDL, Grant EAR-2054926 to ML, and Grant EAR-1853911 to EG. We are grateful for detailed comments by reviewers Barbara Romanowicz, Bernhard Steinberger, Poulami Roy, an anonymous reviewer, and editor Valerio Acocella that have helped us to improve the manuscript. We thank Shun Karato for helpful discussions.

References

AlpArray Seismic Network. (2015). *Z3—AlpArray seismic network (AASN) temporary component*. AlpArray Working Group. https://doi.org/10.12686/ALPARRAY/Z3_2015

Amaru, M. (2007). *Global travel time tomography with 3-D reference models* (Vol. 274). Utrecht University.

Ammann, M. W., Brodholt, J. P., Wookey, J., & Dobson, D. P. (2010). First-principles constraints on diffusion in lower-mantle minerals and a weak D″ layer. *Nature*, *465*(7297), 462–465. https://doi.org/10.1038/nature09052

Ando, M. (1984). ScS polarization anisotropy around the Pacific Ocean. *Journal of Physics of the Earth*, *32*(3), 179–195. https://doi.org/10.4294/jpe1952.32.179

Andrault, D., Pesce, G., Bouhifd, M., Bolfan, N., Hénot, J.-M., & Mezouar, M. (2014). Melting of subducted basalt at the core-mantle boundary. *Science*, *344*(6186), 892–895. https://doi.org/10.1126/science.125046

Asplet, J., Wookey, J., & Kendall, M. (2020). A potential post-perovskite province in D″ beneath the eastern Pacific: Evidence from new analysis of discrepant SKS–SKKS shear-wave splitting. *Geophysical Journal International*, *221*(3), 2075–2090. https://doi.org/10.1093/gji/ggaa114

Asplet, J., Wookey, J., & Kendall, M. (2023). Inversion of shear wave waveforms reveal deformation in the lowermost mantle. *Geophysical Journal International*, *232*(1), 97–114. https://doi.org/10.1093/gji/ggac328

Auer, L., Boschi, L., Becker, T. W., Nissen-Meyer, T., & Giardini, D. (2014). Savani: A variable resolution whole-mantle model of anisotropic shear velocity variations based on multiple data sets. *Journal of Geophysical Research: Solid Earth*, *119*(4), 3006–3034. https://doi.org/10.1002/2013JB010773

Backus, G. E. (1962). Long-wave elastic anisotropy produced by horizontal layering. *Journal of Geophysical Research*, *67*(11), 4427–4440. https://doi.org/10.1029/JZ067i011p04427

Backus, G. E. (1970). A geometrical picture of anisotropic elastic tensors. *Reviews of Geophysics*, *8*(3), 633–671. https://doi.org/10.1029/RG008i003p00633

Ballmer, M., Houser, C., Hernlund, J., Wentzcovitch, R., & Hirose, K. (2017). Persistence of strong silica-enriched domains in the earth's lower mantle. *Nature Geoscience*, *10*(3), 236–240. https://doi.org/10.1038/ngeo2898

Becker, T. W., & Lebedev, S. (2021). Dynamics of the upper mantle in light of seismic anisotropy. In *Mantle convection and surface expressions* (pp. 257–282). American Geophysical Union (AGU). https://doi.org/10.1002/9781119528609.ch10

Becker, T. W., Lebedev, S., & Long, M. D. (2012). On the relationship between azimuthal anisotropy from shear wave splitting and surface wave tomography. *Journal of Geophysical Research*, *117*(B1), B01306. https://doi.org/10.1029/2011JB008705

Beghein, C., Trampert, J., & van Heijst, H. J. (2006). Radial anisotropy in seismic reference models of the mantle. *Journal of Geophysical Research*, *111*(B2), B02303. https://doi.org/10.1029/2005JB003728

Borgeaud, A. F., Konishi, K., Kawai, K., & Geller, R. J. (2016). Finite frequency effects on apparent S-wave splitting in the D″ layer: Comparison between ray theory and full-wave synthetics. *Geophysical Journal International*, *207*(1), 12–28. https://doi.org/10.1093/gji/ggw254

Boschi, L., & Dziewonski, A. M. (2000). Whole Earth tomography from delay times of P, PcP, and PKP phases: Lateral heterogeneities in the outer core or radial anisotropy in the mantle? *Journal of Geophysical Research*, *105*(B6), 13675–13696. https://doi.org/10.1029/2000JB900059

Bower, D. J., Gurnis, M., & Seton, M. (2013). Lower mantle structure from paleogeographically constrained dynamic Earth models. *Geochemistry, Geophysics, Geosystems*, *14*(1), 44–63. https://doi.org/10.1029/2012GC004267

Bowman, J. R., & Ando, M. (1987). Shear-wave splitting in the upper-mantle wedge above the Tonga subduction zone. *Geophysical Journal of the Royal Astronomical Society*, *88*(1), 25–41. https://doi.org/10.1111/j.1365-246X.1987.tb01367.x

Browaeys, J. T., & Chevrot, S. (2004). Decomposition of the elastic tensor and geophysical applications. *Geophysical Journal International*, *159*(2), 667–678. https://doi.org/10.1111/j.1365-246X.2004.02415.x

Bull, A., McNamara, A., Becker, T., & Ritsema, J. (2010). Global scale models of the mantle flow field predicted by synthetic tomography models. *Physics of the Earth and Planetary Interiors*, *182*(3–4), 129–138. https://doi.org/10.1016/j.pepi.2010.03.004

Bullen, K. E. (1950). An Earth model based on a compressibility-pressure hypothesis. *Geophysical Journal International*, *6*, 50–59. https://doi.org/10.1111/j.1365-246X.1950.tb02973.x

Bunge, H.-P., Hagelberg, C. R., & Travis, B. J. (2003). Mantle circulation models with variational data assimilation: Inferring past mantle flow and structure from plate motion histories and seismic tomography. *Geophysical Journal International*, *152*(2), 280–301. https://doi.org/10.1046/j.1365-246X.2003.01823.x

Burke, K., Steinberger, B., Torsvik, T. H., & Smethurst, M. A. (2008). Plume generation zones at the margins of large low shear velocity provinces on the core–mantle boundary. *Earth and Planetary Science Letters*, *265*(1–2), 49–60. https://doi.org/10.1016/j.epsl.2007.09.042

Čadek, O., & Fleitout, L. (2006). Effect of lateral viscosity variations in the core-mantle boundary region on predictions of the long-wavelength geoid. *Studia Geophysica et Geodaetica*, *50*(2), 217–232. https://doi.org/10.1007/s11200-006-0013-0

Chandler, B. C., Chen, L.-W., Li, M., Romanowicz, B., & Wenk, H.-R. (2021). Seismic anisotropy, dominant slip systems and phase transitions in the lowermost mantle. *Geophysical Journal International*, *227*(3), 1665–1681. https://doi.org/10.1093/gji/ggab278

Chang, S.-J., Ferreira, A. M., Ritsema, J., van Heijst, H. J., & Woodhouse, J. H. (2014). Global radially anisotropic mantle structure from multiple datasets: A review, current challenges, and outlook. *Tectonophysics*, *617*, 1–19. https://doi.org/10.1016/j.tecto.2014.01.033

Chang, S.-J., Ferreira, A. M. G., Ritsema, J., van Heijst, H. J., & Woodhouse, J. H. (2015). Joint inversion for global isotropic and radially anisotropic mantle structure including crustal thickness perturbations. *Journal of Geophysical Research: Solid Earth*, *120*(6), 4278–4300. https://doi.org/10.1002/2014JB011824

Chevrot, S. (2000). Multichannel analysis of shear wave splitting. *Journal of Geophysical Research*, *105*(B9), 21579–21590. https://doi.org/10.1029/2000JB900199

Christensen, U. R., & Hofmann, A. W. (1994). Segregation of subducted oceanic crust in the convecting mantle. *Journal of Geophysical Research*, *99*(B10), 19867–19884. https://doi.org/10.1029/93JB03403

Čížková, H., van den Berg, A. P., Spakman, W., & Matyska, C. (2012). The viscosity of Earth's lower mantle inferred from sinking speed of subducted lithosphere. *Physics of the Earth and Planetary Interiors*, *200–201*, 56–62. https://doi.org/10.1016/j.pepi.2012.02.010

Cobden, L., Thomas, C., & Trampert, J. (2015). Seismic detection of post-perovskite inside the earth. In *The earth's heterogeneous mantle: A geophysical, geodynamical, and geochemical perspective* (pp. 391–440). https://doi.org/10.1007/978-3-319-15627-9_13

Cordier, P., Gouriet, K., Weidner, T., Van Orman, J., Castelnau, O., Jackson, J., & Carrez, P. (2023). Periclase deforms more slowly than bridgmanite under mantle conditions. *Nature*, *613*(7943), 303–307. https://doi.org/10.1038/s41586-022-05410-9

Cottaar, S., Li, M., McNamara, A. K., Romanowicz, B., & Wenk, H.-R. (2014). Synthetic seismic anisotropy models within a slab impinging on the core–mantle boundary. *Geophysical Journal International*, *199*(1), 164–177. https://doi.org/10.1093/gji/ggu244

Cottaar, S., & Romanowicz, B. (2013). Observations of changing anisotropy across the southern margin of the African LLSVP. *Geophysical Journal International*, *195*(2), 1184–1195. https://doi.org/10.1093/gji/ggt285

Crampin, S., & Lovell, J. H. (1991). A decade of shear-wave splitting in the earth's crust: What does it mean? What use can we make of it? And what should we do next? *Geophysical Journal International*, *107*(3), 387–407. https://doi.org/10.1111/j.1365-246X.1991.tb01401.x

Creasy, N., Long, M. D., & Ford, H. A. (2017). Deformation in the lowermost mantle beneath Australia from observations and models of seismic anisotropy. *Journal of Geophysical Research: Solid Earth*, *122*(7), 5243–5267. https://doi.org/10.1002/2016JB013901

Creasy, N., Miyagi, L., & Long, M. D. (2020). A library of elastic tensors for lowermost mantle seismic anisotropy studies and comparison with seismic observations. *Geochemistry, Geophysics, Geosystems*, *21*(4), e2019GC008883. https://doi.org/10.1029/2019GC008883

Creasy, N., Pisconti, A., Long, M. D., & Thomas, C. (2021). Modeling of seismic anisotropy observations reveals plausible lowermost mantle flow directions beneath Siberia. *Geochemistry, Geophysics, Geosystems*, *22*(10), e2021GC009924. https://doi.org/10.1029/2021GC009924

Creasy, N., Pisconti, A., Long, M. D., Thomas, C., & Wookey, J. (2019). Constraining lowermost mantle anisotropy with body waves: A synthetic modelling study. *Geophysical Journal International*, *217*(2), 766–783. https://doi.org/10.1093/gji/ggz049

Davaille, A., & Romanowicz, B. (2020). Deflating the LLSVPs: Bundles of mantle thermochemical plumes rather than thick stagnant "piles". *Tectonics*, *39*(10), e2020TC006265. https://doi.org/10.1029/2020TC006265

Davies, D. R., & Davies, J. (2009). Thermally-driven mantle plumes reconcile multiple hot-spot observations. *Earth and Planetary Science Letters*, *278*(1–2), 50–54. https://doi.org/10.1016/j.epsl.2008.11.027

Davies, D. R., Goes, S., & Lau, H. (2015). Thermally dominated deep mantle LLSVPs: A review. In *The earth's heterogeneous mantle: A geophysical, geodynamical, and geochemical perspective* (pp. 441–477). https://doi.org/10.1007/978-3-319-15627-9_14

Deng, J., Long, M. D., Creasy, N., Wagner, L., Beck, S., Zandt, G., et al. (2017). Lowermost mantle anisotropy near the eastern edge of the pacific LLSVP: Constraints from SKS-SKKS splitting intensity measurements. *Geophysical Journal International*, *210*(2), 774–786. https://doi.org/10.1093/gji/ggx190

Deuss, A. (2014). Heterogeneity and anisotropy of earth's inner core. *Annual Review of Earth and Planetary Sciences*, *42*(1), 103–126. https://doi.org/10.1146/annurev-earth-060313-054658

Ding, X., & Helmberger, D. V. (1997). Modelling D″ structure beneath Central America with broadband seismic data. *Physics of the Earth and Planetary Interiors*, *101*(3–4), 245–270. https://doi.org/10.1016/S0031-9201(97)00001-0

Dobrosavljevic, V. V., Sturhahn, W., & Jackson, J. M. (2019). Evaluating the role of iron-rich (Mg,Fe)O in ultralow velocity zones. *Minerals*, *9*(12), 762. https://doi.org/10.3390/min9120762

Dobrosavljevic, V. V., Zhang, D., Sturhahn, W., Chariton, S., Prakapenka, V., Zhao, J., et al. (2023). Melting and defect transitions in FeO up to pressures of Earth's core-mantle boundary. *Nature Communications*, *14*(1), 7336. https://doi.org/10.1038/s41467-023-43154-w

Dobson, D. P., Lindsay-Scott, A., Hunt, S. A., Bailey, E., Wood, I. G., Brodholt, J. P., et al. (2019). Anisotropic diffusion creep in postperovskite provides a new model for deformation at the core-mantle boundary. *Proceedings of the National Academy of Sciences*, *116*(52), 26389–26393. https://doi.org/10.1073/pnas.1914826116

Dziewonski, A. M., & Anderson, D. L. (1981). Preliminary reference earth model. *Physics of the Earth and Planetary Interiors*, *25*(4), 297–356. https://doi.org/10.1016/0031-9201(81)90046-7

Eilon, Z. C., Gaherty, J. B., Zhang, L., Russell, J., McPeak, S., Phillips, J., et al. (2021). The Pacific OBS research into convecting asthenosphere (ORCA) experiment. *Seismological Research Letters*, *93*(1), 477–493. https://doi.org/10.1785/0220210173

Fernando, B., Wolf, J., Leng, K., Nissen-Meyer, T., Eaton, W., Styczinski, M., et al. (2024). Axisem3d—An introduction to using the code and its applications. *EarthArXiv*. https://doi.org/10.31223/X5TH7P

Ferrick, A. L., & Korenaga, J. (2023). Long-term core–mantle interaction explains W-He isotope heterogeneities. *Proceedings of the National Academy of Sciences*, *120*(4), e2215903120. https://doi.org/10.1073/pnas.2215903120

Flament, N. (2018). Present-day dynamic topography and lower-mantle structure from palaeogeographically constrained mantle flow models. *Geophysical Journal International*, *216*(3), 2158–2182. https://doi.org/10.1093/gji/ggy526

Flament, N., Gurnis, M., & Müller, R. D. (2013). A review of observations and models of dynamic topography. *Lithosphere*, *5*(2), 189–210. https://doi.org/10.1130/L245.1

Flament, N., Williams, S., Müller, R. D., Gurnis, M., & Bower, D. J. (2017). Origin and evolution of the deep thermochemical structure beneath Eurasia. *Nature Communications*, *8*(1), 14164. https://doi.org/10.1038/ncomms14164

Ford, H. A., Long, M. D., He, X., & Lynner, C. (2015). Lowermost mantle flow at the eastern edge of the African large low shear velocity province. *Earth and Planetary Science Letters*, *420*, 12–22. https://doi.org/10.1016/j.epsl.2015.03.029

Ford, H. A., Long, M. D., & Wirth, E. A. (2016). Midlithospheric discontinuities and complex anisotropic layering in the mantle lithosphere beneath the Wyoming and Superior Provinces. *Journal of Geophysical Research: Solid Earth*, *121*(9), 6675–6697. https://doi.org/10.1002/2016JB012978

Ford, S. R., Garnero, E. J., & McNamara, A. K. (2006). A strong lateral shear velocity gradient and anisotropy heterogeneity in the lowermost mantle beneath the southern pacific. *Journal of Geophysical Research*, *111*(B3), B03306. https://doi.org/10.1029/2004JB003574

Forte, A. M., Simmons, N. A., & Grand, S. P. (2015). Constraints on seismic models from other disciplines—Implications for the global mantle convective flow. In *Treatise on geophysics* (pp. 853–907). https://doi.org/10.1016/B978-044452748-6.00027-4

Fouch, M. J., Fischer, K. M., & Wysession, M. E. (2001). Lowermost mantle anisotropy beneath the Pacific: Imaging the source of the Hawaiian plume. *Earth and Planetary Science Letters*, *190*(3–4), 167–180. https://doi.org/10.1016/S0012-821X(01)00380-6

French, S. W., & Romanowicz, B. A. (2014). Whole-mantle radially anisotropic shear velocity structure from spectral-element waveform tomography. *Geophysical Journal International*, *199*(3), 1303–1327. https://doi.org/10.1093/gji/ggu334

Fröhlich, Y., Grund, M., & Ritter, J. (2022). On the effects of wrongly aligned seismogram components for shear wave splitting analysis. *Annals of Geophysics*, *65*(22), SE207. https://doi.org/10.4401/ag-8781

Frost, D. A., Garnero, E., Creasy, N., Wolf, J., Bozdag, E., Long, M., et al. (2024). Heterogeneous mantle effects on the behavior of SmKS waves and outermost core imaging. *Geophysical Journal International*, *237*(3), 1655–1673. https://doi.org/10.1093/gji/ggae135

Fukao, Y., & Obayashi, M. (2013). Subducted slabs stagnant above, penetrating through, and trapped below the 660 km discontinuity. *Journal of Geophysical Research: Solid Earth*, *118*(11), 5920–5938. https://doi.org/10.1002/2013JB010466

Garnero, E. J., Grand, S. P., & Helmberger, D. V. (1993). Low P-wave velocity at the base of the mantle. *Geophysical Research Letters*, *20*(17), 1843–1846. https://doi.org/10.1029/93GL02009

Garnero, E. J., & Lay, T. (1997). Lateral variations in lowermost mantle shear wave anisotropy beneath the north Pacific and Alaska. *Journal of Geophysical Research*, *102*(B4), 8121–8135. https://doi.org/10.1029/96JB03830

Garnero, E. J., & Lay, T. (2003). D″ shear velocity heterogeneity, anisotropy and discontinuity structure beneath the Caribbean and Central America. *Physics of the Earth and Planetary Interiors*, *140*(1–3), 219–242. https://doi.org/10.1016/j.pepi.2003.07.014

Garnero, E. J., Maupin, V., Lay, T., & Fouch, M. J. (2004). Variable azimuthal anisotropy in Earth's lowermost Mantle. *Science*, *306*(5694), 259–261. https://doi.org/10.1126/science.1103411

Garnero, E. J., McNamara, A., & Shim, S.-H. (2016). Continent-sized anomalous zones with low seismic velocity at the base of Earth's mantle. *Nature Geoscience*, *9*(7), 481–489. https://doi.org/10.1038/ngeo2733

Garnero, E. J., & McNamara, A. K. (2008). Structure and dynamics of earth's lower mantle. *Science*, *320*(5876), 626–628. https://doi.org/10.1126/science.1148028

Garnero, E. J., Moore, M. M., Lay, T., & Fouch, M. J. (2004). Isotropy or weak vertical transverse isotropy in D″ beneath the Atlantic Ocean. *Journal of Geophysical Research*, *109*(B8), 1–10. https://doi.org/10.1029/2004JB003004

Ghosh, A., Becker, T. W., & Zhong, S. J. (2010). Effects of lateral viscosity variations on the geoid. *Geophysical Research Letters*, *37*(1), L01301. https://doi.org/10.1029/2009GL040426

Girard, J., Amulele, G., Farla, R., Mohiuddin, A., & ichiro Karato, S. (2016). Shear deformation of bridgmanite and magnesiowüstite aggregates at lower mantle conditions. *Science*, *351*(6269), 144–147. https://doi.org/10.1126/science.aad3113

Goryaeva, A., Carrez, P., & Cordier, P. (2016). Low viscosity and high attenuation in $MgSiO_3$ post-perovskite inferred from atomic-scale calculations. *Scientific Reports*, *6*(1), 34771. https://doi.org/10.1038/srep34771

Goryaeva, A., Carrez, P., & Cordier, P. (2017). Modeling defects and plasticity in $MgSiO_3$ post-perovskite: Part 3—Screw and edge [001] dislocations. *Physics and Chemistry of Minerals*, *44*(7), 521–533. https://doi.org/10.1007/s00269-017-0879-0

Grand, S., van der Hilst, R., & Widiyantoro, S. (1997). Global seismic tomography: A snapshot of convection in the earth. *Geological Society America Today*, *7*, 1–7.

Grund, M., & Ritter, J. R. (2019). Widespread seismic anisotropy in Earth's lowermost mantle beneath the Atlantic and Siberia. *Geology*, *47*(2), 123–126. https://doi.org/10.1130/G45514.1

Hager, B. H. (1984). Subducted slabs and the geoid: Constraints on mantle rheology and flow. *Journal of Geophysical Research*, *89*(B7), 6003–6015. https://doi.org/10.1029/JB089iB07p06003

Hager, B. H., Clayton, R., Richards, M., Comer, R., & Am, D. (1985). Lower mantle heterogeneity, dynamic topography and the geoid. *Nature*, *313*(6003), 541–545. https://doi.org/10.1038/313541a0

Hager, B. H., & O'Connell, R. (1981). A simple global model of plate dynamics and mantle convection. *Journal of Geophysical Research*, *86*(B6), 4843–4867. https://doi.org/10.1029/jb086ib06p04843

Hager, B. H., & Richards, M. A. (1989). Long-wavelength variations in earth's geoid: Physical models and dynamical implications. *Philosophical Transactions of the Royal Society of London*, *328*(1599), 309–327. https://doi.org/10.1098/rsta.1989.0038

Hansen, L. N., Faccenda, M., & Warren, J. M. (2021). A review of mechanisms generating seismic anisotropy in the upper mantle. *Physics of the Earth and Planetary Interiors*, *313*, 106662. https://doi.org/10.1016/j.pepi.2021.106662

Hansen, S. E., Garnero, E. J., Li, M., Shim, S.-H., & Rost, S. (2023). Globally distributed subducted materials along the Earth's core-mantle boundary: Implications for ultralow velocity zones. *Science Advances*, *9*(14), eadd4838. https://doi.org/10.1126/sciadv.add4838

Hernlund, J., Thomas, C., & Tackley, P. (2005). A doubling of the post-perovskite phase boundary and structure of the Earth's lowermost mantle. *Nature*, *434*(7035), 882–886. https://doi.org/10.1016/10.1038/nature03472

Heyn, B. H., Conrad, C. P., & Trønnes, R. G. (2020). How thermochemical piles can (periodically) generate plumes at their edges. *Journal of Geophysical Research: Solid Earth*, *125*(6), e2019JB018726. https://doi.org/10.1029/2019JB018726

Hirose, K., Fei, Y., Ma, Y., & Mao, H.-K. (1999). The fate of subducted basaltic crust in the Earth's lower mantle. *Nature*, *6714*, 53–56. https://doi.org/10.1038/16225

Horbach, A., Bunge, H.-P., & Oeser, J. (2014). The adjoint method in geodynamics: Derivation from a general operator formulation and application to the initial condition problem in a high resolution mantle circulation model. *GEM International Journal on Geomathematics*, *5*(2), 163–194. https://doi.org/10.1007/s13137-014-0061-5

Houser, C., Masters, G., Shearer, P., & Laske, G. (2008). Shear and compressional velocity models of the mantle from cluster analysis of long-period waveforms. *Geophysical Journal International*, *174*(1), 195–212. https://doi.org/10.1111/j.1365-246X.2008.03763.x

Hudson, T., Asplet, J., & Walker, A. (2023). Automated shear-wave splitting analysis for single- and multi-layer anisotropic media. *Seismica*, *2*, 3. https://doi.org/10.26443/seismica.v2i2.1031

Hunt, S., Weidner, D., Li, L., Wang, L., Walte, N., Brodholt, J., & Dobson, D. (2009). Weakening of calcium iridate during its transformation from perovskite to post-perovskite. *Nature Geoscience*, *2*(11), 794–797. https://doi.org/10.1038/ngeo663

Irifune, T., & Tsuchiya, T. (2007). Mineralogy of the earth—Phase transitions and mineralogy of the lower mantle. In *Treatise on geophysics* (Vol. 2, pp. 33–62). https://doi.org/10.1016/B978-044452748-6.00030-4

IRIS Transportable Array. (2003). *USArray transportable array*. International Federation of Digital Seismograph Networks. https://doi.org/10.7914/SN/TA

Ishii, M., & Tromp, J. (1999). Normal-Mode and free-air gravity constraints on lateral variations in velocity and density of earth's mantle. *Science*, *285*(5431), 1231–1236. https://doi.org/10.1126/science.285.5431.1231

Karato, S.-I. (1998). Some remarks on the origin of seismic anisotropy in the D′′ layer. *Earth Planets and Space*, *50*(11–12), 1019–1028. https://doi.org/10.1186/BF03352196

Karato, S.-I. (2011). Rheological structure of the mantle of a super-earth: Some insights from mineral physics. *Icarus*, *212*(1), 14–23. https://doi.org/10.1016/j.icarus.2010.12.005

Karato, S.-I. (2014). Does partial melting explain geophysical anomalies? *Physics of the Earth and Planetary Interiors*, *228*, 300–306. https://doi.org/10.1016/j.pepi.2013.08.006

Karato, S.-I., Jung, H., Katayama, I., & Skemer, P. (2008). Geodynamic significance of seismic anisotropy of the upper mantle: New insights from laboratory studies. *Annual Review of Earth and Planetary Sciences*, *36*(1), 59–95. https://doi.org/10.1146/annurev.earth.36.031207.124120

Karato, S.-I., & Wu, P. (1993). Rheology of the upper mantle: A synthesis. *Science*, *260*(5109), 771–778. https://doi.org/10.1126/science.260.5109.771

Karki, B. B., Wentzcovitch, R. M., de Gironcoli, S., & Baroni, S. (1999). First-Principles determination of elastic anisotropy and wave velocities of MgO at lower mantle conditions. *Science*, *286*(5445), 1705–1707. https://doi.org/10.1126/science.287.5450.41f

Kawai, K., & Geller, R. J. (2010). Waveform inversion for localized seismic structure and an application to D″ structure beneath the Pacific. *Journal of Geophysical Research*, *115*(B1), B07308. https://doi.org/10.1029/2009JB006503

Kawai, K., & Tsuchiya, T. (2009). Temperature profile in the lowermost mantle from seismological and mineral physics joint modeling. *Proceedings of the National Academy of Sciences*, *106*(52), 22119–22123. https://doi.org/10.1073/pnas.0905920106

Keller, D., Tassara, S., Robbins, L., Lee, C.-T., Ague, J., & Dasgupta, R. (2023). Links between large igneous province volcanism and subducted iron formations. *Nature Geoscience*, *16*(6), 1–7. https://doi.org/10.1038/s41561-023-01188-1

Kellogg, L. H. (1997). Growing the Earth's D′′ layer: Effect of density variations at the core-mantle boundary. *Geophysical Research Letters*, *24*(22), 2749–2752. https://doi.org/10.1029/97GL02952

Kendall, J.-M., & Silver, P. (1996). Constraints from seismic anisotropy on the nature of the lower mantle. *Nature*, *381*(6581), 409–412. https://doi.org/10.1038/381409a0

Kendall, J.-M., & Silver, P. (1998). Investigating causes of D′′ anisotropy, in the Core-Mantle Boundary Region. Core–mantle boundary region. *Geodynamics Series*, *28*, 97–118.

Kennett, B. L. N., & Engdahl, E. R. (1991). Traveltimes for global earthquake location and phase identification. *Geophysical Journal International*, *105*(2), 429–465. https://doi.org/10.1111/j.1365-246X.1991.tb06724.x

Kido, M., Yuen, D. A., Čadek, O., & Nakakuki, T. (1998). Mantle viscosity derived by genetic algorithm using oceanic geoid and seismic tomography for whole-mantle versus blocked-flow situations. *Physics of the Earth and Planetary Interiors*, *107*(4), 307–326. https://doi.org/10.1016/S0031-9201(98)00077-6

Kiefer, W. S., & Kellogg, L. H. (1998). Geoid anomalies and dynamic topography from time-dependent, spherical axisymmetric mantle convection. *Physics of the Earth and Planetary Interiors*, *106*(3–4), 237–256. https://doi.org/10.1016/S0031-9201(98)00078-8

Ko, B., Chariton, S., Prakapenka, V., Chen, B., Garnero, E. J., Li, M., & Shim, S.-H. (2022). Water-induced diamond formation at earth's core-mantle boundary. *Geophysical Research Letters*, *49*(16), e2022GL098271. https://doi.org/10.1029/2022GL098271

Kocks, U., Tomé, C., & Wenk, H. (2000). *Texture and anisotropy: Preferred orientations in polycrystals and their effect on materials properties*. Cambridge University Press.

Koelemeijer, P., Deuss, A., & Ritsema, J. (2017). Density structure of Earth's lowermost mantle from Stoneley mode splitting observations. *Earth and Planetary Science Letters*, *8*, 1–10. https://doi.org/10.1038/ncomms15241

Koelemeijer, P., Ritsema, J., Deuss, A., & van Heijst, H.-J. (2015). SP12RTS: A degree-12 model of shear- and compressional-wave velocity for earth's mantle. *Geophysical Journal International*, *204*(2), 1024–1039. https://doi.org/10.1093/gji/ggv481

Koelemeijer, P., Schuberth, B., Davies, D., Deuss, A., & Ritsema, J. (2018). Constraints on the presence of post-perovskite in Earth's lowermost mantle from tomographic-geodynamic model comparisons. *Earth and Planetary Science Letters*, *494*, 226–238. https://doi.org/10.1016/j.epsl.2018.04.056

Kohlstedt, D., & Hansen, L. (2015). Constitutive equations, rheological behavior, and viscosity of rocks. In *Mineral physics* (pp. 441–472). https://doi.org/10.1016/B978-0-444-53802-4.00042-7

Komatitsch, D., Vinnik, L. P., & Chevrot, S. (2010). SH_{diff}-SV_{diff} splitting in an isotropic Earth. *Journal of Geophysical Research*, *115*(B7), B07312. https://doi.org/10.1029/2009JB006795

Kustowski, B., Ekström, G., & Dziewoński, A. M. (2008). Anisotropic shear-wave velocity structure of the earth's mantle: A global model. *Journal of Geophysical Research*, *113*(B6), B06306. https://doi.org/10.1029/2007JB005169

Labrosse, S., Hernlund, J., & Coltice, N. (2008). A crystallizing dense magma ocean at the base of the Earth's mantle. *Nature*, *450*(7171), 866–869. https://doi.org/10.1038/nature06355

Lai, H., & Garnero, E. J. (2020). Travel time and waveform measurements of global multibounce seismic waves using virtual station seismogram stacks. *Geochemistry, Geophysics, Geosystems*, *21*(1), e2019GC008679. https://doi.org/10.1029/2019GC008679

Lai, V. H., Helmberger, D. V., Dobrosavljevic, V. V., Wu, W., Sun, D., Jackson, J. M., & Gurnis, M. (2022). Strong ULVZ and slab interaction at the northeastern edge of the Pacific LLSVP favors plume generation. *Geochemistry, Geophysics, Geosystems*, *23*(2), e2021GC010020. https://doi.org/10.1029/2021GC010020

Lau, H., Mitrovica, J., Davis, J., Tromp, J., Yang, H.-Y., & Al-Attar, D. (2017). Tidal tomography constrains Earth's deep-mantle buoyancy. *Nature*, *551*(7680), 321–326. https://doi.org/10.1038/nature24452

Lay, T., & Helmberger, D. V. (1983). The shear-wave velocity gradient at the base of the mantle. *Journal of Geophysical Research*, *88*(B10), 8160–8170. https://doi.org/10.1029/JB088iB10p08160

Lay, T., Hernlund, J., & Buffett, B. (2008). Core–mantle boundary heat flow. *Nature Geoscience*, *1*, 25–32. https://doi.org/10.1038/ngeo.2007.44

Lay, T., Williams, Q., Garnero, E. J., Kellogg, L., & Wysession, M. E. (1998). Seismic wave anisotropy in the D′′ region and its implications. In *The core-mantle boundary region* (pp. 299–318). American Geophysical Union (AGU). https://doi.org/10.1029/GD028p0299

Lay, T., & Young, C. J. (1991). Analysis of seismic SV waves in the core's penumbra. *Geophysical Research Letters*, *18*(8), 1373–1376. https://doi.org/10.1029/91GL01691

Lebensohn, R., & Tomé, C. (1993). A self-consistent anisotropic approach for the simulation of plastic deformation and texture development of polycrystals: Application to zirconium alloys. *Acta Metallurgica et Materialia*, *41*(9), 2611–2624. https://doi.org/10.1016/0956-7151(93)90130-K

Lei, W., Ruan, Y., Bozdağ, E., Peter, D., Lefebvre, M., Komatitsch, D., et al. (2020). Global adjoint tomography—Model GLAD-M25. *Geophysical Journal International*, *223*, 1–21. https://doi.org/10.1093/gji/ggaa253

Lekic, V., Cottaar, S., Dziewonski, A., & Romanowicz, B. (2012). Cluster analysis of global lower mantle tomography: A new class of structure and implications for chemical heterogeneity. *Earth and Planetary Science Letters*, *357–358*, 68–77. https://doi.org/10.1016/j.epsl.2012.09.014

Leng, K., Nissen-Meyer, T., & van Driel, M. (2016). Efficient global wave propagation adapted to 3-D structural complexity: A pseudospectral/spectral-element approach. *Geophysical Journal International*, *207*(3), 1700–1721. https://doi.org/10.1093/gji/ggw363

Leng, K., Nissen-Meyer, T., van Driel, M., Hosseini, K., & Al-Attar, D. (2019). AxiSEM3D: Broad-band seismic wavefields in 3-D global earth models with undulating discontinuities. *Geophysical Journal International*, *217*(3), 2125–2146. https://doi.org/10.1093/gji/ggz092

Li, M. (2020). The formation of hot thermal anomalies in cold subduction-influenced regions of earth's lowermost mantle. *Journal of Geophysical Research: Solid Earth*, *125*(6), e2019JB019312. https://doi.org/10.1029/2019JB019312

Li, M. (2021). The cycling of subducted oceanic crust in the earth's deep mantle. In *Mantle convection and surface expressions* (pp. 303–328). American Geophysical Union (AGU). https://doi.org/10.1002/9781119528609.ch12

Li, M. (2023a). The influence of uncertain mantle density and viscosity structures on the calculations of deep mantle flow and lateral motion of plumes. *Geophysical Journal International*, *233*(3), 1916–1937. https://doi.org/10.1093/gji/ggad040

Li, M. (2023b). Variable distribution of subducted oceanic crust beneath subduction regions of the lowermost mantle. *Physics of the Earth and Planetary Interiors*, *341*, 107063. https://doi.org/10.1016/j.pepi.2023.107063

Li, M., & McNamara, A. K. (2022). Evolving morphology of crustal accumulations in earth's lowermost mantle. *Earth and Planetary Science Letters*, *577*, 117265. https://doi.org/10.1016/j.epsl.2021.117265

Li, M., Wolf, J., Garnero, E., & Long, M. (2024). Flow and deformation in Earth's deepest mantle from geodynamic modeling and implications for seismic anisotropy. *ESS Open Archive*. https://doi.org/10.22541/essoar.171052495.57595075/v1

Li, M., & Zhong, S. (2017). The source location of mantle plumes from 3D spherical models of mantle convection. *Earth and Planetary Science Letters*, *478*, 47–57. https://doi.org/10.1016/j.epsl.2017.08.033

Li, M., & Zhong, S. (2019). Lateral motion of mantle plumes in 3-d geodynamic models. *Geophysical Research Letters*, *46*(9), 4685–4693. https://doi.org/10.1029/2018GL081404

Lin, F., Hilairet, N., Raterron, P., Addad, A., Immoor, J., Marquardt, H., et al. (2017). Elasto-viscoplastic self consistent modeling of the ambient temperature plastic behavior of periclase deformed up to 5.4 GPa. *Journal of Applied Physics*, *122*(20), 205902. https://doi.org/10.1063/1.4999951

Lin, Y., Zhao, L., & Hung, S.-H. (2014). Full-wave effects on shear wave splitting. *Geophysical Research Letters*, *41*(3), 799–804. https://doi.org/10.1002/2013GL058742

Link, F., Reiss, M. C., & Rümpker, G. (2022). An automatized XKS-splitting procedure for large data sets: Extension package for SplitRacer and application to the USArray. *Computers & Geosciences*, *158*, 104961. https://doi.org/10.1016/j.cageo.2021.104961

Lithgow-Bertelloni, C., & Silver, P. (1998). Dynamic topography, plate driving forces and the African Superswell. *Nature*, *395*(6699), 269–272. https://doi.org/10.1038/26212

Liu, L., & Gurnis, M. (2008). Simultaneous inversion of mantle properties and initial conditions using an adjoint of mantle convection. *Journal of Geophysical Research*, *113*(B8), B08405. https://doi.org/10.1029/2008JB005594

Liu, X., & Zhong, S. (2016). Constraining mantle viscosity structure for a thermochemical mantle using the geoid observation. *Geochemistry, Geophysics, Geosystems*, *17*(3), 895–913. https://doi.org/10.1002/2015GC006161

Long, M. D. (2009). Complex anisotropy in D′′ beneath the eastern Pacific from SKS–SKKS splitting discrepancies. *Earth and Planetary Science Letters*, *283*(1–4), 181–189. https://doi.org/10.1016/j.epsl.2009.04.019

Long, M. D. (2013). Constraints on subduction geodynamics from seismic anisotropy. *Reviews of Geophysics*, *51*(1), 76–112. https://doi.org/10.1002/rog.20008

Long, M. D., & Becker, T. (2010). Mantle dynamics and seismic anisotropy. *Earth and Planetary Science Letters*, *297*(3–4), 341–354. https://doi.org/10.1016/j.epsl.2010.06.036

Long, M. D., & Silver, P. G. (2009). Shear wave splitting and mantle anisotropy: Measurements, interpretations, and new directions. *Surveys in Geophysics*, *30*(4–5), 407–461. https://doi.org/10.1007/s10712-009-9075-1

Long, M. D., Xiao, X., Jiang, Z., Evans, B., & ichiro Karato, S. (2006). Lattice preferred orientation in deformed polycrystalline (Mg,Fe)O and implications for seismic anisotropy in D″. *Physics of the Earth and Planetary Interiors*, *156*(1–2), 75–88. https://doi.org/10.1016/j.pepi.2006.02.006

Lowman, J. P., King, S. D., & Gable, C. W. (2004). Steady plumes in viscously stratified, vigorously convecting, three-dimensional numerical mantle convection models with mobile plates. *Geochemistry, Geophysics, Geosystems*, *5*(1), Q01L01. https://doi.org/10.1029/2003GC000583

Lutz, K., Long, M., Creasy, N., & Deng, J. (2020). Seismic anisotropy in the lowermost mantle beneath North America from SKS-SKKS splitting intensity discrepancies. *Physics of the Earth and Planetary Interiors*, *305*, 106504. https://doi.org/10.1016/j.pepi.2020.106504

Lynner, C., & Long, M. D. (2013). Sub-slab seismic anisotropy and mantle flow beneath the Caribbean and Scotia subduction zones: Effects of slab morphology and kinematics. *Earth and Planetary Science Letters*, *361*, 367–378. https://doi.org/10.1016/j.epsl.2012.11.007

Lynner, C., & Long, M. D. (2014). Lowermost mantle anisotropy and deformation along the boundary of the African LLSVP. *Geophysical Research Letters*, *41*(10), 3447–3454. https://doi.org/10.1002/2014GL059875

Manga, M., & Jeanloz, R. (1996). Implications of a metal-bearing chemical boundary layer in D″ for mantle dynamics. *Geophysical Research Letters*, *23*(22), 3091–3094. https://doi.org/10.1029/96GL03021

Mao, W., & Zhong, S. (2019). Controls on global mantle convective structures and their comparison with seismic models. *Journal of Geophysical Research: Solid Earth*, *124*(8), 9345–9372. https://doi.org/10.1029/2019JB017918

Mao, W., & Zhong, S. (2021). Constraints on mantle viscosity from intermediate-wavelength geoid anomalies in mantle convection models with plate motion history. *Journal of Geophysical Research: Solid Earth*, *126*(4), e2020JB021561. https://doi.org/10.1029/2020JB021561

Marquardt, H., & Miyagi, L. (2015). Slab stagnation in the shallow lower mantle linked to an increase in mantle viscosity. *Nature Geoscience*, *8*(4), 311–314. https://doi.org/10.1038/ngeo2393

Matzel, E., Sen, M. K., & Grand, S. P. (1996). Evidence for anisotropy in the deep mantle beneath Alaska. *Geophysical Research Letters*, *23*(18), 2417–2420. https://doi.org/10.1029/96GL02186

Maupin, V., Garnero, E. J., Lay, T., & Fouch, M. J. (2005). Azimuthal anisotropy in the D″ layer beneath the Caribbean. *Journal of Geophysical Research*, *110*(B8), B08301. https://doi.org/10.1029/2004JB003506

McNamara, A. K. (2019). A review of large low shear velocity provinces and ultra low velocity zones. *Tectonophysics*, *760*, 199–220. https://doi.org/10.1016/j.tecto.2018.04.015

McNamara, A. K., Garnero, E. J., & Rost, S. (2010). Tracking deep mantle reservoirs with ultra-low velocity zones. *Earth and Planetary Science Letters*, *299*(1–2), 1–9. https://doi.org/10.1016/j.epsl.2010.07.042

McNamara, A. K., van Keken, P., & Karato, S.-I. (2002). Development of anisotropic structure in the Earth's lower mantle by solid-state convection. *Nature*, *416*(6878), 310–314. https://doi.org/10.1038/416310a

McNamara, A. K., van Keken, P. E., & Karato, S.-I. (2003). Development of finite strain in the convecting lower mantle and its implications for seismic anisotropy. *Journal of Geophysical Research*, *108*(B5), 2230. https://doi.org/10.1029/2002JB001970

McNamara, A. K., & Zhong, S. (2005). Degree-one mantle convection: Dependence on internal heating and temperature-dependent rheology. *Geophysical Research Letters*, *32*(1), L01301. https://doi.org/10.1029/2004GL021082

Meade, C., Silver, P. G., & Kaneshima, S. (2005). Laboratory and seismological observations of lower mantle isotropy. *Geophysical Research Letters*, *22*(10), 1293–1296. https://doi.org/10.1029/95GL01091

Megnin, C., & Romanowicz, B. (2000). The shear velocity structure of the mantle from the inversion of of body, surface and higher modes waveforms. *Geophysical Journal International*, *143*(3), 709–728. https://doi.org/10.1046/j.1365-246X.2000.00298.x

Merkel, S., McNamara, A. K., Kubo, A., Speziale, S., Miyagi, L., Meng, Y., et al. (2007). Deformation of (Mg,Fe)SiO_3 post-perovskite and D″ anisotropy. *Science*, *316*(5832), 1729–1732. https://doi.org/10.1126/science.1140609

Mitchell, B. J., & Helmberger, D. V. (1973). Shear velocities at the base of the mantle from observations of s and scs. *Journal of Geophysical Research*, *78*(26), 6009–6020. https://doi.org/10.1029/JB078i026p06009

Mitrovica, J., & Forte, A. (2004). A new inference of mantle viscosity based upon joint inversion of convection and glacial isostatic adjustment data. *Earth and Planetary Science Letters*, *225*(1–2), 177–189. https://doi.org/10.1016/j.epsl.2004.06.005

Miyagi, L., Nishiyama, N., Wang, Y., Kubo, A., West, D. V., Cava, R. J., et al. (2008). Deformation and texture development in $CaIrO_3$ post-perovskite phase up to 6 GPa and 1300 K. *Earth and Planetary Science Letters*, *268*(3–4), 515–525. https://doi.org/10.1016/j.epsl.2008.02.005

Montagner, J.-P., & Kennett, B. L. N. (1996). How to reconcile body-wave and normal-mode reference earth models. *Geophysical Journal International*, *125*(1), 229–248. https://doi.org/10.1111/j.1365-246X.1996.tb06548.x

Moore, M. M., Garnero, E. J., Lay, T., & Williams, Q. (2004). Shear wave splitting and waveform complexity for lowermost mantle structures with low-velocity lamellae and transverse isotropy. *Journal of Geophysical Research*, *109*(B2), 1–26. https://doi.org/10.1029/2003JB002546

Moulik, P., & Ekström, G. (2014). An anisotropic shear velocity model of the Earth's mantle using normal modes, body waves, surface waves and long-period waveforms. *Geophysical Journal International*, *199*(3), 1713–1738. https://doi.org/10.1093/gji/ggu356

Mundl-Petermeier, A. (2021). Core mantle interactions. In D. Alderton & S. A. Elias (Eds.), *Encyclopedia of geology* (2nd ed., pp. 270–277). Academic Press. https://doi.org/10.1016/B978-0-08-102908-4.00094-1

Murakami, M., Hirose, K., Kawamura, K., Sata, N., & Ohishi, Y. (2004). Post-perovskite phase transition in $MgSiO_3$. *Science*, *304*(5672), 855–858. https://doi.org/10.1126/science.1095932

Nakada, M., & Karato, S.-I. (2012). Low viscosity of the bottom of the earth's mantle inferred from the analysis of chandler wobble and tidal deformation. *Physics of the Earth and Planetary Interiors*, *192–193*, 68–80. https://doi.org/10.1016/j.pepi.2011.10.001

Nakagawa, T., Tackley, P. J., Deschamps, F., & Connolly, J. A. (2010). The influence of MORB and harzburgite composition on thermo-chemical mantle convection in a 3-D spherical shell with self-consistently calculated mineral physics. *Earth and Planetary Science Letters*, *296*(3–4), 403–412. https://doi.org/10.1016/j.epsl.2010.05.026

Niu, F., & Perez, A. M. (2004). Seismic anisotropy in the lower mantle: A comparison of waveform splitting of SKS and SKKS. *Geophysical Research Letters*, *31*(24), L24612. https://doi.org/10.1029/2004GL021196

Nowacki, A., & Cottaar, S. (2021). Toward imaging flow at the base of the mantle with seismic, mineral physics, and geodynamic constraints. In *Mantle convection and surface expressions* (pp. 329–352). American Geophysical Union (AGU). https://doi.org/10.1002/9781119528609.ch13

Nowacki, A., & Wookey, J. (2016). The limits of ray theory when measuring shear wave splitting in the lowermost mantle with ScS waves. *Geophysical Journal International*, *207*(3), 1573–1583. https://doi.org/10.1093/gji/ggw358

Nowacki, A., Wookey, J., & Kendall, J.-M. (2010). Deformation of the lowermost mantle from seismic anisotropy. *Nature*, *467*(7319), 1091–1094. https://doi.org/10.1038/nature09507

Nowacki, A., Wookey, J., & Kendall, J.-M. (2011). New advances in using seismic anisotropy, mineral physics and geodynamics to understand deformation in the lowermost mantle. *Journal of Geodynamics*, *52*(3–4), 205–228. https://doi.org/10.1016/j.jog.2011.04.003

Otsuka, K., & Karato, S.-I. (2012). Deep penetration of molten iron into the mantle caused by a morphological instability. *Nature*, *492*(7428), 243–246. https://doi.org/10.1038/nature11663

Panasyuk, S. V., & Hager, B. H. (2000). Models of isostatic and dynamic topography, geoid anomalies, and their uncertainties. *Journal of Geophysical Research*, *105*(B12), 28199–28209. https://doi.org/10.1029/2000JB900249

Panning, M., Lekić, V., & Romanowicz, B. A. (2010). Importance of crustal corrections in the development of a new global model of radial anisotropy. *Journal of Geophysical Research*, *115*(B12), B12325. https://doi.org/10.1029/2010JB007520

Panning, M., & Romanowicz, B. (2006). A three-dimensional radially anisotropic model of shear velocity in the whole mantle. *Geophysical Journal International*, *167*(1), 361–379. https://doi.org/10.1111/j.1365-246X.2006.03100.x

Parisi, L., Ferreira, A. M. G., & Ritsema, J. (2018). Apparent splitting of S waves propagating through an isotropic lowermost mantle. *Journal of Geophysical Research: Solid Earth*, *123*(5), 3909–3922. https://doi.org/10.1002/2017JB014394

Pisconti, A., Creasy, N., Wookey, J., Long, M. D., & Thomas, C. (2023). Mineralogy, fabric and deformation domains in D″ across the southwestern border of the African LLSVP. *Geophysical Journal International*, *232*(1), 705–724. https://doi.org/10.1093/gji/ggac359

Pisconti, A., Thomas, C., & Wookey, J. (2019). Discriminating between causes of D″ anisotropy using reflections and splitting measurements for a single path. *Journal of Geophysical Research: Solid Earth*, *124*(5), 4811–4830. https://doi.org/10.1029/2018JB016993

Pulliam, J., & Sen, M. K. (1998). Seismic anisotropy in the core—Mantle transition zone. *Geophysical Journal International*, *135*(1), 113–128. https://doi.org/10.1046/j.1365-246X.1998.00612.x

Qayyum, A., Lom, N., Advokaat, E. L., Spakman, W., van der Meer, D. G., & van Hinsbergen, D. J. J. (2022). Subduction and slab detachment under moving trenches during ongoing India-Asia convergence. *Geochemistry, Geophysics, Geosystems*, *23*(11), e2022GC010336. https://doi.org/10.1029/2022GC010336

Rao, P. B., Kumar, M., & Singh, A. (2017). Anisotropy in the lowermost mantle beneath the Indian Ocean Geoid Low from ScS splitting measurements. *Geochemistry, Geophysics, Geosystems*, *18*, 13385–13393. https://doi.org/10.1002/2016GC006604

Reiss, M. C., Long, M. D., & Creasy, N. (2019). Lowermost mantle anisotropy beneath Africa from differential SKS-SKKS shear-wave splitting. *Journal of Geophysical Research: Solid Earth*, *124*(8), 8540–8564. https://doi.org/10.1029/2018JB017160

Reiss, M. C., & Rümpker, G. (2017). SplitRacer: MATLAB code and GUI for semiautomated analysis and interpretation of teleseismic shear-wave splitting. *Seismological Research Letters*, *88*(2A), 392–409. https://doi.org/10.1785/0220160191

Richards, F. D., Hoggard, M. J., Ghelichkhan, S., Koelemeijer, P., & Lau, H. C. (2023). Geodynamic, geodetic, and seismic constraints favour deflated and dense-cored LLVPs. *Earth and Planetary Science Letters*, *602*, 117964. https://doi.org/10.1016/j.epsl.2022.117964

Ritsema, J. (2000). Evidence for shear velocity anisotropy in the lowermost mantle beneath the Indian Ocean. *Geophysical Research Letters*, *27*(7), 1041–1044. https://doi.org/10.1029/1999GL011037

Ritsema, J., Deuss, A., van Heijst, H. J., & Woodhouse, J. H. (2011). S40RTS: A degree-40 shear-velocity model for the mantle from new Rayleigh wave dispersion, teleseismic traveltime and normal-mode splitting function measurements. *Geophysical Journal International*, *184*(3), 1223–1236. https://doi.org/10.1111/j.1365-246X.2010.04884.x

Ritsema, J., Garnero, E., & Lay, T. (1997). A strongly negative shear velocity gradient and lateral variability in the lowermost mantle beneath the Pacific. *Journal of Geophysical Research*, *102*(B9), 20395–20411. https://doi.org/10.1029/97JB01507

Ritsema, J., Lay, T., Garnero, E. J., & Benz, H. (1998). Seismic anisotropy in the lowermost mantle beneath the Pacific. *Geophysical Research Letters*, *25*(8), 1229–1232. https://doi.org/10.1029/98GL00913

Ritsema, J., Ni, S., Helmberger, D. V., & Crotwell, H. P. (1998). Evidence for strong shear velocity reductions and velocity gradients in the lower mantle beneath Africa. *Geophysical Research Letters*, *25*(23), 4245–4248. https://doi.org/10.1029/1998GL900127

Rokosky, J. M., Lay, T., & Garnero, E. J. (2006). Small-scale lateral variations in azimuthally anisotropic D″ structure beneath the Cocos Plate. *Earth and Planetary Science Letters*, *248*(1–2), 411–425. https://doi.org/10.1016/j.epsl.2006.06.005

Rokosky, J. M., Lay, T., Garnero, E. J., & Russell, S. A. (2004). High-resolution investigation of shear wave anisotropy in D″ beneath the Cocos Plate. *Geophysical Research Letters*, *31*(7), L07605. https://doi.org/10.1029/2003GL018902

Romanowicz, B., & Wenk, H.-R. A. (2017). Anisotropy in the deep earth. *Physics of the Earth and Planetary Interiors*, *269*, 58–90. https://doi.org/10.1016/j.pepi.2017.05.005

Rubey, M., Brune, S., Heine, C., Davies, D. R., Williams, S., & Müller, D. (2017). Global patterns in earth's dynamic topography since the Jurassic: The role of subducted slabs. *Solid Earth*, *8*(5), 899–919. https://doi.org/10.5194/se-8-899-2017

Rudolph, M., Leki, V., & Lithgow-Bertelloni, C. (2015). Viscosity jump in Earth's mid-mantle. *Science*, *350*(6266), 1349–1352. https://doi.org/10.1126/science.aad1929

Russell, S. A., Lay, T., & Garnero, E. J. (1998). Seismic evidence for small-scale dynamics in the lowermost mantle at the root of the Hawaiian hotspot. *Nature*, *396*(6708), 255–258. https://doi.org/10.1038/24364

Russell, S. A., Lay, T., & Garnero, E. J. (1999). Small-scale lateral shear velocity and anisotropy heterogeneity near the core-mantle boundary beneath the central Pacific imaged using broadband ScS waves. *Journal of Geophysical Research*, *104*(B6), 13183–13199. https://doi.org/10.1029/1999JB900114

Schneider, S., & Deuss, A. (2020). A new catalogue of toroidal-mode overtone splitting function measurements. *Geophysical Journal International*, *225*(1), 329–341. https://doi.org/10.1093/gji/ggaa567

Schuberth, B. S. A., Bunge, H.-P., Steinle-Neumann, G., Moder, C., & Oeser, J. (2009). Thermal versus elastic heterogeneity in high-resolution mantle circulation models with pyrolite composition: High plume excess temperatures in the lowermost mantle. *Geochemistry, Geophysics, Geosystems*, *10*(1), Q01W01. https://doi.org/10.1029/2008GC002235

Shahraki, M., Schmeling, H., Kaban, M. K., & Petrunin, A. G. (2015). Effects of the postperovskite phase change on the observed geoid. *Geophysical Research Letters*, *42*(1), 44–52. https://doi.org/10.1002/2014GL060255

Shim, S.-H. (2008). The postperovskite transition. *Annual Review of Earth and Planetary Sciences*, *36*(1), 569–599. https://doi.org/10.1146/annurev.earth.36.031207.124309

Sigloch, K., McQuarrie, N., & Nolet, G. (2008). Two-stage subduction history under North America inferred from finite-frequency tomography. *Nature Geoscience*, *1*(7), 458–462. https://doi.org/10.1038/ngeo231

Silver, P. G., & Chan, W. W. (1991). Shear wave splitting and subcontinental mantle deformation. *Journal of Geophysical Research*, *96*(B10), 16429–16454. https://doi.org/10.1029/91JB00899

Silver, P. G., & Savage, M. K. (1994). The interpretation of shear-wave splitting parameters in the presence of two anisotropic layers. *Geophysical Journal International*, *119*(3), 949–963. https://doi.org/10.1111/j.1365-246X.1994.tb04027.x

Simmons, N. A., Forte, A. M., Boschi, L., & Grand, S. P. (2010). GyPSuM: A joint tomographic model of mantle density and seismic wave speeds. *Journal of Geophysical Research*, *115*(B12), 523. https://doi.org/10.1029/2010JB007631

Simmons, N. A., Forte, A. M., & Grand, S. P. (2009). Joint seismic, geodynamic and mineral physical constraints on three-dimensional mantle heterogeneity: Implications for the relative importance of thermal versus compositional heterogeneity. *Geophysical Journal International*, *177*(3), 1284–1304. https://doi.org/10.1111/j.1365-246X.2009.04133.x

Simmons, N. A., & Grand, S. P. (2002). Partial melting in the deepest mantle. *Geophysical Research Letters*, *29*(11), 47-1. https://doi.org/10.1029/2001GL013716

Spasojevic, S., Liu, L., & Gurnis, M. (2009). Adjoint models of mantle convection with seismic, plate motion, and stratigraphic constraints: North America since the Late Cretaceous. *Geochemistry, Geophysics, Geosystems*, *10*(5), Q05W02. https://doi.org/10.1029/2008GC002345

Stackhouse, S., Brodholt, J. P., Wookey, J., Kendall, J.-M., & Price, G. D. (2005). The effect of temperature on the seismic anisotropy of the perovskite and post-perovskite polymorphs of $MgSiO_3$. *Earth and Planetary Science Letters*, *230*(1–2), 1–10. https://doi.org/10.1016/j.epsl.2004.11.021

Steinberger, B. (2000). Plumes in a convecting mantle: Models and observations for individual hotspots. *Journal of Geophysical Research*, *105*(B5), 11127–11152. https://doi.org/10.1029/1999JB900398

Steinberger, B., & Calderwood, A. R. (2006). Models of large-scale viscous flow in the Earth's mantle with constraints from mineral physics and surface observations. *Geophysical Journal International*, *167*(3), 1461–1481. https://doi.org/10.1111/j.1365-246X.2006.03131.x

Steinberger, B., Conrad, C. P., Osei Tutu, A., & Hoggard, M. J. (2019). On the amplitude of dynamic topography at spherical harmonic degree two. *Tectonophysics*, *760*, 221–228. (Linking plate tectonics and volcanism to deep earth dynamics—A tribute to Trond H. Torsvik). https://doi.org/10.1016/j.tecto.2017.11.032

Steinberger, B., & Holme, R. (2008). Mantle flow models with core-mantle boundary constraints and chemical heterogeneities in the lowermost mantle. *Journal of Geophysical Research*, *113*(B5), B05403. https://doi.org/10.1029/2007JB005080

Steinberger, B., & O'Connell, R. J. (1998). Advection of plumes in mantle flow: Implications for hotspot motion, mantle viscosity and plume distribution. *Geophysical Journal International*, *132*(2), 412–434. https://doi.org/10.1046/j.1365-246x.1998.00447.x

Steinberger, B., & Steinberger, A. (2023). Chapter 17—Mantle plumes and their interactions. In *Dynamics of plate tectonics and mantle convection* (pp. p. 407–426). Elsevier. https://doi.org/10.1016/B978-0-323-85733-8.00021-4

Steinberger, B., & Torsvik, T. H. (2012). A geodynamic model of plumes from the margins of large low shear velocity provinces. *Geochemistry, Geophysics, Geosystems*, *13*(1), Q01W09. https://doi.org/10.1029/2011GC003808

Stixrude, L., & Lithgow-Bertelloni, C. (2011). Thermodynamics of mantle minerals—II. phase equilibria. *Geophysical Journal International*, *184*(3), 1180–1213. https://doi.org/10.1111/j.1365-246X.2010.04890.x

Suzuki, Y., Kawai, K., & Geller, R. J. (2021). Imaging paleoslabs and inferring the Clapeyron slope in D′′ beneath the northern Pacific based on high-resolution inversion of seismic waveforms for 3-D transversely isotropic structure. *Physics of the Earth and Planetary Interiors*, *321*, 106751. https://doi.org/10.1016/j.pepi.2021.106751

Tackley, P. J. (2000). Mantle convection and plate tectonics: Toward an integrated physical and chemical theory. *Science*, *288*(5473), 2002–2007. https://doi.org/10.1126/science.288.5473.2002

Tackley, P. J. (2011). Living dead slabs in 3-D: The dynamics of compositionally-stratified slabs entering a "slab graveyard" above the core-mantle boundary. *Physics of the Earth and Planetary Interiors*, *188*(3–4), 150–162. https://doi.org/10.1016/j.pepi.2011.04.013

Tandon, G. P., & Weng, G. J. (1984). The effect of aspect ratio of inclusions on the elastic properties of unidirectionally aligned composites. *Polymer Composites*, *5*(4), 327–333. https://doi.org/10.1002/pc.750050413

Tesoniero, A., Leng, K., Long, M. D., & Nissen-Meyer, T. (2020). Full wave sensitivity of SK(K)S phases to arbitrary anisotropy in the upper and lower mantle. *Geophysical Journal International*, *222*(1), 412–435. https://doi.org/10.1093/gji/ggaa171

Thomas, C., Wookey, J., Brodholt, J., & Fieseler, T. (2011). Anisotropy as cause for polarity reversals of D′′ reflections. *Earth and Planetary Science Letters*, *307*(3–4), 369–376. https://doi.org/10.1016/j.epsl.2011.05.011

Thorne, M. S., Leng, K., Pachhai, S., Rost, S., Wicks, J., & Nissen-Meyer, T. (2021). The most parsimonious ultralow-velocity zone distribution from highly anomalous SPdKS waveforms. *Geochemistry, Geophysics, Geosystems*, *22*(1), e2020GC009467. https://doi.org/10.1029/2020GC009467

Thorne, M. S., Takeuchi, N., & Shiomi, K. (2019). Melting at the edge of a slab in the deepest mantle. *Geophysical Research Letters*, *46*(14), 8000–8008. https://doi.org/10.1029/2019GL082493

Tkalčić, H. (2015). Complex inner core of the earth: The last Frontier of global seismology. *Reviews of Geophysics*, *53*(1), 59–94. https://doi.org/10.1002/2014RG000469

Tkalčić, H., Young, M., Muir, J., Davies, D. R., & Mattesini, M. (2015). Strong, multi-scale heterogeneity in earth's lowermost mantle. *Scientific Reports*, *5*(1), 18416. https://doi.org/10.1038/srep18416

To, A., Romanowicz, B., Capdeville, Y., & Takeuchi, N. (2005). 3D effects of sharp boundaries at the borders of the African and Pacific superplumes: Observation and modeling. *Earth and Planetary Science Letters*, *233*(1–2), 137–153. https://doi.org/10.1016/j.epsl.2005.01.037

Torsvik, T. (2019). Earth history: A journey in time and space from base to top. *Tectonophysics*, *760*, 297–313. https://doi.org/10.1016/j.tecto.2018.09.009

Trønnes, R. G. (2010). Structure, mineralogy and dynamics of the lowermost mantle. *Mineralogy and Petrology*, *99*(3–4), 243–261. https://doi.org/10.1007/s00710-009-0068-z

Usui, Y., Hiramatsu, Y., Furumoto, M., & Kanao, M. (2008). Evidence of seismic anisotropy and a lower temperature condition in the D″ layer beneath Pacific Antarctic Ridge in the Antarctic Ocean. *Physics of the Earth and Planetary Interiors*, *167*(3–4), 205–216. https://doi.org/10.1016/j.pepi.2008.04.006

Vanacore, E., & Niu, F. (2011). Characterization of the D″ beneath the Galapagos Islands using SKKS and SKS waveforms. *Earthquake Science*, *24*(1), 87–99. https://doi.org/10.1007/s11589-011-0772-8

van der Hilst, R., Widiyantoro, S., & Engdahl, E. (1997). Evidence for deep mantle circulation from global tomography. *Nature*, *386*(6625), 578–584. https://doi.org/10.1038/386578a0

van der Meer, D. G., van Hinsbergen, D. J., & Spakman, W. (2018). Atlas of the underworld: Slab remnants in the mantle, their sinking history, and a new outlook on lower mantle viscosity. *Tectonophysics*, *723*, 309–448. https://doi.org/10.1016/j.tecto.2017.10.004

Vinnik, L., Bréger, L., & Romanowicz, B. (1998a). Anisotropic structures at the base of the Earth's mantle. *Nature*, *393*(6685), 564–567. https://doi.org/10.1038/31208

Vinnik, L., Bréger, L., & Romanowicz, B. (1998b). On the inversion of Sd particle motion for seismic anisotropy in D′. *Geophysical Research Letters*, *25*(5), 679–682. https://doi.org/10.1029/98GL00190

Vinnik, L., Farra, V., & Romanowicz, B. (1989a). Azimuthal anisotropy in the earth from observations of SKS at GEOSCOPE and NARS broadband stations. *Bulletin of the Seismological Society of America*, *79*, 1542–1558. https://doi.org/10.1785/BSSA0790051542

Vinnik, L., Farra, V., & Romanowicz, B. (1989b). Observational evidence for diffracted sv in the shadow of the earth's core. *Geophysical Research Letters*, *16*(6), 519–522. https://doi.org/10.1029/GL016i006p00519
Vinnik, L., Romanowicz, B., Le Stunff, Y., & Makeyeva, L. (1995). Seismic anisotropy in the D″ layer. *Geophysical Research Letters*, *22*(13), 1657–1660. https://doi.org/10.1029/95GL01327
Walker, A. M., Forte, A. M., Wookey, J., Nowacki, A., & Kendall, J.-M. (2011). Elastic anisotropy of D′′ predicted from global models of mantle flow. *Geochemistry, Geophysics, Geosystems*, *12*(10), Q10006. https://doi.org/10.1029/2011GC003732
Walsh, E., Arnold, R., & Savage, M. K. (2013). Silver and Chan revisited. *Journal of Geophysical Research: Solid Earth*, *118*(10), 5500–5515. https://doi.org/10.1002/jgrb.50386
Wang, Y., & Li, M. (2020). Constraining mantle viscosity structure from a statistical analysis of slab stagnation events. *Geochemistry, Geophysics, Geosystems*, *21*(11), e2020GC009286. https://doi.org/10.1029/2020GC009286
Wang, Y., & Wen, L. (2004). Mapping the geometry and geographic distribution of a very low velocity province at the base of the Earth's mantle. *Journal of Geophysical Research*, *109*(B10), B10305. https://doi.org/10.1029/2003JB002674
Wang, Y., & Wen, L. (2007). Complex seismic anisotropy at the border of a very low velocity province at the base of the Earth's mantle. *Journal of Geophysical Research*, *112*(B9), B09305. https://doi.org/10.1029/2006JB004719
Wenk, H.-R., Cottaar, S., Tomé, C. N., McNamara, A., & Romanowicz, B. (2011). Deformation in the lowermost mantle: From polycrystal plasticity to seismic anisotropy. *Earth and Planetary Science Letters*, *306*(1–2), 33–45. https://doi.org/10.1016/j.epsl.2011.03.021
Wenk, H.-R., & Houtte, P. V. (2004). Texture and anisotropy. *Reports on Progress in Physics*, *67*(8), 1367–1428. https://doi.org/10.1088/0034-4885/67/8/R02
Wenk, H.-R., Speziale, S., McNamara, A., & Garnero, E. (2006). Modeling lower mantle anisotropy development in a subducting slab. *Earth and Planetary Science Letters*, *245*(1–2), 302–314. https://doi.org/10.1016/j.epsl.2006.02.028
Williams, Q., & Garnero, E. J. (1996). Seismic evidence for partial melt at the base of earth's mantle. *Science*, *273*(5281), 1528–1530. https://doi.org/10.1126/science.273.5281.1528
Wolf, J., Creasy, N., Pisconti, A., Long, M. D., & Thomas, C. (2019). An investigation of seismic anisotropy in the lowermost mantle beneath Iceland. *Geophysical Journal International*, *219*(Supplement_1), S152–S166. https://doi.org/10.1093/gji/ggz312
Wolf, J., & Evans, D. A. D. (2022). Reconciling supercontinent cycle models with ancient subduction zones. *Earth and Planetary Science Letters*, *578*, 117293. https://doi.org/10.1016/j.epsl.2021.117293
Wolf, J., Frost, D. A., Long, M. D., Garnero, E., Aderoju, A. O., Creasy, N., & Bozdağ, E. (2023). Observations of mantle seismic anisotropy using array techniques: Shear-wave splitting of beamformed SmKS phases. *Journal of Geophysical Research: Solid Earth*, *128*(1), e2022JB025556. https://doi.org/10.1029/2022JB025556
Wolf, J., Li, M., Haws, A. A., & Long, M. D. (2024). Strong seismic anisotropy due to upwelling flow at the root of the Yellowstone mantle plume. *Geology*, *52*(5), 379–382. https://doi.org/10.1130/G51919.1
Wolf, J., & Long, M. (2024). ScS shear-wave splitting in the lowermost mantle: Practical challenges and new global measurements. *Seismica*, *3*(1), 1573. https://doi.org/10.26443/seismica.v3i1.1128
Wolf, J., & Long, M. D. (2022). Slab-driven flow at the base of the mantle beneath the northeastern Pacific Ocean. *Earth and Planetary Science Letters*, *594*, 117758. https://doi.org/10.1016/j.epsl.2022.117758
Wolf, J., & Long, M. D. (2023). Lowermost mantle structure beneath the central Pacific Ocean: Ultralow velocity zones and seismic anisotropy. *Geochemistry, Geophysics, Geosystems*, *24*(6), e2022GC010853. https://doi.org/10.1029/2022GC010853
Wolf, J., Long, M. D., Creasy, N., & Garnero, E. (2023). On the measurement of Sdiff splitting caused by lowermost mantle anisotropy. *Geophysical Journal International*, *233*(2), 900–921. https://doi.org/10.1093/gji/ggac490
Wolf, J., Long, M. D., & Frost, D. A. (2024). Ultralow velocity zone and deep mantle flow beneath the himalayas linked to subducted slab. *Nature Geoscience*, *17*(4), 1–7. https://doi.org/10.1038/s41561-024-01386-5
Wolf, J., Long, M. D., Frost, D. A., & Nissen-Meyer, T. (2024). The expression of mantle seismic anisotropy in the global seismic wavefield. *Geophysical Journal International*. https://doi.org/10.1093/gji/ggae164
Wolf, J., Long, M. D., Leng, K., & Nissen-Meyer, T. (2022a). Constraining deep mantle anisotropy with shear wave splitting measurements: Challenges and new measurement strategies. *Geophysical Journal International*, *230*(1), 507–527. https://doi.org/10.1093/gji/ggac055
Wolf, J., Long, M. D., Leng, K., & Nissen-Meyer, T. (2022b). Sensitivity of SK(K)S and ScS phases to heterogeneous anisotropy in the lowermost mantle from global wavefield simulations. *Geophysical Journal International*, *228*(1), 366–386. https://doi.org/10.1093/gji/ggab347
Wolf, J., Long, M. D., Li, M., & Garnero, E. (2023). Global compilation of deep mantle anisotropy observations and possible correlation with low velocity provinces. *Geochemistry, Geophysics, Geosystems*, *24*(10), e2023GC011070. https://doi.org/10.1029/2023GC011070
Wookey, J., & Kendall, J.-M. (2008). Constraints on lowermost mantle mineralogy and fabric beneath siberia from seismic anisotropy. *Earth and Planetary Science Letters*, *275*(1–2), 32–42. https://doi.org/10.1016/j.epsl.2008.07.049
Wookey, J., Kendall, J.-M., & Rümpker, G. (2005). Lowermost mantle anisotropy beneath the north Pacific from differential S-ScS splitting. *Geophysical Journal International*, *161*(3), 829–838. https://doi.org/10.1111/j.1365-246X.2005.02623.x
Wookey, J., Stackhouse, S., Kendall, J.-M., Brodholt, J., & Price, G. (2005). Efficacy of the post-perovskite phase as an explanation for lowermost-mantle seismic properties. *Nature*, *438*(7070), 1004–1007. https://doi.org/10.1038/nature04345
Wu, X., Lin, J., Kaercher, P., Mao, Z., Liu, J., Wenk, H. R., & Prakapenka, V. B. (2017). Seismic anisotropy of the D′′ layer induced by (001) deformation of post-perovskite. *Nature Communications*, *8*(1), 14669. https://doi.org/10.1038/ncomms14669
Wüstefeld, A., Bokelmann, G., Barruol, G., & Montagner, J.-P. (2009). Identifying global seismic anisotropy patterns by correlating shear-wave splitting and surface-wave data. *Physics of the Earth and Planetary Interiors*, *176*(3–4), 198–212. https://doi.org/10.1016/j.pepi.2009.05.006
Wüstefeld, A., Bokelmann, G., Zaroli, C., & Barruol, G. (2008). Splitlab: A shear-wave splitting environment in MATLAB. *Computers & Geosciences*, *34*(5), 515–528. https://doi.org/10.1016/j.cageo.2007.08.002
Wysession, M. E., Langenhorst, A., Fouch, M. J., Fischer, K. M., Al-Eqabi, G. I., Shore, P. J., & Clarke, T. J. (1999). Lateral variations in compressional/shear velocities at the base of the mantle. *Science*, *284*(5411), 120–125. https://doi.org/10.1126/science.284.5411.120
Yamazaki, D., & Karato, S.-I. (2001). High-pressure rotational deformation apparatus to 15 GPa. *Review of Scientific Instruments*, *72*(11), 4207–4211. https://doi.org/10.1063/1.1412858
Yamazaki, D., & Karato, S.-I. (2002). Fabric development in (Mg,Fe)O during large strain, shear deformation: Implications for seismic anisotropy in earth's lower mantle. *Physics of the Earth and Planetary Interiors*, *131*(3), 251–267. https://doi.org/10.1016/S0031-9201(02)00037-7
Yamazaki, D., & Karato, S.-I. (2007). Lattice-preferred orientation of lower mantle materials and seismic anisotropy in the D′′ layer. In *Washington DC American geophysical union geophysical monograph series* (pp. 69–78). https://doi.org/10.1029/174GM07
Yamazaki, D., Shinmei, T., Inoue, T., Irifune, T., Nozawa, A., & Funakoshi, K. (2006). Generation of pressures to 60 GPa in Kawai-type apparatus and stability of $MnGeO_3$ perovskite at high pressure and high temperature. *American Mineralogist*, *91*(8–9), 1342–1345. https://doi.org/10.2138/am.2006.2175

Yamazaki, D., Yoshino, T., Ohfuji, H., Ichi Ando, J., & Yoneda, A. (2006). Origin of seismic anisotropy in the D′′ layer inferred from shear deformation experiments on post-perovskite phase. *Earth and Planetary Science Letters*, *252*(3–4), 372–378. https://doi.org/10.1016/j.epsl.2006.10.004

Yang, T., & Gurnis, M. (2016). Dynamic topography, gravity and the role of lateral viscosity variations from inversion of global mantle flow. *Geophysical Journal International*, *207*(2), 1186–1202. https://doi.org/10.1093/gji/ggw335

Yoshida, M. (2008a). Core-mantle boundary topography estimated from numerical simulations of instantaneous mantle flow. *Geochemistry, Geophysics, Geosystems*, *9*(7), Q07002. https://doi.org/10.1029/2008GC002008

Yoshida, M. (2008b). Mantle convection with longest-wavelength thermal heterogeneity in a 3-D spherical model: Degree one or two? *Geophysical Research Letters*, *35*(23), L23302. https://doi.org/10.1029/2008GL036059

Yu, S., & Garnero, E. J. (2018). Ultralow velocity zone locations: A global assessment. *Geochemistry, Geophysics, Geosystems*, *19*(2), 396–414. https://doi.org/10.1002/2017GC007281

Yuan, Q., & Li, M. (2022). Vastly different heights of LLVPs caused by different strengths of historical slab push. *Geophysical Research Letters*, *49*(17), e2022GL099564. https://doi.org/10.1029/2022GL099564

Yuan, Q., Li, M., Desch, S., Ko, B., Deng, H., Garnero, E., et al. (2023). Moon-forming impactor as a source of Earth's basal mantle anomalies. *Nature*, *623*(7985), 95–99. https://doi.org/10.1038/s41586-023-06589-1

Zhang, N., Zhong, S., Leng, W., & Li, Z.-X. (2010). A model for the evolution of the Earth's mantle structure since the Early Paleozoic. *Journal of Geophysical Research*, *115*(B6), B06401. https://doi.org/10.1029/2009JB006896

Zhao, L., & Jordan, T. H. (2006). Structural sensitivities of finite-frequency seismic waves: A full-wave approach. *Geophysical Journal International*, *165*(3), 981–990. https://doi.org/10.1111/j.1365-246X.2006.02993.x

Zhong, S., & Rudolph, M. L. (2015). On the temporal evolution of long-wavelength mantle structure of the Earth since the early Paleozoic. *Geochemistry, Geophysics, Geosystems*, *16*(5), 1599–1615. https://doi.org/10.1002/2015GC005782

Zhong, S., Zhang, N., Li, Z.-X., & Roberts, J. H. (2007). Supercontinent cycles, true polar wander, and very long-wavelength mantle convection. *Earth and Planetary Science Letters*, *261*(3), 551–564. https://doi.org/10.1016/j.epsl.2007.07.049